The Dissertation Committee for Yu Leng
certifies that this is the approved version of the following dissertation:

Numerical analysis of reproducing kernel collocation method for linear nonlocal models

Committee:

John T. Foster, Supervisor

Xiaochuan Tian, Co-supervisor

Leszek F. Demkowicz

Kamy Sepehrnoori

Mukul M. Sharma

Mary F. Wheeler

Numerical analysis of reproducing kernel collocation method for linear nonlocal models

by

Yu Leng

Dissertation

Presented to the Faculty of the Graduate School of
The University of Texas at Austin
in Partial Fulfillment
of the Requirements
for the Degree of

Doctor of Philosophy

The University of Texas at Austin
May 2020

Acknowledgments

I want to thank Prof. John Foster for giving me the opportunity to come to UT and for his patience and support on my research. I can not thank him enough for the freedom he has given me to explore my research interests. More importantly, He directed me back on track when I got lost, has provided me with lots of opportunities to work with other brilliant collaborators, and sent me to conferences worldwide, which opened my eyes in various ways.

I have been fortunate enough to work with Dr. Xiaochuan Tian on nonlocal models. Her knowledge and insights in applied mathematics have helped me overcome various challenges throughout this dissertation. Her enthusiasm for research and meticulous attention to details have encouraged me to push myself further in academics.

I would like to express my sincere appreciation to Prof. Demkowicz. He opened another door to me and I saw a new world of numerical analysis through his eyes. His dedication to research has motivated me to become a researcher like him; he is a true role model for young researchers.

I also want to thank, Prof. Wheeler for her valuable questions during my PhD proposal which directed me to numerical analysis, and Profs. Sepehrnoori and Sharma for serving on my committee. It's my great privilege to have worked with some excellent researchers, Prof. J.S. Chen, Drs. Nat Trask, Marta D'Elia, Marco Pasetto, and Pablo Seleson. The fruitful conversions with them have enlightened me and sparked many ideas. Moreover, The Oden Institute has many distinguished faculties whom I've taken classes from and been allowed to work next to, which has

had intangibly great effect on me.

There are many others who have helped me walk through this journey in Austin. I want to thank UT staffs, who have helped me with non-academic work, and also my friends and family who have shaped me in a positive way.

Numerical analysis of reproducing kernel collocation method for linear nonlocal models

Yu Leng, Ph.D.

The University of Texas at Austin, 2020

Supervisor: John T. Foster
Co-supervisor: Xiaochuan Tian

Hydraulic fracturing has played a major role in north America's "shale revolution" over the past decades. Modeling of the hydraulic fracture propagation is challenging. Peridynamics, a nonlocal theory of continuum mechanics, has been used to model complex hydraulic fracturing processes in recent years. While the peridynamics-based hydraulic fracturing model has shown promising simulations results, its current numerical discretization lacks any mathematical analysis.

This dissertation is motivated by the numerical solution of the peridynamics-based hydraulic fracturing model. The major objective is to develop a robust numerical method, under the change of the modeling parameters, for linear nonlocal diffusion models and peridynamic Navier equation, which are decoupled models of the peridynamics-based hydraulic fracturing model. Reproducing kernel (RK) collocation method is of our interest due to its mesh-free nature. By choosing special RK support sizes, we have developed a RK collocation method for nonlocal models and numerical solutions converge to the nonlocal solution and also to the corresponding local limit independent of the modeling parameters as the nonlocal interactions vanish.

Accurate evaluation of the stiffness matrix for nonlocal models is computationally prohibitive even for collocation method. To save computational costs, the concept of RK approximation is generalized to approximate integrals and the quasi-discrete nonlocal operator, which uses a finite number of symmetric quadrature points to evaluate the integral, is proposed. We have shown RK collocation on the quasi-discrete nonlocal diffusion and peridynamic Navier equation converge to their classical counterparts.

Finally, for the pure displacement form of the classical linear elasticity model, finite element solutions deteriorate when the material is nearly incompressible. A common remedy is to introduce an additional variable, pressure, and rewrite the equation in a mixed formulation, but the discrete functional spaces need to satisfy the famous inf-sup condition. For the the mixed form of the quasi-discrete peridynamic Navier equation, the discretization obtained using RK collocation with equal order interpolation for displacements and pressure passes the inf-sup test; the solution does not suffer from instability. Hence, with the use of penalty techniques or artificial compressibility, the proposed RK collocation method is promising in solving the peridynamics-based hydraulic fracturing model, which has an embedded saddle-point problem.

Table of Contents

Acknowledgments iv

Abstract vi

List of Figures x

Chapter 1. Introduction 1
- 1.1 Motivation . . . 1
- 1.2 State of the art . . . 5
  - 1.2.1 Numerical methods . . . 5
  - 1.2.2 Computational cost . . . 10
  - 1.2.3 RK approximation . . . 11
- 1.3 Overview . . . 12
  - 1.3.1 Objectives . . . 12
  - 1.3.2 Outline . . . 13

Chapter 2. Super-convergence of RK approximation 15
- 2.1 RK approximation . . . 16
  - 2.1.1 Continuous RK approximation . . . 17
  - 2.1.2 Discrete RK approximation . . . 18
- 2.2 Super-convergence for continuous RK approximation . . . 20
- 2.3 Discrete RK approximation error estimates for selected RK support sizes 27
  - 2.3.1 B-spline functions as window functions . . . 31
- 2.4 Multi-dimensional RK approximation . . . 33
- 2.5 Numerical experiments . . . 37
- 2.6 The discussion on general RK support sizes . . . 41

Chapter 3. Nonlocal diffusion 46
- 3.1 Nonlocal diffusion operator and model equation . . . 47
- 3.2 RK collocation method . . . 48
- 3.3 Convergence analysis of the RK collocation method for nonlocal diffusion 53
  - 3.3.1 Stability . . . 53
  - 3.3.2 Consistency . . . 59
- 3.4 Numerical example . . . 65

Chapter 4. Quasi-discrete nonlocal diffusion **68**
4.1 Quasi-discrete nonlocal operators 69
4.1.1 Quasi-discrete nonlocal diffusion 69
4.1.2 Quadrature weights using the RK approximation 71
4.1.3 Quadrature weights using GMLS 74
4.1.4 Truncation error of the quasi-discrete nonlocal operator 76
4.2 Convergence analysis of the RK collocation for the quasi-discrete nonlocal diffusion 77
4.2.1 Stability 78
4.2.2 Consistency 82
4.3 Numerical example 84

Chapter 5. Peridynamic Navier equation **86**
5.1 Peridynamic Navier equation 87
5.1.1 Nonlocal operators 88
5.1.2 Quasi-discrete nonlocal operators 90
5.1.3 RK collocation scheme 92
5.2 Convergence analysis of RK collocation method for the peridynamic Navier equation 93
5.2.1 Stability 93
5.2.2 Consistency 102
5.3 Convergence analysis of the RK collocation for the quasi-discrete peridynamic Navier equation 107
5.3.1 Stability 108
5.3.2 Consistency 112
5.4 Numerical example 116
5.4.1 RK collocation for the peridynamic Navier equation 117
5.4.2 RK collocation for the quasi-discrete peridynamic Navier equation 117
5.5 Near incompressibility 118

Chapter 6. Conclusions **124**

Bibliography **128**

List of Figures

1.1 Simulation results using the peridynamics-based hydraulic fracturing model. 4

2.1 Domain decomposition in 1d. $\overline{\overline{\Omega}} = \Omega_{bl} \cup \Omega$ and $\Omega_{bl} = \Omega_L \cup \Omega_R$ 16

2.2 Error distribution of approximating a linear function $u(x) = x$ using constant RK interpolation with $h = 0.1$ and $\epsilon = 2h$. Cubic B-spline is the window function 38

2.3 Convergence study of approximating $u(x) = e^x$ using constant RK interpolation with $\epsilon = 2h$. r is the rate of convergence and cubic B-spline is the window function 39

2.4 Convergence study of approximating $u(x) = e^x$ using linear RK interpolation with $\epsilon = 2h$. r is the rate of convergence and cubic B-spline is the window function 39

2.5 Convergence study of approximating $u(x) = e^x$ using quadratic RK interpolation with $\epsilon = 3h$. r is the rate of convergence and fifth order B-spline is the window function 40

2.6 Error distribution of approximating a linear function $u(x) = x$ using constant RK interpolation with $h = 0.2$ and $\epsilon = h$. Cubic B-spline is the window function. 42

2.7 Error distribution of approximating a linear function $u(x) = x$ using constant RK interpolation with support sizes $\epsilon = 1.7h$ and $\epsilon = 2.7h$. Cubic B-spline is the window function 43

2.8 Convergence study of approximating $u(x) = e^x$ using constant and quadratic RK interpolation with support sizes $\epsilon = 1.7h, 2.7h$ and $3.7h$. Cubic B-spline is the window function 45

3.1 The dashed lines form the grid for the RK collocation method 49

3.2 Meshfree discretization of a two-dimensional unit square domain with integration points within the neighborhood of each node. The dashed lines represent the limits of the neighborhoods of nodes A and B. . . 67

3.3 Convergence profiles using the RK collocation method. 67

4.1 Quadrature points (blue dots) are shown in the horizon of $\boldsymbol{x} \in \Omega$. The dashed lines form the grid for the RK collocation scheme that will be applied later in section 4.2. $\boldsymbol{x}$ is not necessarily the grid point. The quadrature points are independent of the collocation points on the grid. 70

4.2 Convergence profiles using the RK collocation method for the quasi-discrete nonlocal diffusion. 85

5.1 Convergence profiles using the RK collocation method. 117
5.2 Convergence profiles using the RK collocation for quasi-discrete peridynamic Navier equation. 118
5.3 Inf-sup test of the RK collocation for quasi-discrete peridynamic Navier equation. 121
5.4 Exact and numerical solution of eq. (5.89) with uniform grid (64×64) on $\Omega = (0,1)^2$, $h = 0.015625$, $\nu = 0.499$, and $\delta = 3h$. 123

Chapter 1

Introduction

1.1 Motivation

In recent decades, hydraulic fracturing, in combination with horizontal drilling, has made commercial oil and gas production from shale and tight formations possible. As of 2015, more than half of oil production and about two-thirds of gas production in the U.S. come from hydraulic fractured wells [27, 115]. It is predicted that by 2040, tight oil will make up two-thirds of oil production and tight gas about 60% of gas production [116]. During the hydraulic fracturing process, a mixture of water, sand, and chemicals is injected into the formation to initiate and propagate fractures. The geometry of induced fractures is a result of multiple factors such as rock properties, in-situ stress state [45], natural fractures [90] and more. Modeling the propagation of hydraulic fractures has been an important topic in oil and gas industry.

Modeling of hydraulic fracturing process is a challenging task. Perkins-Kern-Nordgren (PKN) [89, 96] and Khristianovic-Geertsma-de Klerk (KGD) [44, 125] are two classical two-dimensional hydraulic fracturing models. Both models assume constant height fracture growth in the direction away from well-bore and no fluid flow in vertical direction but they differ in the assumption of plane strain direction and fracture cross-section geometry. PKN assumes vertical plane strain and is more applicable for fractures whose length are much larger than height; KGD, however, assumes the plane stress in horizontal planes and can better describe fractures with much larger height than length. Although these two models oversimplify the hydraulic fracturing

process, they still serve as basic models for model verification.

Based on the classical two-dimensional model (PKN), pseudo-three-dimensional (P3D) models allow fracture height to change and can predict hydraulic fracture growth in multi-layered formation. P3D models can be further categorized into cell-based models and lumped models. In cell-based P3D models, the fracture is divided into multiple cells along the horizontal direction [43, 108] and classical two-dimensional model is used to predict fracture profile in each cell and fracture heights may vary between cells. In lumped models, however, the fracture is divided into two sections along the vertical direction (the upper half and lower half) [24] and fracture profiles are solved individually in each vertical section. Most P3D models ignore vertical fluid flow and do not include fully three dimensional elastic response. To overcome these shortcomings of P3D models, planar three-dimensional (PL3D) models which can simulate general shaped fractures have been proposed [25, 26, 31, 102]. Because PL3D models are limited to planar fracture surfaces, fully three-dimensional models are required to describe complex interactions of propagating fractures with layered media and natural fractures.

A simplified three-dimensional displacement discontinuity method [120] can generate non-planar fractures with an initial angle deviating from the direction of maximum horizontal stress or by multiple fracture propagation in close spacing. By using an enriched finite-element basis functions, extended finite element method (XFEM) also known as generalized finite element method (GFEM) is able to simulate discontinuities without re-meshing; the simulation of non-planar three-dimensional hydraulic fractures has been studied using XFEM/GFEM in [29, 46, 47, 48, 65, 86, 97]. XFEM/GFEM has the potential to simulate more complicated fracture geometries. Phase-field modeling, a diffuse crack modeling approach, is another emerging tech-

nique to model the process of hydraulic fracturing; arbitrary non-planar crack propagation is handled naturally in the solution of the model. Phase-field modeling has been successfully applied to hydraulic fracturing simulation in [23, 52, 67, 68, 82, 83, 84, 118, 119].

Peridynamics [103, 105] is a nonlocal theory of continuum mechanics. Unlike classical theory, the peridynamic equation of motion is formulated using spatial integration instead of derivatives, which makes it well-suited for describing discontinuities such as fractures, material separation, and failure. Peridynamics has been applied to hydraulic fracture propagation problems [92], crack branching [10], damage progression in multi-layered glass [49], and among others. A peridynamics model, which incorporates the effects of fluid pressure, is introduced in [114] and it is the first nonlocal poro-elasticity model. Nonetheless, in order to simplify the presentation, they assume the fluid pressure is given everywhere. A peridynamics-based porous flow model is proposed based on a variational formulation of the classical diffusion model [64]. This nonlocal diffusion model is applicable for anisotropic diffusion in heterogeneous materials and slightly compressible fluids. In [93], the nonlocal diffusion model [64] and nonlocal poro-elasticity model [114] are coupled together and a peridynamics-based hydraulic fracturing model is developed to study fluid-driven fracture propagation. The interaction between hydraulic fracture and natural fractures [92], see Figure 1.1a, and the effect of different types of vertical reservoir heterogeneities on fracture propagation [91], see Figure 1.1b, are systematically investigated. This peridynamics-based hydraulic fracturing model has shown promise in modeling non-planar, multiple fracture growth in arbitrarily heterogeneous reservoirs.

This dissertation is motivated by the discretization of the peridynamics-based hydraulic fracturing model. Because mathematical analysis of this nonlocal hydraulic

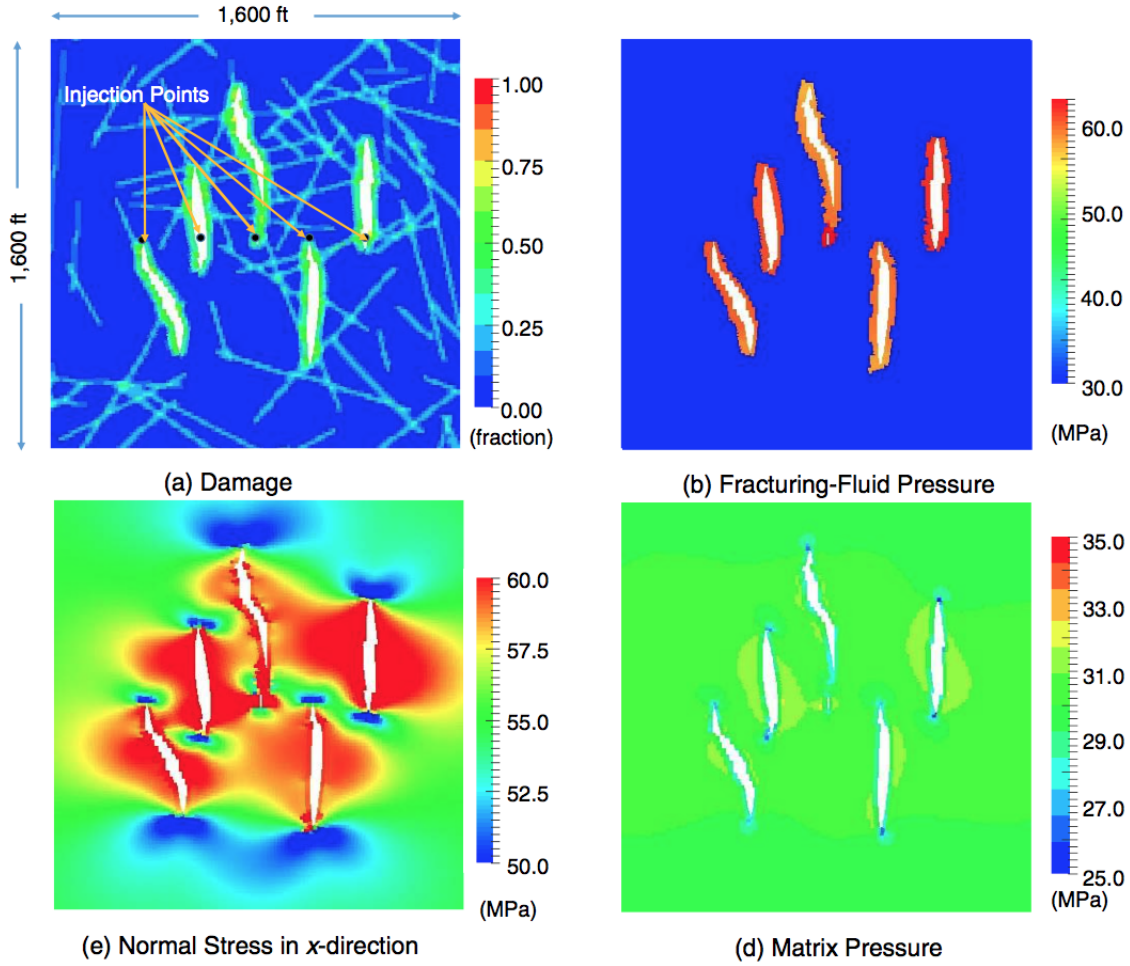

(a) Hydraulic fractures interacts with natural fractures [92]

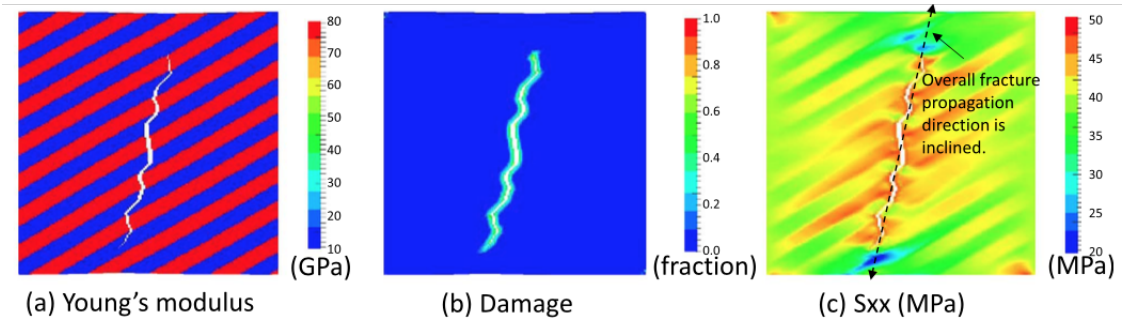

(b) Hydraulic fracture propagation in reservoir with heterogeneities [91]

Figure 1.1: Simulation results using the peridynamics-based hydraulic fracturing model.

fracturing model is still under development, we study the decoupled models: nonlocal diffusion model and the peridynamic Navier equation, which is the nonlocal linear elasticity model. We have developed a robust numerical method for both nonlocal diffusion model and peridynamic Navier equation. Analysis made in this dissertation is applicable to general elliptic nonlocal models. Moreover, we show that the proposed numerical discretization is promising in solving the peridynamics-based hydraulic fracturing model.

1.2 State of the art

1.2.1 Numerical methods

Nonlocal models introduce a length scale δ, called the *horizon* in peridynamics, which takes into account interactions over finite distances. As δ goes to 0, nonlocal interactions vanish and the linear nonlocal model recovers its local limit, i.e. a partial differential equation, provided the limit is well-defined. Mathematical analysis of nonlocal models have been carried out in [33, 34, 35, 80, 81] and it is well understood that the linear nonlocal diffusion and peridynamic Navier equation with Dirichlet boundary conditions are well-posed. Unlike classical elliptic models, the solution of the nonlocal elliptic models depends on the nonlocal kernel. If the nonlocal kernel is integrable, the nonlocal solution is a L^2 (square integrable) function; if the nonlocal kernel is of fractional type but not integrable, the energy space is a fractional Sobolev space between L^2 and H^1 (the function itself and its first derivative are both square integrable) [33]. As δ goes to 0, the nonlocal energy space approaches the H^1 space which is the energy space for the corresponding local model [111].

A mathematical framework of convergence is established for nonlocal models in [33, 80, 81] and the asymptotically compatible (AC) discretization is introduced in

[111]. An AC scheme allows the numerical solution of nonlocal equations to converge to both the nonlocal solutions for a fixed δ and also their local limits as δ goes to zero, independent of the mesh size $h_{\max}$. Several numerical methods have been developed for nonlocal diffusion and peridynamics models [8, 16, 21, 22, 32, 33, 35, 36, 37, 40, 66, 79, 81, 95, 100, 101, 104, 109, 111, 113, 124]. Many numerical methods for nonlocal models are not AC and some standard numerical methods may converge to the wrong local limit [110]. It is, however, a common practice to couple δ with the mesh size h in engineering applications as it leads to banded linear systems amenable to traditional preconditioning techniques, so both the nonlocal and local limits are of our interest.

A meshfree discretization [104] of peridynamic models has been widely used in engineering applications because it is simple to implement. This meshfree method uses the volume of the particles as the integration weights and assumes a constant field value in each nodal element. For the first time, three types of convergence have been numerically investigated for one-dimensional nonlocal model in [11]. When δ approaches zero slower than h, i.e., $\delta = \sqrt{h}$, the numerical solution of the meshfree method converges to the nonlocal limit and to the local limit. If δ is fixed and h goes to zero, the approximation converges to the nonlocal solution. However, when δ goes to zero faster than h, i.e., $\delta = h^2$ or at the same rate, i.e., $\delta = h$, the convergence to the local limit is not guaranteed. This was the early study of numerical robustness for nonlocal models. Moreover, adaptive refinement is discussed in one [11] and two dimensions [9] using variable horizon size.

The aforementioned meshfree method suffers from large quadrature error leading to low order of convergence, especially if the nonlocal kernel is singular or discontinuous over the whole domain. The accuracy can be improved by either changing the quadrature weights or updating the location of the quadrature points. In [123],

different geometric configurations of intersection between the volume of a neighbor and the horizon are classified and evaluated using an adaptive trapezoidal rule with a combined relative-absolute error control. This integration method improves the convergence rate to nearly quadratic. In [53], a Cartesian grid and mesh created by the centroidal Voronoi tessellation (CVT) generator have been compared for peridynamic simulation. Similar accuracy are obtained using both meshes but the CVT generator is less sensitive to the perturbation in the location of the quadrature points. Improved one-point quadrature algorithms are proposed for two dimensional peridynamic models in [99]. By calculating the intersection area of the peridynamic neighborhood and a neighboring particle exactly, and updating the neighboring particle location as the geometric center of the intersecting region, monotonic convergence is obtained. Influence functions with different regularities have also been suggested as means to improve the convergence of the meshfree discretization [100]. Despite these efforts to reduce the integration error, this meshfree method is not an AC scheme [110]. In [113], the quadrature weights are constructed using a generalized moving squares method and numerical results show that solutions obtained using this quadrature rule converge to the correct local limit.

The Finite Element Method (FEM) has been very successful in solving classical partial differential equations (PDEs) and there are many works devoted to solve nonlocal models using FEM [12, 21, 58, 60, 69, 79, 111]. We generalize FEM on nonlocal models as solving the weak form of the nonlocal equations which involves a double integral (in one dimension). A peridynamic grid can be incorporated into the FEM mesh as truss elements as pointed out by [79]. This was the first FEM implementation of peridynamics and it has shown the potential of coupling traditional FEM with peridynamics. Convergence behavior of continuous and discontinuous finite element approximations for one-dimensional nonlocal models are studied in

[21] and they consider both continuous and discontinuous manufactured solutions. They obtain similar convergence rates using piecewise-linear approximations for fixed horizons and for fixed ratios between the horizon and mesh size, i.e., $\delta = mh$, where m is a constant. Moreover, piecewise-constant approximations are robust if the mesh size is small with respect to the horizon. Even though, the concept of AC schemes for nonlocal models had not been proposed yet, they [21] were the first one to investigate the robustness of numerical method for nonlocal models.

In [111], AC schemes, which require the numerical solution of the discrete nonlocal models converges to the continuous nonlocal model as mesh size h goes to zero for a fixed δ and also to the corresponding continuous local limit as h and δ both approach zero, were introduced. This definition lays the foundation for the convergence study of numerical schemes for nonlocal models. Through rigorous analysis, they also found that FEM approximations are AC as long as the finite element space contains continuous piecewise-linear functions, and that piecewise-constant approximations converges to the correct local limit only if δ goes to zero faster than h, these analysis agree with the numerical experiments in [21].

A meshless Galerkin method is used to solve the nonlocal diffusion and the approximation space is constructed using radial basis functions in [12, 69]. They minimize the energy functional using the method of Lagrange multipliers and end up solving a mixed problem [69]. In [58, 60], a class of space-time nonlocal nonlinear fracture models with double well potentials is considered using finite element approximations and a priori convergence rates to the nonlocal solution for a fixed δ are established. However, the convergence to the corresponding local limit has not been studied so it is not clear if the schemes in [12, 69, 58, 60] converge to their corresponding local limit.

The finite difference method (FDM) is another popular numerical technique in solving PDEs but it has more restrictions on the domain of interest. A quadrature-based finite difference discretization is proposed in [110] and it is a reformulation of classical FDM for nonlocal models. This discretization is an AC scheme provided that the parameter is carefully chosen. They also study the limiting behaviors to the local limit for various discrete approximations and demonstrate that some numerical schemes may converge to a wrong local limit. Their work motivates researchers to pay particular attention to the robustness of the numerical method for nonlocal models. Then in [37], the authors extend the discretization to multi-dimensional nonlocal diffusion but the analysis is limited to uniform grids. More applications of this quadrature-based finite difference method to nonlocal convection-diffusion [109] and space-time nonlocal diffusion [16] is available. Finite difference approximations are also considered for the evolutionary nonlocal nonlinear fracture models in [59, 60] and convergence rates to the nonlocal limit are established. A quadrature rule using the trapezoidal rule based on linear interpolation is proposed to approximate the nonlocal diffusion operator and this collocation scheme is shown to be AC [124]. Other numerical methods are also exploited in [40, 66]. Fourier spectral approximations for the one-dimensional nonlocal Allen-Cahn equation are studied in [40]; this discretization is AC but it is limited to periodic boundary conditions. In [66], particle based discretizations are developed for one-dimensional linear nonlocal advection model.

A reproducing kernel (RK) collocation method for nonlocal models has been numerically investigated in [95] but only the convergence to the nonlocal limit is shown. In this dissertation, we provide rigorous convergence analysis for this RK collocation method for nonlocal diffusion and the peridynamic Navier equation, and show the collocation scheme is AC, provided that special RK support sizes are chosen. Showing the stability of collocation methods on integral equations is challenging

because the collocation scheme lacks a discrete maximum principle. The key idea in this dissertation is to compare the Fourier representation of the collocation scheme and the Galerkin scheme which has been shown to be stable [111]; this idea has also appeared in [1, 2]. It is straightforward to calculate the Fourier symbol of the nonlocal diffusion model while the Fourier symbol of the peridynamic Navier operator needs more in-depth derivation because it is a matrix. The uniform consistency, which is crucial to show that the scheme is AC, is established using the synchronized convergence of the linear RK approximation [17, 73, 74].

1.2.2 Computational cost

FEM for nonlocal models can be computationally prohibitive because the weak forms of nonlocal models involve a double integral (in one dimension) and it is necessary to use high-order Gauss quadrature rules to reduce the integration error [21]. Another challenge is the calculation of a geometrically costly mesh intersection [122] with the horizon. These are the two main drawbacks of FEM for nonlocal models. Although the FDM or the collocation method require the evaluation of only one integral, it is still computationally expensive particularly for models with singular kernels. In [95], two Gauss quadrature schemes are studied. The first one has a background mesh for integration but the accuracy of this scheme is compromised due to the intersection of the horizon and background mesh. The second scheme places quadrature points inside the horizon but still requires high-order Gauss quadrature rules to obtain monotonic convergence profiles. Therefore, truly meshfree methods are at advantage because it saves computational costs and more importantly, it is straightforward to include "bond breaking" which provides a way to simulate fractures or material failure [113].

To obviate the need to use high-order Gaussian quadrature rules, we introduce,

in this dissertation, the quasi-discrete nonlocal operators which replace the nonlocal integral with a finite summation of symmetric quadrature points in the horizon with carefully designed quadrature weights satisfying polynomial reproducing conditions for a given nonlocal (even singular) kernel. The quadrature weights are calculated using the generalized RK technique [94] and we modify the RK approach so that the weights are positive. Moreover, it is also more practical to fix the ratio between horizon δ and the grid size $h_{\max}$ because this leads to banded linear systems amenable to traditional preconditioning techniques. Therefore, we provide convergence analysis of the RK collocation scheme on the quasi-discrete nonlocal diffusion model and peridynamic Navier equation to their local equivalents when the ratio $(\delta/h_{\max})$ is fixed and both δ and $h_{\max}$ go to zero.

1.2.3 RK approximation

RK approximations introduced by [77] uses integral transformation with corrected kernel functions, are meshfree methods that construct shape functions from scattered data. Shape functions with arbitrary order of completeness, which are determined by the reproducing conditions, are easy to construct. The reproducing kernel particle methods (RKPM) [20, 77] are meshfree methods based on RK approximations. RKPM has attracted attention from researchers who use this method to solve PDEs in the Galerkin framework, and has been effectively applied to problems, such as, large deformations [18, 19, 63], fracture modeling [5, 6], reservoir engineering [55, 117, 121], and more. The application of RK approximations to peridynamics problems can mitigate shortcomings of the standard meshfree peridynamics discretization [7]. Numerous numerical experiments have been conducted in [95] and super-convergence has been observed.

The conventional error estimates of RKPM in [51, 78] yield same order of con-

vergence as in classical FEM. Many numerical experiments (see e.g. [73, 95]), however, show that these error estimates are rather conservative and super-convergence rates have been observed for even order RKPM. A synchronized convergence phenomenon is introduced in [73] and its applications are exploited in [50, 74, 76, 75]. Their interest is to achieve the same order of convergence rate in high-order error norms as in L^2 error norm in the interior of the domain. To achieve the synchronized convergence, a crucial requirement is that the correction function has to be a constant in the interior of the domain. This condition, to the knowledge of the author, is rather restrictive and it is shown in the literature to be possible only when the interpolation order p is one.

In this dissertation, we show that the convergence rate under all Sobolev norms can be improved for all even order RK approximations over the entire domain of interest. We start with the continuous RK approximation and this helps us understand the origin of the super-convergence phenomenon. It is vital to investigate the approximation error contribution from the boundary and interior regions separately. Then we show the discrete RK approximation is super-convergent only for uniform particle distribution, and special choices of RK window function and support sizes. For general RK support sizes, error estimates do not anticipate super-convergence but numerical experiments have observed higher convergence rates; this is explained using the concept of pseudo super convergence.

1.3 Overview

1.3.1 Objectives

This dissertation is motivated by the numerical solution of the peridynamics-based hydraulic fracturing model which couples the nonlocal diffusion and nonlocal

poro-elasticity models. Because the mathematical analysis of the coupled system is still under development, instead of studying the coupled system, we study the decoupled equations, namely, nonlocal diffusion and peridynamic Navier equation. The major objective is to develop a mathematically rigorous numerical discretization for the nonlocal models. Four steps are followed to achieve the main goal:

1. Explain the super-convergence behaviour of the RK approximation.
2. Develop an AC RK collocation method for nonlocal diffusion.
3. Propose a practical RK collocation method for nonlocal diffusion.
4. Extend the RK collocation method to peridynamic Navier equation.

1.3.2 Outline

This dissertation is organized as follows.

Chapter 2 shows that the convergence rates under all Sobolev norms can be improved for all even order RK approximations over the entire domain of interest, for uniform particle distribution and carefully designated RK support sizes. We also introduce the concept of pseudo super convergence to explain the numerically observed super convergence for general RK support sizes.

Based on the findings of Chapter 2, we choose special RK support size and use the resulting RK approximation to collocate on the nonlocal models. In Chapter 3, we provide the convergence analysis of the RK collocation method for nonlocal diffusion models. Numerical examples are conducted to complement the theoretical results.

Chapter 4 introduces a quasi-discrete nonlocal diffusion operator which replaces the integral with a finite summation of quadrature points inside the horizon.

Solution of the RK collocation on the quasi-discrete nonlocal diffusion converges to the correct local limit.

In Chapter 5, we extend the RK collocation framework developed in Chapters 3 and 4 to the peridynamic Navier equation. In addition, we show the matrices derived from the RK collocation method pass the inf-sup test.

Finally we conclude this dissertation in Chapter 6.

Chapter 2

Super-convergence of RK approximation

In this chapter[1], we provide a theoretical analysis of super-convergence in Sobolev norms for RK approximations when the interpolation order p is even. Super-convergence phenomenon means the convergence rate is higher than the order that is generally expected. We distinguish the continuous RK approximation and the discrete RK approximation. While the continuous RK approximations are proven to be super-convergent when p is even, its discrete counterpart has super-convergence only with uniform particle distribution and special choices of RK window functions and support sizes. Moreover, super-convergence does not exist for the discrete RK approximation with general RK support sizes. The concept of pseudo super convergence is then introduced to explain why in practice the super-convergence phenomenon is sometimes observed for general cases although the theory does not anticipate it. Our analysis is general, for multi-dimensional RK approximations.

This chapter is organized as follows. Section 2.1 introduces the continuous and discrete RK approximations. Super-convergence for continuous RK approximation is shown in section 2.2 and this lays the foundation for the analysis of super-convergence for RK approximations. In section 2.3, super-convergence for discrete RK approximation with selected RK support sizes is presented. To better demonstrate the analysis, we work on one dimension in sections 2.1 to 2.3. The multi-dimensional extension

[1]This chapter is an adaption of [70]. The author's contribution includes theoretical derivation and conducting numerical experiments.

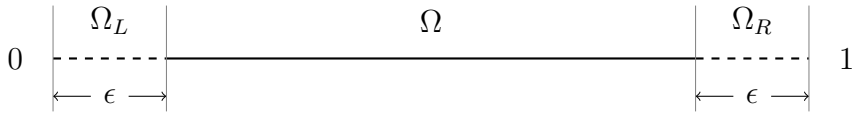

Figure 2.1: Domain decomposition in 1d. $\overline{\overline{\Omega}} = \Omega_{bl} \cup \Omega$ and $\Omega_{bl} = \Omega_L \cup \Omega_R$

is then natural and is presented in section 2.4. Numerical experiments that verify the super-convergence of discrete RK approximation are presented in section 2.5. Then the discussion of discrete RK approximation with arbitrary RK support size is presented in section 2.6, where the concept of pseudo super convergence is introduced.

2.1 RK approximation

The continuous RK approximation of functions uses integral transformation with corrected kernel functions. In practice, integrals are replaced by finite summations, which leads to discrete RK approximations. The corrected kernel functions are determined by the reproducing conditions. Therefore RK approximations exactly reproduce polynomials. We review the notations of the continuous and discrete RK approximation in subsection 2.1.1 and subsection 2.1.2 respectively.

In this section and the following two sections, we work on the 1d domain $\overline{\overline{\Omega}} \subset \mathbb{R}$. The generalization to multi-dimension is natural and is discussed in section 2.4. In Figure 2.1, the domain of interest is given by $\overline{\overline{\Omega}} = (0, 1)$ and the interior of the domain is defined by $\Omega = (\epsilon, 1 - \epsilon)$, where ϵ is a parameter in the RK approximation that will be introduced shortly. Notice that the boundary of the domain $\overline{\overline{\Omega}}$ (denoted by $\Omega_{bl} = \overline{\overline{\Omega}} \backslash \Omega$) is not the usual codimension one boundary, but rather a boundary layer of width ϵ inside $\overline{\overline{\Omega}}$. The main idea of the error analysis in the following sections is to investigate the approximation errors separately on the interior Ω and on the boundary layer Ω_{bl}.

2.1.1 Continuous RK approximation

For a small number $\epsilon > 0$, $u_\epsilon(x)$ is the RK approximation of a given function $u(x)$ on $\overline{\overline{\Omega}}$ defined by

$$u_\epsilon(x) = \int_{\overline{\overline{\Omega}}} \widetilde{\Psi}_\epsilon(x; x-y) u(y) dy \,, \tag{2.1}$$

where $\widetilde{\Psi}_\epsilon(x; x-y)$ is the modified kernel function given by

$$\widetilde{\Psi}_\epsilon(x; x-y) = C(x; x-y)\phi_\epsilon(x-y) \,. \tag{2.2}$$

$C(x; x-y)$ is the correction function obtained by imposing the reproducing conditions such that the RK approximation exactly reproduces polynomials. $\phi_\epsilon(x-y)$ is the kernel function given by

$$\phi_\epsilon(x) = \frac{1}{\epsilon}\phi\left(\frac{x}{\epsilon}\right), \tag{2.3}$$

where $\phi(x)$ is a symmetric non-negative function supported on $[-1, 1]$, which we call the *window function*. Notice that we do not require the integral of the kernel function ϕ to be 1 since any scaling factor can be absorbed into the correction function. Now for p being a non-negative integer, the correction function $C(x; x-y)$ is given by

$$C(x; x-y) = \boldsymbol{H}_p^T(x-y)\boldsymbol{b}_p(x), \tag{2.4}$$

where $\boldsymbol{H}_p^T(x-y)$ is a row vector consisting of monomial basis functions of degree p:

$$\boldsymbol{H}_p^T(x-y) = [1, x-y, (x-y)^2, \cdots, (x-y)^p] \,.$$

$\boldsymbol{b}_p(x)$ is a column vector containing correction function coefficients obtained from the p-th order reproducing condition:

$$\int_{\overline{\overline{\Omega}}} \widetilde{\Psi}_\epsilon(x; x-y) y^\alpha dy = x^\alpha, \quad \alpha = 0, 1, \ldots, p, \tag{2.5}$$

which is equivalent to

$$\int_{\overline{\overline{\Omega}}} \widetilde{\Psi}_\epsilon(x; x-y) \boldsymbol{H}_p(x-y) dy = \boldsymbol{H}_p(0). \tag{2.6}$$

Substitute eqs. (2.2) and (2.4) into eq. (2.6) we obtain

$$\widetilde{\boldsymbol{M}}_p(x)\boldsymbol{b}_p(x) = \boldsymbol{H}_p(0), \tag{2.7}$$

where

$$\widetilde{\boldsymbol{M}}_p(x) = \int_{\overline{\overline{\Omega}}} \boldsymbol{H}_p(x-y)\phi_\epsilon(x-y)\boldsymbol{H}_p^T(x-y)dy, \tag{2.8}$$

is a $(p+1)\times(p+1)$ matrix and is called the moment matrix. Denote $\widetilde{\boldsymbol{M}}(x) = (\widetilde{M}_{ij}(x))_{i,j=0}^{p}$, then each entry $\widetilde{M}_{ij}$ is the $(i+j)$-th moment of ϕ_ϵ given by

$$\widetilde{M}_{ij}(x) = \widetilde{m}_{i+j}(x) := \int_{\overline{\overline{\Omega}}} (x-y)^{i+j}\phi_\epsilon(x-y)dy, \quad 0 \le i,j \le p. \tag{2.9}$$

$\boldsymbol{b}_p(x)$ is then obtained by solving the system of eq. (2.7):

$$\boldsymbol{b}_p(x) = \widetilde{\boldsymbol{M}}_p^{-1}(x)\boldsymbol{H}_p(0). \tag{2.10}$$

By combining eqs. (2.2), (2.4), and (2.10), we obtain the modified kernel function

$$\widetilde{\Psi}_\epsilon(x; x-y) = \boldsymbol{H}_p^T(x-y)\widetilde{\boldsymbol{M}}_p^{-1}(x)\boldsymbol{H}_p(0)\phi_\epsilon(x-y). \tag{2.11}$$

2.1.2 Discrete RK approximation

For practical computations, integrals are replaced by summations. Suppose the domain $\overline{\overline{\Omega}}$ is discretized into a total number of I nodes $\{x_k\}_{k=1}^I$, the discrete RK approximation is then a numerical approximation of eq. (2.1):

$$u(x) \approx u^I(x) = \sum_{k=1}^{I} \Psi_k(x)u(x_k)\,, \tag{2.12}$$

where the modified kernel function $\Psi_k(x)$ is defined by

$$\Psi_k(x) = C(x, x-x_k)\phi_\epsilon(x-x_k)\,. \tag{2.13}$$

$\Psi_k(x)$ is also referred to as the *RK shape function* in the literature. Notice that eq. (2.12) does not contain any quadrature weights because they can be absorbed

into the shape function. The p-th order reproducing condition is then replaced by the discrete reproducing condition:

$$\sum_{k=1}^{I} \Psi_k(x) x_k^{\alpha} = x^{\alpha}, \quad \alpha = 0, 1, \ldots, p. \tag{2.14}$$

which is equivalent to

$$\sum_{k=1}^{I} \Psi_k(x) \boldsymbol{H}_p(x - x_k) = \boldsymbol{H}_p(0). \tag{2.15}$$

Substitute eqs. (2.4) and (2.13) into 2.15 we obtain

$$\boldsymbol{M}_p(x) \boldsymbol{b}_p(x) = \boldsymbol{H}_p(0),$$

where $\boldsymbol{M}_p = (M_{ij})_{i,j=0}^{p}$ is the discrete moment matrix given by

$$\boldsymbol{M}_p(x) = \sum_{k=1}^{I} \boldsymbol{H}_p(x - x_k) \phi_\epsilon(x - x_k) \boldsymbol{H}_p^T(x - x_k)\,. \tag{2.16}$$

Each entry $M_{ij}(x)$ is the $(i + j)$-th discrete moment:

$$M_{ij}(x) = m_{i+j}(x) := \sum_{k=1}^{I} (x - x_k)^{i+j} \phi_\epsilon(x - x_k), \quad 0 \le i, j \le p\,. \tag{2.17}$$

Similar to eq. (2.10), we now have

$$\boldsymbol{b}_p(x) = (\boldsymbol{M}_p)^{-1}(x) \boldsymbol{H}_p(0). \tag{2.18}$$

By substituting eqs. (2.4) and (2.18) into eq. (2.13), the RK shape function is obtained as

$$\Psi_k(x) = \boldsymbol{H}_p^T(x - x_k)(\boldsymbol{M}_p)^{-1}(x) \boldsymbol{H}_p(0) \phi_\epsilon(x - x_k), \ k = 1, \cdots, I\,. \tag{2.19}$$

We call $u^I(x)$ the RK interpolant of $u(x)$. Note that $u^I(x_k)$ does not usually not agree with $u(x_k)$, so $u^I(x)$ is viewed as an interpolant of $u(x)$ in a generalized sense.

2.2 Super-convergence for continuous RK approximation

The error estimates for the RK approximation are done using Taylor expansion (see [51, 78]). We first give a brief review of them for completeness. Notice that we focus on the continuous RK approximation in this section. To give estimates in Sobolev space, we need the so called averaged Taylor polynomial, since derivatives may not exist in the point-wise sense. As in [51], we use the notation $W^{p,q}$ for Sobolev space, where p is the order of derivative and q denotes the L^q norm.

Now suppose that the whole domain $\overline{\overline{\Omega}}$ has a finite cover $\cup_{j=1}^{N(\epsilon)} B_j$, where each set B_j is a ball of diameter ϵ and each point $x \in \overline{\overline{\Omega}}$ is covered by at most a fixed number of sets in $\{B_j\}_{j=1}^{N(\epsilon)}$. Define

$$\hat{B}_j = \{x : \mathrm{dist}(x, B_j) < \epsilon\},$$

then $\cup_{j=1}^{N(\epsilon)} \hat{B}_j$ is again a covering of $\overline{\overline{\Omega}}$. Assume that each point $x \in \overline{\overline{\Omega}}$ is covered by at most K_0 sets in $\{\hat{B}_j\}_{j=1}^{N(\epsilon)}$, where K_0 is a constant independent of ϵ. This can be satisfied, for instance, by choosing $\{B_j\}_{j=1}^{N(\epsilon)}$ to be a collection of uniformly distributed balls over the domain $\overline{\overline{\Omega}}$. Note that the finite cover is not the discretization of the domain $\overline{\overline{\Omega}}$. The error estimation is done locally on each set $B_j \cap \overline{\overline{\Omega}}$. Let $Q_j^p u(x)$ be the Taylor polynomial of degree p of u averaged over B_j (see [13, 41]), and denote the remainder

$$R_j^p u(x) = u(x) - Q_j^p u(x), \quad \forall x \in B_j \cap \overline{\overline{\Omega}}.$$

Then from the results of [13, Section 4.3], we have the following estimates

$$\|R_j^p u\|_{L^\infty(\hat{B}_j \cap \overline{\overline{\Omega}})} \leq C\epsilon^{p+1-1/q} \|u\|_{W^{p+1,q}(\hat{B}_j \cap \overline{\overline{\Omega}})}, \quad \text{and} \tag{2.20}$$

$$\|R_j^p u\|_{W^{l,q}(\hat{B}_j \cap \overline{\overline{\Omega}})} \leq C\epsilon^{p+1-l} \|u\|_{W^{p+1,q}(\hat{B}_j \cap \overline{\overline{\Omega}})} \quad \text{for } l = 0, 1, \cdots, p+1, \tag{2.21}$$

where C only depends on p and q. Notice that in multi-dimension, the power on ϵ in eq. (2.20) becomes $p + 1 - \mathrm{d}/q$, where d is the dimension, and that eq. (2.21) is a

constructive form of the Bramble-Hilbert lemma. Now for $x \in B_j \cap \overline{\overline{\Omega}}$, we can write by applying eq. (2.1) that

$$\begin{aligned} u(x) - u_\epsilon(x) =& Q_j^p u(x) - \int_{\overline{\overline{\Omega}}} \widetilde{\Psi}_\epsilon(x; x-y) Q_j^p u(y) dy \\ &+ R_j^p u(x) - \int_{\overline{\overline{\Omega}}} \widetilde{\Psi}_\epsilon(x; x-y) R_j^p u(y) dy \,. \end{aligned}$$

Since $Q_j^p u(x)$ is a polynomial of degree p, we have by the reproducing condition eq. (2.5) that

$$Q_j^p u(x) = \int_{\overline{\overline{\Omega}}} \widetilde{\Psi}_\epsilon(x; x-y) Q_j^p u(y) dy \,, \quad \forall x \in B_j \cap \overline{\overline{\Omega}}. \tag{2.22}$$

Thus

$$u(x) - u_\epsilon(x) = R_j^p u(x) - \int_{\overline{\overline{\Omega}}} \widetilde{\Psi}_\epsilon(x; x-y) R_j^p u(y) dy \,,$$

for $x \in B_j \cap \overline{\overline{\Omega}}$ and then

$$\begin{aligned} \|u - u_\epsilon\|_{W^{l,q}(B_j \cap \overline{\overline{\Omega}})} \leq & \|R_j^p u\|_{W^{l,q}(B_j \cap \overline{\overline{\Omega}})} \\ &+ \|R_j^p u\|_{L^\infty(\hat{B}_j \cap \overline{\overline{\Omega}})} \sum_{k=0}^{l} \| \int_{\overline{\overline{\Omega}}} \left| D_x^k \widetilde{\Psi}_\epsilon(x; x-y) \right| dy \|_{L^q(B_j \cap \overline{\overline{\Omega}})} \,, \end{aligned} \tag{2.23}$$

where D_x^k stands for the k-th derivative with respect to x. Notice that the support of $\widetilde{\Psi}_\epsilon(x; x-y)$ is $y \in B_\epsilon(x)$ and by the calculations of [78, Lemma 2.1], one has

$$D_x^k C(x; x-y) = O(\epsilon^{-k}), \quad \text{for } y \in B_\epsilon(x) \,,$$

if the window function ϕ is k-th continuously differentiable. So we can obtain by eq. (2.2) that

$$D_x^k \widetilde{\Psi}_\epsilon(x; x-y) = O(\epsilon^{-k-1}), \quad \text{for } y \in B_\epsilon(x) \,. \tag{2.24}$$

Now substitute eqs. (2.20), (2.21), and (2.24) into eq. (2.23), we obtain

$$\|u - u_\epsilon\|_{W^{l,q}(B_j \cap \overline{\overline{\Omega}})} \leq C \epsilon^{p+1-l} \|u\|_{W^{p+1,q}(\hat{B}_j \cap \overline{\overline{\Omega}})} \,, \tag{2.25}$$

for all $l = 0, 1, \cdots, p+1$. Therefore we conclude that

$$\begin{aligned}\|u-u_\epsilon\|_{W^{l,q}(\overline{\overline{\Omega}})} &\leq \sum_{j=1}^{N(\epsilon)} \|u-u_\epsilon\|_{W^{l,q}(B_j\cap\overline{\overline{\Omega}})} \leq C\epsilon^{p+1-l}\sum_{j=1}^{N(\epsilon)}\|u\|_{W^{p+1,q}(\hat{B}_j\cap\overline{\overline{\Omega}})} \\ &\leq \tilde{C}\epsilon^{p+1-l}\|u\|_{W^{p+1,q}(\overline{\overline{\Omega}})}\,, \quad l=0,1,\cdots p+1\,,\end{aligned} \tag{2.26}$$

where $\tilde{C}=CK_0$, and the last step in eq. (2.26) is by the fact that $x\in\overline{\overline{\Omega}}$ is covered by at most K_0 sets in $\{\hat{B}_j\}_{j=1}^{N(\epsilon)}$.

The previous lines of arguments and the final estimate eq. (2.26) share the same idea with [51, 78], although details may differ. Equation (2.26) tells us that the RK approximation of p-th order can achieve at most $(p+1)$-th order convergence in L^2 norm provided that the function u is in the Sobolev space $W^{p+1,2}$. However, many numerical experiments (see [73, 95]) have shown that super-convergence exists for even order RK approximation (p is an even number).

In the following, we provide careful error analysis that explains the super-convergence phenomena for p being an even number. The basic idea is to investigate the errors in the interior and at the boundary of the domain separately. We show that a p-th order RK approximation can actually achieve $(p+1)$-th reproducing condition in the interior of the domain provided p is an even number. This fact is the key to obtain the super-convergence result as we have seen that eq. (2.22) relies totally on the reproducing condition. We begin with a lemma that characterizes the moment function $\widetilde{m}_\alpha(x)$ in the interior of the domain.

Lemma 2.2.1. *For $x\in\Omega$, the moment $\widetilde{m}_\alpha(x)=0$ if α is an odd number.*

Proof. Recall that $\widetilde{m}_\alpha(x)$ is defined by eq. (2.9). First notice that for $x\in\Omega$, we have $B_\epsilon(x)$ fully contained in $\overline{\overline{\Omega}}$. Since kernel function $\phi_\epsilon(z)$ is symmetric, it implies that for any $x\in\Omega$, $\widetilde{m}_\alpha(x)$ is zero when α is an odd number. □

Lemma 2.2.1 is simple enough by observation, but it leads to the following crucial property for the correction coefficients vector.

Lemma 2.2.2. *Let* $\boldsymbol{b}_p(x) = \widetilde{\boldsymbol{M}}_p^{-1}(x)\boldsymbol{H}_p(0)$ *and let* $b_p^{(i)}$ $(0 \le i \le p)$ *be the components of* $\boldsymbol{b}_p$. *In the interior of the domain* $(x \in \Omega)$, *we have*

(a) $b_p^{(i)}(x) = 0$ *for* i *being an odd number, and*

(b) $b_p^{(i)}(x) = b_{p+1}^{(i)}(x)$ *for* $p = 2k$, *where* $k \in \mathbb{N}$.

Proof. We are going to show (a) first. Here we always assume that $x \in \Omega$ and we drop the x-dependence of the vectors for convenience. The proof of (a) contains two cases where p is even or odd. For p being an even number, we assume that $p = 2k$, where $k \in \mathbb{N}$. Since all the odd order moments vanish by Lemma 2.2.1, eq. (2.7) becomes

$$\begin{bmatrix} \widetilde{m}_0 & 0 & \cdots & \widetilde{m}_{2k} \\ 0 & \widetilde{m}_2 & \cdots & 0 \\ \vdots & \vdots & \ddots & \vdots \\ \widetilde{m}_{2k} & 0 & \cdots & \widetilde{m}_{4k} \end{bmatrix} \begin{bmatrix} b_{2k}^{(0)} \\ b_{2k}^{(1)} \\ \vdots \\ b_{2k}^{(2k)} \end{bmatrix} = \begin{bmatrix} 1 \\ 0 \\ \vdots \\ 0 \end{bmatrix}, \tag{2.27}$$

which can be written into two independent systems based on even and odd rows of $\boldsymbol{b}_{2k}$:

$$\begin{bmatrix} \widetilde{m}_0 & \widetilde{m}_2 & \cdots & \widetilde{m}_{2k} \\ \widetilde{m}_2 & \widetilde{m}_4 & \cdots & \widetilde{m}_{2k+2} \\ \vdots & \vdots & \ddots & \vdots \\ \widetilde{m}_{2k} & \widetilde{m}_{2k+2} & \cdots & \widetilde{m}_{4k} \end{bmatrix} \begin{bmatrix} b_{2k}^{(0)} \\ b_{2k}^{(2)} \\ \vdots \\ b_{2k}^{(2k)} \end{bmatrix} = \begin{bmatrix} 1 \\ 0 \\ \vdots \\ 0 \end{bmatrix}, \tag{2.28}$$

and

$$\begin{bmatrix} \widetilde{m}_2 & \widetilde{m}_4 & \cdots & \widetilde{m}_{2k} \\ \widetilde{m}_4 & \widetilde{m}_6 & \cdots & \widetilde{m}_{2k+2} \\ \vdots & \vdots & \ddots & \vdots \\ \widetilde{m}_{2k} & \widetilde{m}_{2k+2} & \cdots & \widetilde{m}_{4k-2} \end{bmatrix} \begin{bmatrix} b_{2k}^{(1)} \\ b_{2k}^{(3)} \\ \vdots \\ b_{2k}^{(2k-1)} \end{bmatrix} = \begin{bmatrix} 0 \\ 0 \\ \vdots \\ 0 \end{bmatrix}. \tag{2.29}$$

As shown in [78], since the moment matrix is a Gram matrix which is invertible, it is apparent that the matrices in the two linear systems eqs. (2.28) and (2.29) are also invertible. So the solution to eq. (2.29) is $\mathbf{0}$, i.e. $b_{2k}^{(i)}(x) = 0$ for i being an odd number.

For the second case where $p = 2k+1, k \in \mathbb{N}$, follow the same procedure as before we have

$$\begin{bmatrix} \widetilde{m}_0 & 0 & \cdots & \widetilde{m}_{2k} & 0 \\ 0 & \widetilde{m}_2 & \cdots & 0 & \widetilde{m}_{2k+2} \\ \vdots & \vdots & \ddots & \vdots & \vdots \\ \widetilde{m}_{2k} & 0 & \cdots & \widetilde{m}_{4k} & 0 \\ 0 & \widetilde{m}_{2k+2} & \cdots & 0 & \widetilde{m}_{4k+2} \end{bmatrix} \begin{bmatrix} b_{2k+1}^{(0)} \\ b_{2k+1}^{(1)} \\ \vdots \\ b_{2k+1}^{(2k)} \\ b_{2k+1}^{(2k+1)} \end{bmatrix} = \begin{bmatrix} 1 \\ 0 \\ \vdots \\ 0 \\ 0 \end{bmatrix}. \tag{2.30}$$

Rewrite eq. (2.30) into the two independent systems

$$\begin{bmatrix} \widetilde{m}_0 & \widetilde{m}_2 & \cdots & \widetilde{m}_{2k} \\ \widetilde{m}_2 & \widetilde{m}_4 & \cdots & \widetilde{m}_{2k+2} \\ \vdots & \vdots & \ddots & \vdots \\ \widetilde{m}_{2k} & \widetilde{m}_{2k+2} & \cdots & \widetilde{m}_{4k} \end{bmatrix} \begin{bmatrix} b_{2k+1}^{(0)} \\ b_2^{2k+1} \\ \vdots \\ b_{2k+1}^{(2k)} \end{bmatrix} = \begin{bmatrix} 1 \\ 0 \\ \vdots \\ 0 \end{bmatrix}, \tag{2.31}$$

and

$$\begin{bmatrix} \widetilde{m}_2 & \widetilde{m}_4 & \cdots & \widetilde{m}_{2k+2} \\ \widetilde{m}_4 & \widetilde{m}_6 & \cdots & \widetilde{m}_{2k+4} \\ \vdots & \vdots & \ddots & \vdots \\ \widetilde{m}_{2k} & \widetilde{m}_{2k+2} & \cdots & \widetilde{m}_{4k} \\ \widetilde{m}_{2k+2} & \widetilde{m}_{2k+4} & \cdots & \widetilde{m}_{4k+2} \end{bmatrix} \begin{bmatrix} b_{2k+1}^{(1)} \\ b_{2k+1}^{(3)} \\ \vdots \\ b_{2k+1}^{(2k-1)} \\ b_{2k+1}^{(2k+1)} \end{bmatrix} = \begin{bmatrix} 0 \\ 0 \\ \vdots \\ 0 \\ 0 \end{bmatrix}. \tag{2.32}$$

Equation (2.32) has only the trivial solution, i.e., $b_{2k+1}^{(i)} = 0$ for i being an odd number. Combine the two cases, (a) is shown.

Now observe that the coefficient matrices in eqs. (2.28) and (2.31) are exactly the same, therefore their solutions are identical, i.e., $b_{2k+1}^{(i)} = b_{2k}^{(i)}$, for $i = 2n, n \in \mathbb{N}$. This completes the proof of (b).

□

By the result of Lemma 2.2.2, we can identify the modified kernel function $\widetilde{\Psi}_\epsilon$ of an even order to that of an odd order. For convenience we denote $\widetilde{\Psi}_\epsilon(p, x; x-y)$ to be the modified kernel function with respect to the RK approximation of p-th order, then we have the following result.

Lemma 2.2.3. *If p is even, then the modified kernel functions of p-th and $(p+1)$-th order are identical in the interior of the domain, that is*

$$\widetilde{\Psi}_\epsilon(p, x; x-y) = \widetilde{\Psi}_\epsilon(p+1, x; x-y), \quad x \in \Omega.$$

Proof. If p is even, use Lemma 2.2.2, we have for $x \in \Omega$ that

$$\boldsymbol{b}_{p+1}^T(x) = [\boldsymbol{b}_p^T(x), \ \ 0].$$

Then by eqs. (2.2) and (2.4) we have obviously that $\widetilde{\Psi}_\epsilon(p, x; x-y)$ and $\widetilde{\Psi}_\epsilon(p+1, x; x-y)$ are identical. □

Lemma 2.2.3 essentially says that for even number p, the p-th order RK approximation can achieve $(p+1)$-th reproducing condition in the interior of the domain, which is crucial in proving super-convergence. When showing the final theorem, we need functions to be approximated free from pathological behavior in the boundary layer. More specially, we want that the Sobolev norm of a function u has uniform density in the boundary layer and in the interior of the domain. We thus give the following definition.

Definition 2.2.4. *Suppose that $\overline{\overline{\Omega}} \subset \mathbb{R}^{\mathrm{d}}$, and $\Omega_{bl} = \{x \in \overline{\overline{\Omega}} : dist(x, \partial\Omega) < \epsilon\}$. We say that a function $u \in W^{p,q}(\overline{\overline{\Omega}})$ is proper if*

$$\|u\|_{W^{p,q}(\Omega_{bl})} \leq C\epsilon^{\mathrm{d}/q}\|u\|_{W^{p,q}(\overline{\overline{\Omega}})}. \tag{2.33}$$

One can easily check that if $u \in W^{p,q}(\overline{\overline{\Omega}}) \cap C^p(\overline{\overline{\Omega}})$, then eq. (2.33) is satisfied.

We now go back to the 1d case and show the convergence theorem for the continuous RK approximation.

Theorem 2.2.5. *Assume that the window function $\phi \in C^{p+2}$, and $u \in W^{p+2,q}(\overline{\overline{\Omega}})$ is proper. Then the error estimate for the continuous RK approximation is as follows: if p is odd,*

$$\|u - u_\epsilon\|_{W^{l,q}(\overline{\overline{\Omega}})} \leq C\epsilon^{p+1-l}\|u\|_{W^{p+1,q}(\overline{\overline{\Omega}})}\,,$$

and if p is even,

$$\|u - u_\epsilon\|_{W^{l,q}(\overline{\overline{\Omega}})} \leq C\epsilon^{p+1+1/q-l}\|u\|_{W^{p+2,q}(\overline{\overline{\Omega}})}\,,$$

for $l = 0, 1, \cdots p+1$.

Proof. If p is an odd number, the error estimate is the same one as eq. (2.26) shows. Now assume that p is even, then we divide the domain $\overline{\overline{\Omega}}$ into two parts, as shown in Figure 2.1, and investigate approximation errors on them separately.

For $x \in \Omega$, by Lemma 2.2.3 and eq. (2.5), we have

$$\int_{\overline{\overline{\Omega}}} \widetilde{\Psi}_\epsilon(p, x; x-y) y^\alpha dy = x^\alpha, \quad \alpha = 0, 1, \ldots, p+1\,. \tag{2.34}$$

So we can write

$$\begin{aligned} u(x) - u_\epsilon(x) =& Q_j^{p+1}u(x) - \int_{\overline{\overline{\Omega}}} \widetilde{\Psi}_\epsilon(p, x; x-y) Q_j^{p+1}u(y)dy \\ &+ R_j^{p+1}u(x) - \int_{\overline{\overline{\Omega}}} \widetilde{\Psi}_\epsilon(p, x; x-y) R_j^{p+1}u(y)dy\,, \end{aligned}$$

where $Q_j^{p+1}u$ is the Taylor polynomial of degree $p+1$ of u averaged over B_j, and $R_j^{p+1}u$ is the remainder. By eq. (2.34), we have

$$Q_j^{p+1}u(x) = \int_{\overline{\overline{\Omega}}} \widetilde{\Psi}_\epsilon(p, x; x-y) Q_j^{p+1}u(y)dy, \quad x \in \Omega\,.$$

So one can follow the previous arguments to show that

$$\|u - u_\epsilon\|_{W^{l,q}(B_j \cap \Omega)} \leq C\epsilon^{p+2-l} \|u\|_{W^{p+2,q}(\hat{B}_j \cap \Omega)} ,$$

for $l = 0, 1, \cdots, p+2$. Now combine with fact that

$$\|u - u_\epsilon\|_{W^{l,q}(B_j \cap \Omega_{bl})} \leq C\epsilon^{p+1-l} \|u\|_{W^{p+1,q}(\hat{B}_j \cap \Omega_{bl})} ,$$

for $l = 0, 1, \cdots, p+1$, we have finally

$$\begin{aligned}
\|u(x) - u_\epsilon(x)\|_{W^{l,q}(\overline{\overline{\Omega}})} &\leq \sum_{j: B_j \cap \Omega \neq \emptyset} \|u - u_\epsilon\|_{W^{l,q}(\hat{B}_j \cap \Omega)} + \sum_{j: B_j \cap \Omega_{bl} \neq \emptyset} \|u - u_\epsilon\|_{W^{l,q}(B_j \cap \Omega)} , \\
&\leq C\epsilon^{p+2-l} \|u\|_{W^{p+2,q}(\Omega)} + C\epsilon^{p+1-l} \|u\|_{W^{p+1,q}(\Omega_{bl})} , \\
&\leq C\epsilon^{p+2-l} \|u\|_{W^{p+2,q}(\Omega)} + C\epsilon^{p+1+1/q-l} \|u\|_{W^{p+1,q}(\overline{\overline{\Omega}})} , \\
&\leq C\epsilon^{p+1+1/q-l} \|u\|_{W^{p+2,q}(\overline{\overline{\Omega}})} .
\end{aligned}$$

□

2.3 Discrete RK approximation error estimates for selected RK support sizes

In this section we investigate the super-convergence of the discrete RK approximation. The continuous RK approximation discussed in section 2.2 is rarely used in practice, though it gives us insights on how to obtain super-convergence in the discrete RK approximation. In the previous section we have established a clear understanding of the origin of the super-convergence. Intuitively, we can expect super-convergence to happen for even order discrete RK approximation if the discrete moment m_α vanishes for α being an odd number. However, this condition is hard to satisfy if particles are not uniformly distributed. Therefore in this section, we only consider the uniform discretization of the domain $\overline{\overline{\Omega}}$. We assume that $\{x_k\}_{k=1}^I$ is uniformly distributed with

$h = x_k - x_{k-1}$ being the spacing. By construction, the p-th order discrete RK approximation also satisfies p-th order reproducing condition, then similar to the continuous case, the L^2 approximation error is at least $O(\epsilon^{p+1})$ for the p-th order discrete RK approximation. We do not repeat the arguments here since they are almost identical to the continuous case. The super-convergence, however, is different.

Unlike the continuous moment, if α is odd, the discrete moment $m_\alpha(x)$ is not always zero for $x \in \Omega$. However, we show in the following that this can be made true with carefully selected window functions and RK support sizes. To achieve this, we need to utilize the Strang-Fix condition discussed in [62] to characterize the kernel functions. We recall that a function $f(x)$ is said to satisfy the k-th order Strang-Fix condition, if the following two conditions are satisfied:

$$\widehat{f}(0) = 1, \text{ and} \tag{2.35}$$

$$D_\xi^\alpha \widehat{f}(\xi)\Big|_{2\pi j} = 0, \quad \forall j \in \mathbb{Z}\backslash\{0\},\ \alpha \le k\,. \tag{2.36}$$

Here $\widehat{f}(\xi)$ is the Fourier transform of $f(x)$ defined as

$$\widehat{f}(\xi) = \int_{-\infty}^{\infty} f(x) e^{-i\xi x} dx\,,$$

and $D_\xi^\alpha \widehat{f}$ is the α-th derivative of $\widehat{f}$. Since the scaling factor can always be absorbed into the correction function, the condition eq. (2.35) can actually be dropped because it is a normalization of the function f. In addition, we use a more generalized version of eq. (2.36):

$$D_\xi^\alpha \widehat{f}(\xi)\Big|_{\frac{2\pi j}{h}} = 0, \quad \forall j \in \mathbb{Z}\backslash\{0\}\,,$$

where h is the mesh spacing. So following the notation in [77], we define a special class of functions that satisfies the generalized k-th order Strang-Fix condition as

$$\mathcal{SF}_h^{(k)} = \{f : D_\xi^\alpha \widehat{f}(\xi)\Big|_{\frac{2\pi j}{h}} = 0, \quad \forall j \in \mathbb{Z}\backslash\{0\},\ 0 \le \alpha \le k\} \tag{2.37}$$

It turns out that the discrete moment $m_\alpha(x)$ for x in the interior of the domain has an equivalent form as in the following lemma.

Lemma 2.3.1. *Assume that the window function $\phi_\epsilon \in \mathcal{SF}_h^{(k)}$, then the discrete moment $m_\alpha(x)$ defined by eq. (2.17) does not depend on x in the interior of domain and is given by*

$$m_\alpha(x) = \frac{1}{h}\int_{\mathbb{R}} z^\alpha \phi_\epsilon(z)dz\,, \tag{2.38}$$

for $\alpha \le k$ and $x \in \Omega$.

Proof. First we recall Poisson's summation formula (see e.g. [30]):

$$\sum_{j\in\mathbb{Z}} f(x+jh) = \frac{1}{h}\sum_{j\in\mathbb{Z}} \widehat{f}\left(2\pi\frac{j}{h}\right) e^{i2\pi x\frac{j}{h}}\,.$$

Assume that $x_k = kh$ without loss of generality. For $x \in \Omega$, the discrete moment can be written as

$$\begin{aligned} m_\alpha(x) &= \sum_{j=1}^{I}(x-x_j)^\alpha\phi_\epsilon(x-x_j) = \sum_{j\in\mathbb{Z}}(x+jh)^\alpha\phi_\epsilon(x+jh), \\ &= \frac{i^\alpha}{h}\sum_{j\in\mathbb{Z}} D_\xi^\alpha\widehat{\phi_\epsilon}\left(2\pi\frac{j}{h}\right)e^{i2\pi x\frac{j}{h}}, \\ &= \frac{i^\alpha}{h}D_\xi^\alpha\widehat{\phi_\epsilon}(0), \end{aligned} \tag{2.39}$$

where we have used the Poisson's summation formula and the generalized Strang-Fix condition for ϕ_ϵ. Now since

$$D_\xi^\alpha\widehat{\phi_\epsilon}(\xi) = \int_{\mathbb{R}}(-ix)^\alpha\phi_\epsilon(x)e^{-i\xi x}dx\,,$$

we have

$$\frac{i^\alpha}{h}D_\xi^\alpha\widehat{\phi_\epsilon}(0) = \frac{1}{h}\int_{\mathbb{R}} x^\alpha\phi_\epsilon(x)dx\,.$$

□

From eq. (2.38), it is easily seen that the discrete moment $m_\alpha(x)$ vanishes for $x \in \Omega$ if α is an odd number, by the fact that ϕ_ϵ is a symmetric kernel. Then it is straightforward to go through the same process from Lemma 2.2.1 to Lemma 2.2.3. Here we only present a discrete version of Lemma 2.2.3. For convenience we denote $\Psi_k(p,x)(k=1,\cdots,I)$ to be the RK shape function of p-th order.

Lemma 2.3.2. *Assume that the kernel function $\phi_\epsilon \in \mathcal{SF}_h^{(2p_0+1)}$, where p_0 is some non-negative integer, then for all $p \le p_0$ and p being an even number, the RK shape functions of p-th and $(p+1)$-th order are identical in the interior of the domain, namely*

$$\Psi_k(p,x) = \Psi_k(p+1,x), \quad x \in \Omega,\ p \le p_0,\ p \text{ is even}.$$

Proof. This is a result of Lemma 2.3.1. The proof is essentially the same as the arguments in Lemma 2.2.2 and 2.2.3. □

Finally, we assume that the particle distribution is always (ϵ, p)-regular, a notion introduced by [51], so that all the analytical tools in [51] can be used. the theorem for discrete RK approximation error estimates is the following.

Theorem 2.3.3. *Assume that the window function $\phi \in C^{p+2}$, and $u \in W^{p+2,q}(\overline{\overline{\Omega}})$ is proper. Suppose $\phi_\epsilon \in \mathcal{SF}_h^{(2p+1)}$, the error estimate for the discrete RK approximation is as follows:*

if p is odd,

$$\|u - u^I\|_{W^{l,q}(\overline{\overline{\Omega}})} \le C\epsilon^{p+1-l}\|u\|_{W^{p+1,q}(\overline{\overline{\Omega}})},$$

and if p is even,

$$\|u - u^I\|_{W^{l,q}(\overline{\overline{\Omega}})} \le C\epsilon^{p+1+1/q-l}\|u\|_{W^{p+2,q}(\overline{\overline{\Omega}})},$$

for $l = 0, 1, \cdots, p+1$.

Proof. The proof is a discrete adaptation of the previous continuous result, which can also be obtained following the analysis of [51]. The super-convergence for p being even is realized by the application of Lemma 2.3.2. □

2.3.1 B-spline functions as window functions

Theorem 2.3.3 says that in general, we expect the discrete RK approximation of even order to have super-convergence if we select sufficiently smooth window function such that $\phi_\epsilon \in \mathcal{SF}_h^{(2p+1)}$. In practice, the window function $\phi(x)$ is usually chosen to be B-spline functions. The following lemma reveals the good properties of B-spline functions that allow the discrete RK approximation to have super-convergence.

Lemma 2.3.4. *Assume that the window function ϕ is supported on $[-1,1]$ and it is the B-spline of degree $n \geq 2p+1$. Assume also that the RK support size is chosen to be $\epsilon = \frac{n+1}{2} r_0 h$, for r_0 being a positive integer, then $\phi_\epsilon \in \mathcal{SF}_h^{(2p+1)}$, and thus the convergence results in Theorem 2.3.3 are achieved.*

Proof. We introduce a rectangular function

$$\beta^0(x) = \begin{cases} 1, & x \in [-\frac{1}{2}, \frac{1}{2}], \\ 0, & \text{otherwise}, \end{cases}$$

and its Fourier transform is given by

$$\widehat{\beta^0}(\xi) = \frac{\sin(\xi/2)}{\xi/2}.$$

B-spline function of degree n, can be written as the convolution of $n+1$ rectangular functions, see also [98],

$$\beta^n(x) = \beta^0 * \beta^0 * \cdots * \beta^0(x),$$

and thus

$$\widehat{\beta^n}(\xi) = \left[\frac{\sin(\xi/2)}{\xi/2}\right]^{n+1}.$$

Here we normalize the support of the B-spline to $[-1,1]$ to get our window function

$$\phi(x) = \beta^n\left(\frac{n+1}{2}x\right), \tag{2.40}$$

and

$$\phi_\epsilon(x) = \frac{1}{\epsilon}\phi\left(\frac{x}{\epsilon}\right) = \frac{1}{\epsilon}\beta^n\left(\frac{x}{r_0 h}\right),$$

where we have used $\epsilon = \frac{n+1}{2}r_0 h$. Thus we have

$$\widehat{\phi_\epsilon}(\xi) = \frac{r_0 h}{\epsilon}\widehat{\beta^n}\left(r_0 h\xi\right) = \frac{r_0 h}{\epsilon}\left[\frac{\sin(r_0 h\xi/2)}{r_0 h\xi/2}\right]^{n+1}. \tag{2.41}$$

The derivatives of $\widehat{\phi_\epsilon}$ are given by

$$D_\xi^\alpha\widehat{\phi_\epsilon}(\xi) = \frac{r_0 h}{\epsilon}\sum_{k=0}^{\alpha}\binom{\alpha}{k}D_\xi^{\alpha-k}(\sin\left(r_0 h\xi/2\right))^{n+1}D_\xi^k\left(\left(\frac{1}{r_0 h\xi/2}\right)^{n+1}\right).$$

Now since

$$\sin\left(r_0 h\xi/2\right)\Big|_{\xi=\frac{2\pi j}{h}} = 0, \quad j\in\mathbb{Z},$$

and if $\alpha \le n$, $\sin\left(r_0 h\xi/2\right)$ is in every term of $D_\xi^\alpha\widehat{\phi_\epsilon}(\xi)$, we have

$$D_\xi^\alpha\widehat{\phi_\epsilon}(\xi)\Big|_{\xi=2\pi j} = 0, \quad j\in\mathbb{Z}\backslash\{0\},$$

which proves that $\phi_\epsilon \in \mathcal{SF}_h^{(2p+1)}$. □

Lemma 2.3.4 shows that the popular choices of B-spline functions as window functions satisfy the assumptions made in Theorem 2.3.3. Therefore, Lemma 2.3.4 can be used as guidelines on selecting window function and RK support in order to achieve super-convergence. Numerical experiments that verify our theorem are presented in section 2.5.

2.4 Multi-dimensional RK approximation

We have worked with one-dimensional problems previously for better presentation of the work. Our method can actually be easily generalized to multi-dimensional RK approximation. Let $\mathrm{d} > 1$, we consider an open bounded domain $\overline{\overline{\Omega}} \subset \mathbb{R}^{\mathrm{d}}$. The boundary layer of $\overline{\overline{\Omega}}$ is given by

$$\Omega_{bl} = \{\boldsymbol{x} \in \overline{\overline{\Omega}} : \mathrm{dist}(x, \partial\Omega) < \epsilon\}\,.$$

The interior of $\overline{\overline{\Omega}}$ is then the complement of Ω_{bl} in $\overline{\overline{\Omega}}$. A point in $\mathbb{R}^{\mathrm{d}}$ is denoted by $\boldsymbol{x} = (x_1, \ldots, x_{\mathrm{d}})^T$. A multi-index is a collection of d non-negative integers, $\boldsymbol{\alpha} = (\alpha_1, \ldots, \alpha_{\mathrm{d}})$ and its length is expressed as $|\boldsymbol{\alpha}| = \sum_{i=1}^{d} \alpha_i$. For a given $\boldsymbol{\alpha}$, we write $\boldsymbol{x}^{\boldsymbol{\alpha}} = x_1^{\alpha_1} \ldots x_{\mathrm{d}}^{\alpha_{\mathrm{d}}}$.

Now instead of eq. (2.3), the kernel function $\phi_\epsilon(\boldsymbol{x})$ in multi-dimension is defined as

$$\phi_\epsilon(\boldsymbol{x}) = \frac{1}{\epsilon^{\mathrm{d}}}\phi\left(\frac{|\boldsymbol{x}|}{\epsilon}\right), \quad \boldsymbol{x} \in \mathbb{R}^{\mathrm{d}}\,. \tag{2.42}$$

The row vector $\boldsymbol{H}_p^T(\boldsymbol{x}-\boldsymbol{y})$ consists of multivariate monomial basis functions of degree p arranged in a certain lexicographical order:

$$\boldsymbol{H}_p^T(\boldsymbol{x}-\boldsymbol{y}) = [(\boldsymbol{x}-\boldsymbol{y})^{\boldsymbol{\alpha}}]_{|\boldsymbol{\alpha}|\le p} \in \mathbb{R}^{N_p}\,,$$

where N_p is the dimension of the polynomial space of degree p and is defined as

$$N_p = \binom{p+\mathrm{d}}{\mathrm{d}}\,.$$

The continuous moment matrix $\widetilde{\boldsymbol{M}}_p(\boldsymbol{x}) \in \mathbb{R}^{N_p \times N_p}$ is given by

$$\widetilde{\boldsymbol{M}}_p(\boldsymbol{x}) = \int_{\overline{\overline{\Omega}}} \boldsymbol{H}_p(\boldsymbol{x}-\boldsymbol{y})\phi_\epsilon(\boldsymbol{x}-\boldsymbol{y})\boldsymbol{H}_p^T(\boldsymbol{x}-\boldsymbol{y})d\boldsymbol{y},$$

and each entry of $\widetilde{\boldsymbol{M}}_p(\boldsymbol{x})$ is written as

$$\widetilde{m}_{\boldsymbol{\alpha}}(\boldsymbol{x}) = \int_{\overline{\overline{\Omega}}} (\boldsymbol{x}-\boldsymbol{y})^{\boldsymbol{\alpha}}\phi_\epsilon(\boldsymbol{x}-\boldsymbol{y})d\boldsymbol{y}, \quad |\boldsymbol{\alpha}| \le 2p\,. \tag{2.43}$$

Therefore, we arrive at the continuous approximation in multi-dimension as

$$u_{\boldsymbol{\epsilon}}(\boldsymbol{x}) = \int_{\overline{\Omega}} \widetilde{\Psi}_{\epsilon}(\boldsymbol{x}; \boldsymbol{x}-\boldsymbol{y}) u(\boldsymbol{y}) d\boldsymbol{y}\,,$$

where

$$\widetilde{\Psi}_{\epsilon}(\boldsymbol{x}; \boldsymbol{x}-\boldsymbol{y}) = \boldsymbol{H}_p^T(\boldsymbol{x}-\boldsymbol{y}) \widetilde{\boldsymbol{M}}_p^{-1}(\boldsymbol{x}) \boldsymbol{H}_p(\boldsymbol{0}) \phi_{\epsilon}(\boldsymbol{x}-\boldsymbol{y})\,.$$

With the continuous multi-dimensional RK approximation defined, it is straightforward to define the corresponding discrete RK approximation following the work in 1d, which we omit here.

Now by the definition of the moment $\widetilde{m}_{\boldsymbol{\alpha}}(\boldsymbol{x})$ in eq. (2.43), we observe that it is zero for $\boldsymbol{x}$ in the interior of the domain if any one of components of $\boldsymbol{\alpha}$ is an odd number, which is a multi-dimensional generalization of Lemma 2.2.1. We first define some notations for convenience of presentation. We define the set $\mathcal{I} = \{\boldsymbol{\alpha} = (\alpha_1, \alpha_2, \cdots, \alpha_{\mathrm{d}}) \in \mathbb{N}^{\mathrm{d}} : |\boldsymbol{\alpha}| \leq p\}$, and define two subsets of $\mathcal{I}$ as

$$\begin{aligned}
&\mathcal{E} = \{\boldsymbol{\alpha} \in \mathcal{I} : \alpha_i \text{ are even numbers for all } 1 \leq i \leq \mathrm{d}\}, \text{ and} \\
&\mathcal{O} = \mathcal{I} \backslash \mathcal{E}\,.
\end{aligned}$$

Notice that $\mathcal{O}$ is the set of all indices $\boldsymbol{\alpha}$ with at least one component being an odd number. Now the multi-dimensional version of Lemma 2.2.1 is the following.

Lemma 2.4.1. *For $\boldsymbol{x} \in \Omega$, the moment $\widetilde{m}_{\boldsymbol{\alpha}}(\boldsymbol{x}) = 0$ if $\boldsymbol{\alpha} \in \mathcal{O}$.*

Proof. For $\boldsymbol{x}$ in the interior of the domain, the moment given by eq. (2.43) is actually

$$\widetilde{m}_{\boldsymbol{\alpha}}(\boldsymbol{x}) = \int_{\mathbb{R}^{\mathrm{d}}} \boldsymbol{z}^{\boldsymbol{\alpha}} \phi_{\epsilon}(\boldsymbol{z}) d\boldsymbol{z}\,. \tag{2.44}$$

Since ϕ_{ϵ} is a radially symmetric function, it is obvious that if one of the components of α is an odd number, then the integral given by eq. (2.44) is zero. □

We now present a multi-dimensional version of Lemma 2.2.2.

Lemma 2.4.2. *Let* $\boldsymbol{b}_p(\boldsymbol{x}) = \widetilde{\boldsymbol{M}}_p^{-1}(\boldsymbol{x})\boldsymbol{H}_p(\boldsymbol{0})$ *and let* $b_p^{(\boldsymbol{\alpha})}(|\boldsymbol{\alpha}| \leq p)$ *be the components of* $\boldsymbol{b}_p$. *For* $\boldsymbol{x} \in \Omega$, *we have*

(a) $b_p^{(\boldsymbol{\alpha})}(\boldsymbol{x}) = 0$ *if* $\boldsymbol{\alpha} \in \mathcal{O}$, *and*

(b) $b_p^{(\boldsymbol{\alpha})}(\boldsymbol{x}) = b_{p+1}^{(\boldsymbol{\alpha})}(\boldsymbol{x})$ *for* $p = 2k$, *where* $k \in \mathbb{N}$.

Proof. The basic idea of the proof is again by splitting the system $\widetilde{\boldsymbol{M}}_p(\boldsymbol{x})\boldsymbol{b}_p(\boldsymbol{x}) = \boldsymbol{H}_p(\boldsymbol{0})$ into two linear systems. Notice that in 1d, the linear systems eqs. (2.27) and (2.30) are decomposed into two smaller systems. The common feature is that after decomposition, the smaller systems eqs. (2.28) and (2.31) contain only the components of $\boldsymbol{b}_p$ with even upper indices. Here such decomposition for multi-dimensional problem follows similarly.

Now we split the vector $\boldsymbol{b}_p(\boldsymbol{x})$ into two sub-vectors by defining

$$\boldsymbol{b}_p^{even}(\boldsymbol{x}) = [\boldsymbol{b}_p^{(\boldsymbol{\alpha})}(\boldsymbol{x})]_{\boldsymbol{\alpha}\in\mathcal{E}}, \text{ and } \boldsymbol{b}_p^{odd}(\boldsymbol{x}) = [\boldsymbol{b}_p^{(\boldsymbol{\alpha})}(\boldsymbol{x})]_{\boldsymbol{\alpha}\in\mathcal{O}}\,.$$

We then define sub-matrices of $\widetilde{\boldsymbol{M}}_p(\boldsymbol{x})$ as

$$\widetilde{\boldsymbol{M}}_p^{even}(\boldsymbol{x}) = (\widetilde{m}_{\boldsymbol{\alpha}+\boldsymbol{\beta}}(\boldsymbol{x}))_{\boldsymbol{\alpha}\in\mathcal{E},\boldsymbol{\beta}\in\mathcal{E}}\,, \text{ and}$$
$$\widetilde{\boldsymbol{M}}_p^{odd}(\boldsymbol{x}) = (\widetilde{m}_{\boldsymbol{\alpha}+\boldsymbol{\beta}}(\boldsymbol{x}))_{\boldsymbol{\alpha}\in\mathcal{O},\boldsymbol{\beta}\in\mathcal{O}}\,.$$

It is obvious that $\widetilde{\boldsymbol{M}}_p^{even}(\boldsymbol{x})$ and $\widetilde{\boldsymbol{M}}_p^{odd}(\boldsymbol{x})$ are both invertible if the original matrix $\widetilde{\boldsymbol{M}}_p(\boldsymbol{x})$ is invertible. Notice that the other two sub-matrices of $\widetilde{\boldsymbol{M}}_p(\boldsymbol{x})$ given by $(\widetilde{m}_{\boldsymbol{\alpha}+\boldsymbol{\beta}}(\boldsymbol{x}))_{\boldsymbol{\alpha}\in\mathcal{E},\boldsymbol{\beta}\in\mathcal{O}}$ and $(\widetilde{m}_{\boldsymbol{\alpha}+\boldsymbol{\beta}}(\boldsymbol{x}))_{\boldsymbol{\alpha}\in\mathcal{O},\boldsymbol{\beta}\in\mathcal{E}}$ are in fact zero since by Lemma 2.4.2 the moment $\widetilde{m}_{\boldsymbol{\gamma}}(\boldsymbol{x})$ is zero if $\boldsymbol{\gamma} \in \mathcal{O}$. We can then rearrange the rows and columns in the system $\widetilde{\boldsymbol{M}}_p(\boldsymbol{x})\boldsymbol{b}_p(\boldsymbol{x}) = \boldsymbol{H}_p(\boldsymbol{0})$ such that it is given by the following block matrices

$$\begin{bmatrix} \widetilde{\boldsymbol{M}}_p^{even}(\boldsymbol{x}) & \boldsymbol{0} \\ \boldsymbol{0} & \widetilde{\boldsymbol{M}}_p^{odd}(\boldsymbol{x}) \end{bmatrix} \begin{bmatrix} \boldsymbol{b}_p^{even}(\boldsymbol{x}) \\ \boldsymbol{b}_p^{odd}(\boldsymbol{x}) \end{bmatrix} = \begin{bmatrix} \boldsymbol{e}_1 \\ \boldsymbol{0} \end{bmatrix}, \tag{2.45}$$

where $\boldsymbol{e}_1 = [1, 0, \cdots, 0]^T$. Naturally, eq. (2.45) splits into two linear systems

$$\widetilde{\boldsymbol{M}}_p^{even}(\boldsymbol{x})\boldsymbol{b}_p^{even}(\boldsymbol{x}) = \boldsymbol{e}_1\,, \text{ and} \tag{2.46}$$

$$\widetilde{\boldsymbol{M}}_p^{odd}(\boldsymbol{x})\boldsymbol{b}_p^{odd}(\boldsymbol{x}) = \boldsymbol{0}\,. \tag{2.47}$$

Equation (2.47) implies that $\boldsymbol{b}_p^{odd}(\boldsymbol{x}) = \boldsymbol{0}$, which is exactly (a). Moreover, (b) is not hard to seen by looking at eq. (2.46) for $p = 2k$ and $p = 2k + 1$. □

As soon as one has the multi-dimensional version of Lemma 2.2.2, it is clear that there is no obstacle in obtaining the convergence theorem in multi-dimension. We believe that the proof is similar enough to the 1d case so that it is omitted here. For completeness, we give the final theorem for the multi-dimensional continuous RK approximation is given as follows.

Theorem 2.4.3. *Assume that the window function $\phi \in C^{p+2}$, and $u \in W^{p+2,q}(\overline{\overline{\Omega}})$ is proper. Then the error estimate for the* d*-dimensional continuous RK approximation is as follows:*

if p is odd,

$$\|u - u_\epsilon\|_{W^{l,q}(\overline{\overline{\Omega}})} \leq C\epsilon^{p+1-l}\|u\|_{W^{p+1,q}(\overline{\overline{\Omega}})}\,,$$

and if p is even,

$$\|u - u_\epsilon\|_{W^{l,q}(\overline{\overline{\Omega}})} \leq C\epsilon^{p+1+d/q-l}\|u\|_{W^{p+2,q}(\overline{\overline{\Omega}})}\,,$$

for $l = 0, 1, \cdots p + 1$.

For the discrete RK approximation, we need to modify the definition of the set of functions with Strang-Fix property. Instead of eq. (2.37), we now define

$$\mathcal{SF}_h^{(k)} = \{f : D_{\boldsymbol{\xi}}^{\boldsymbol{\alpha}}\widehat{f}(\boldsymbol{\xi})\Big|_{\frac{2\pi\boldsymbol{j}}{h}} = 0, \quad \forall\, j \in \mathbb{Z}^{\mathrm{d}}\backslash\{0\},\, 0 \leq \alpha \leq k\}\,, \tag{2.48}$$

where $D_{\boldsymbol{\xi}}^{\boldsymbol{\alpha}} = D_{\xi_1}^{\alpha_1} D_{\xi_2}^{\alpha_2} \cdots D_{\xi_{\mathrm{d}}}^{\alpha_{\mathrm{d}}}$. Then the multi-dimensional version of Theorem 2.3.3 is given as follows.

Theorem 2.4.4. *Assume that the window function $\phi \in C^{p+2}$, and $u \in W^{p+2,q}(\overline{\overline{\Omega}})$ is proper. Suppose $\phi_\epsilon \in \mathcal{SF}_h^{(2p+1)}$, then the error estimate for the* d*-dimensional discrete RK approximation is as follows:*

if p is odd,

$$\|u - u^I\|_{W^{l,q}(\overline{\overline{\Omega}})} \leq C\epsilon^{p+1-l}\|u\|_{W^{p+1,q}(\overline{\overline{\Omega}})},$$

and if p is even,

$$\|u - u^I\|_{W^{l,q}(\overline{\overline{\Omega}})} \leq C\epsilon^{p+1+d/q-l}\|u\|_{W^{p+2,q}(\overline{\overline{\Omega}})},$$

for $l = 0, 1, \cdots p+1$.

2.5 Numerical experiments

Cubic B-spline is widely used as the window function in RK approximations, because it guarantees that $u^I \in C^2(\overline{\overline{\Omega}})$. In this section, $\phi(x)$ is defined by eq. (2.40) with $n = 3$. By Lemma 2.3.4 and Theorem 2.3.3, we have super-convergence of the constant RK interpolation ($p = 0$) if the RK support $\epsilon = \frac{n+1}{2} r_0 h = 2r_0 h$, where $r_0 \in \mathbb{N}$. We are going to verify Theorem 2.3.3 with $l = 0$ and $q = 2$, namely we look at the L^2 error between a function and its discrete RK approximation with the expectation of half-order super-convergence for the case $p = 0$.

Figure 2.2 shows the point-wise error of using constant RK interpolation ($p = 0$) to approximate linear function the $u(x) = x$ on the domain $\overline{\overline{\Omega}} = (0, 1)$. In Figure 2.2, 11 particles are positioned uniformly and RK support $\epsilon = 2h$ ($r_0 = 1$). We see that the approximation error is zero everywhere in the interior of the domain. This is to say the constant RK approximation reproduces exactly linear functions in the interior of the domain. In general, the RK shape function of constant interpolation satisfies first order reproducing condition for points in the interior of the domain with support size $\epsilon = 2r_0 h$, where r_0 is a positive integer.

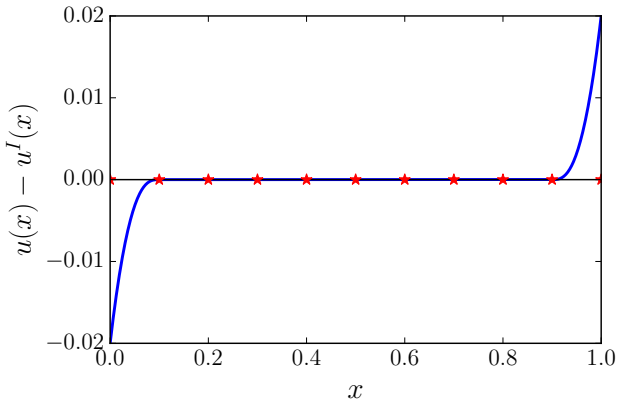

Figure 2.2: Error distribution of approximating a linear function $u(x) = x$ using constant RK interpolation with $h = 0.1$ and $\epsilon = 2h$. Cubic B-spline is the window function

.

Convergence studies of approximating $u(x) = e^x$ are shown in Figures 2.3 to 2.5. In Figure 2.3, constant RK interpolation ($p = 0$) is used with RK support $\epsilon = 2h$. The L^2 convergence rate on Ω is observed to be second order and the L^2 convergence rate over the whole domain $\overline{\overline{\Omega}}$ is observed to be $O(h^{1.5})$, which agrees with our theorem. Figure 2.3 can be compared with Figure 2.4, where linear RK interpolation ($p = 1$) is used with RK support $\epsilon = 2h$. The L^2 convergence rates are second order on both Ω and $\overline{\overline{\Omega}}$. Similar behaviors are observed for all support size $\epsilon = 2r_0h$, where r_0 is a positive integer. More generally, to see the super-convergence of RK approximation for $p \geq 2$, higher order B-spline functions need to be used, using the guidelines given by Lemma 2.3.2. In Figure 2.5, quadratic RK interpolation ($p = 2$) is employed with RK support $\epsilon = 3h$ and the window function is the fifth order B-spline. The L^2, H^1 and H^2 convergence rates on Ω are 4.0, 3.0 and 2.0 respectively and they are 3.5, 2.5 and 1.5 on $\overline{\overline{\Omega}}$. Therefore, we observe super-convergence for constant and quadratic RK interpolation and our numerical experiments verify the results of Lemma 2.3.2.

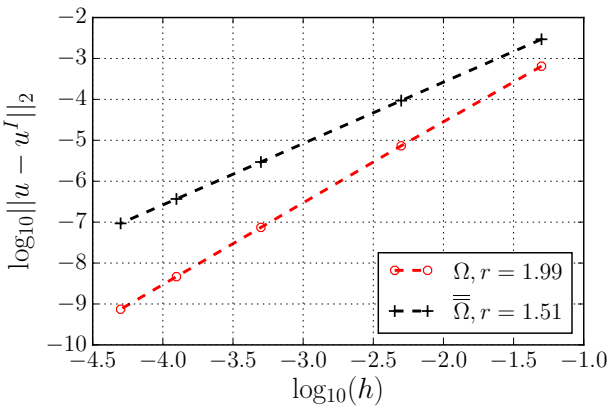

Figure 2.3: Convergence study of approximating $u(x) = e^x$ using constant RK interpolation with $\epsilon = 2h$. r is the rate of convergence and cubic B-spline is the window function

.

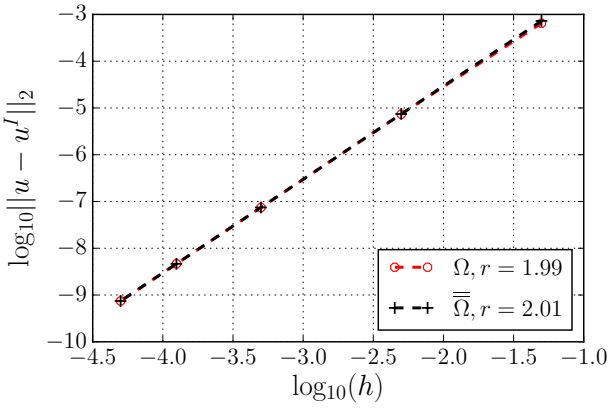

Figure 2.4: Convergence study of approximating $u(x) = e^x$ using linear RK interpolation with $\epsilon = 2h$. r is the rate of convergence and cubic B-spline is the window function

.

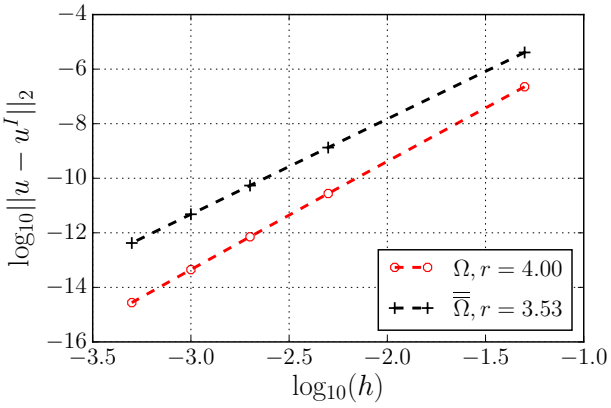

(a) L^2 norm

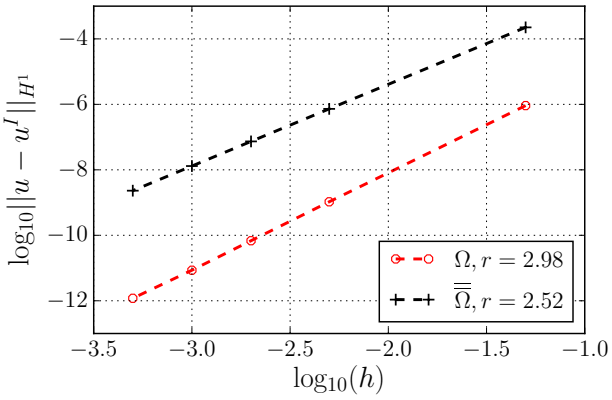

(b) H^1 norm

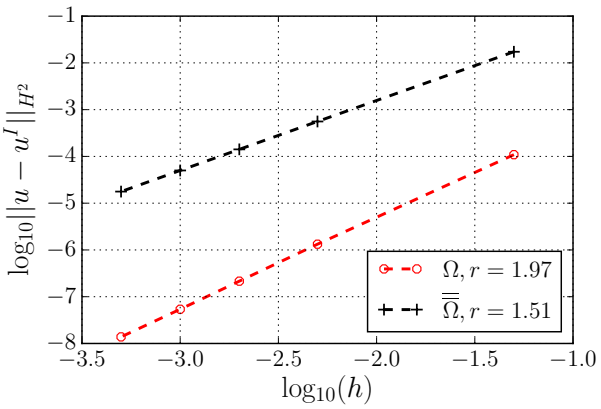

(c) H^2 norm

Figure 2.5: Convergence study of approximating $u(x) = e^x$ using quadratic RK interpolation with $\epsilon = 3h$. r is the rate of convergence and fifth order B-spline is the window function

.

2.6 The discussion on general RK support sizes

The analysis in section 2.3 does not hold for general RK support sizes except for these discussed in Lemma 2.3.4 because $\phi_\epsilon \notin \mathcal{SF}_h^{(2p+1)}$ for arbitrary ϵ. Thus one do not expect super-convergence of RK approximation with arbitrary RK support size. We present the error estimates of RK approximation with arbitrary RK support sizes which can be found in [51, 73] as follows:

$$\|u - u^I\|_{W^{l,q}(\overline{\overline{\Omega}})} \leq C\epsilon^{p+1-l}\|u\|_{W^{p+1,q}(\overline{\overline{\Omega}})}, \quad \text{for } l = 0, 1, \cdots, p+1\,. \tag{2.49}$$

In Section 2.3, we showed that in general if B-spline of order n is the window function, then we have super-convergence for even order RK interpolation with support size $\epsilon = \frac{n+1}{2} r_0 h$. In general, for an arbitrary RK support size, we do not expect such super-convergence. Figure 2.6 shows the error distribution of using constant RK interpolation to approximate linear function the $u(x) = x$, but with a support size $\epsilon = h$. We do not see the exact reproduction of linear function in the interior of the domain, in comparison with Figure 2.2 using the support size $\epsilon = 2h$. However, we do observe that the error vanishes at the grid points ($x = x_i$) and midpoints between grid points ($x = (x_i + x_{i+1})/2$). This is a general fact for all support sizes because the grids are symmetrically distributed centered at these special points $x = x_i$ and $x = (x_i + x_{i+1})/2$, which makes the odd order discrete moments at these points to be zero, and we can easily derive a higher order reproducing relation at those special points for even order RK approximation.

In practice, however, one often observes super-convergence within certain range of numerical resolution in L^2 norm for even order RK interpolation with a support size ϵ not exactly equal to $\frac{n+1}{2} r_0 h$, as shown in [73, 95]. These observations

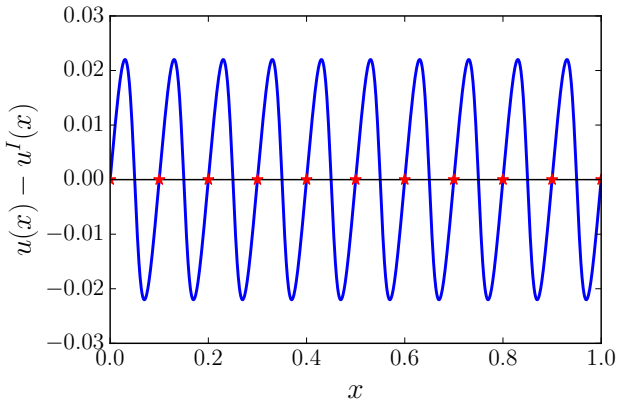

Figure 2.6: Error distribution of approximating a linear function $u(x) = x$ using constant RK interpolation with $h = 0.2$ and $\epsilon = h$. Cubic B-spline is the window function.

do not contradict eq. (2.49) and we call this phenomenon the *pseudo super convergence*.

Remark 2.6.1. *Pseudo super convergence is the phenomenon that some numerical examples exhibit super-convergence within certain range of numerical resolution but is not truly super-convergent after sufficient grid refinement.*

First, at a generic point x ($x \neq x_i$ and $x \neq (x_i + x_{i+1})/2$) in the interior of the domain, although the odd order discrete moments do not vanish completely, but they are diminishing as the ratio ϵ/h grows, since more sampling points are used to calculate the numerical integral of anti-symmetric functions. We see clearly in Figure 2.7 that with the increase of the ratio ϵ/h, the errors in the interior of the domain relative to the boundary are diminishing for the case of approximating linear functions by the constant RK approximation. Thus in the region where h is not refined enough, the dominant error comes from the boundary and thus we observe super-convergence for p being even. However, for a fixed ratio ϵ/h, the approximation error on Ω will eventually play the significant role with the refinement of h. Thus

convergence rate drops back to $p+1$ in the region where h is smaller than some threshold. The differentiation of two regions is typical in a RK approximation with pseudo super convergence.

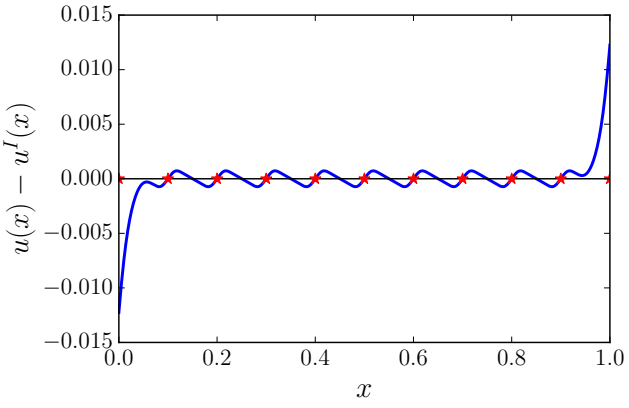

(a) $h = 0.1, \epsilon = 1.7h$

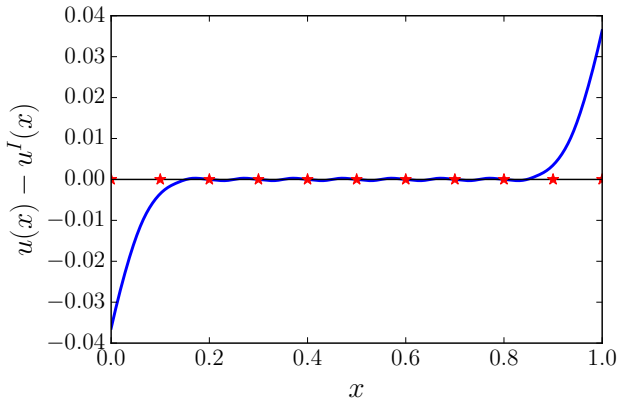

(b) $h = 0.1, \epsilon = 2.7h$

Figure 2.7: Error distribution of approximating a linear function $u(x) = x$ using constant RK interpolation with support sizes $\epsilon = 1.7h$ and $\epsilon = 2.7h$. Cubic B-spline is the window function

.

Figure 2.8 studies pseudo super convergence phenomena. We approximate $u(x) = e^x$ by RK with constant interpolation using cubic B-spline as the window function. Figure 2.8 shows the clear transition between two different regions of convergence rates. In Figure 2.8a, the support size $\epsilon = 1.7h$ is used. When $h > 1E-2.5$,

the major approximation error comes from the boundary, thus we see a convergence rate of $r = 1.5$. When $h < 1E-2.5$, the error on Ω starts to play the dominant role. The convergence rate over the whole domain gradually changes from $r = 1.5$ to $r = 1.0$. We observe similar pattern of such transition in Figure 2.8b where $\epsilon = 2.7h$. The difference is that with a larger ratio ϵ/h, the transition of error contribution comes at a smaller mesh size where $h \approx 1E-4.5$. The transition point moves further when we keep increasing the ratio ϵ/h. If one further increases the ratio ϵ/h, then the transition happens at even smaller h. When the ratio ϵ/h is large enough such that the transition point is around machine precision, i.e., Figure 2.8c, one always observes super-convergence in numerical experiments. However, such super-convergence is not a mathematical property but just a numerical artifact, and thus it bears the name pseudo super convergence.

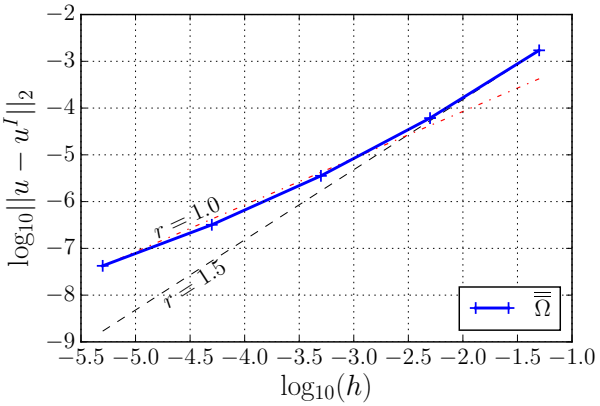

(a) $\epsilon = 1.7h$, constant RK interpolation

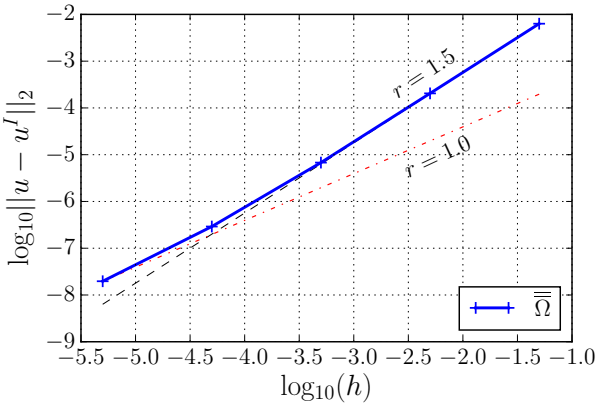

(b) $\epsilon = 2.7h$, constant RK interpolation

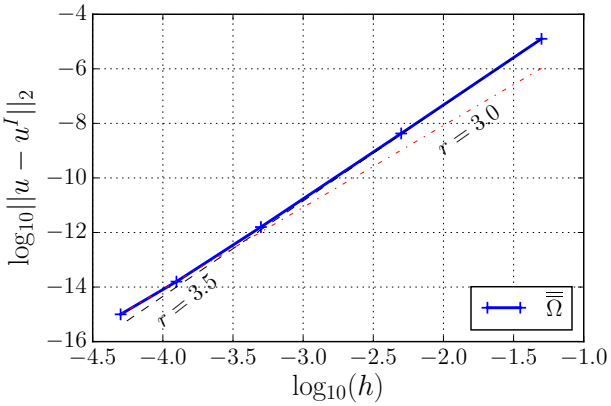

(c) $\epsilon = 3.7h$, quadratic RK interpolation

Figure 2.8: Convergence study of approximating $u(x) = e^x$ using constant and quadratic RK interpolation with support sizes $\epsilon = 1.7h, 2.7h$ and $3.7h$. Cubic B-spline is the window function

.

Chapter 3

Nonlocal diffusion

In this chapter[1], we introduce the RK collocation method and show the collocation scheme for nonlocal diffusion models with Dirichlet boundary condition is AC. The scheme is shown to be convergent to both nonlocal diffusion and its corresponding local limit as the nonlocal interaction vanishes. Stability of collocation methods on integral equations is not a trivial task, due to the lack of a discrete maximum principle. As in [1, 2, 28], a helpful view is to compare collocation schemes with Galerkin scheme for which stability comes naturally. We use the Fourier approach as in [28] and demonstrate that the Fourier symbol of the RK collocation scheme for nonlocal diffusion can be bounded below by that of the standard Galerkin scheme on the grids. Consequently, we show that the collocation scheme is stable because the standard Galerkin approximation is uniformly stable (i.e. the stability constant does not depends on δ). Then, consistency is established using the properties of the RK approximation discussed in Chapter 2. Finally, theoretical results are validated using numerical experiments.

This chapter is organized as follows. In section 3.1, we introduce the nonlocal diffusion model equations with Dirichlet boundary conditions. Section 3.3 discusses the convergence of the RK collocation method to both the nonlocal diffusion equation for fixed δ and the local diffusion equation as δ goes to zero so that the RK collocation

[1]This chapter is a part of [71]. The author's contribution includes theoretical derivation and conducting numerical experiments.

scheme is AC. section 3.4 gives numerical examples to complement our theoretical analysis.

3.1 Nonlocal diffusion operator and model equation

We use the following notation throughout this chapter. d is a positive integer denoting spatial dimension. Let $\Omega \subset \mathbb{R}^{\mathrm{d}}$ be a bounded, open domain. The corresponding interaction domain is then defined as

$$\Omega_{\mathcal{I}} = \{\boldsymbol{x} \in \mathbb{R}^{\mathrm{d}} \backslash \Omega : \mathrm{dist}(\boldsymbol{x}, \Omega) \leq \delta\},$$

and let $\Omega_\delta = \Omega \cup \Omega_{\mathcal{I}}$. Following the same notations as in [33], we define the nonlocal diffusion operator $\mathcal{L}_\delta$, for a given $u(\boldsymbol{x}) : \Omega_\delta \to \mathbb{R}$, as

$$\mathcal{L}_\delta u(\boldsymbol{x}) = \int_{\Omega_\delta} \rho_\delta(\boldsymbol{x}, \boldsymbol{y})(u(\boldsymbol{y}) - u(\boldsymbol{x}))d\boldsymbol{y}, \quad \forall\, \boldsymbol{x} \in \Omega, \tag{3.1}$$

where δ is the nonlocal length and $\rho_\delta(\boldsymbol{x}, \boldsymbol{y})$ is the nonlocal diffusion kernel which is non-negative and symmetric, i.e., $\rho_\delta(\boldsymbol{x}, \boldsymbol{y}) = \rho_\delta(\boldsymbol{y}, \boldsymbol{x})$. Let us consider a nonlocal diffusion problem with homogeneous Dirichlet volumetric constraint,

$$\begin{cases} -\mathcal{L}_\delta u = f, & \text{in } \Omega, \\ u = 0, & \text{on } \Omega_{\mathcal{I}}. \end{cases} \tag{3.2}$$

In this work, we study the kernels of radial type, i.e., $\rho_\delta(\boldsymbol{x}, \boldsymbol{y}) = \rho_\delta(|\boldsymbol{x} - \boldsymbol{y}|)$. We denote the following scaling of the kernel

$$\rho_\delta(|\boldsymbol{s}|) = \frac{1}{\delta^{\mathrm{d}+2}} \rho\left(\frac{|\boldsymbol{s}|}{\delta}\right), \tag{3.3}$$

where $\rho(|\boldsymbol{s}|)$ is compactly supported in $B_1(\mathbf{0})$, a unit ball about $\mathbf{0}$ (we denote $B_\delta(\mathbf{0})$ as B_δ for the rest of the dissertation). We further assume $\rho(|\boldsymbol{s}|)$ is a non-increasing function and has a bounded second-order moment, i.e.

$$\int_{B_\delta} \rho_\delta(|\boldsymbol{s}|)|\boldsymbol{s}|^2 d\boldsymbol{s} = \int_{B_1} \rho(|\boldsymbol{s}|)|\boldsymbol{s}|^2 d\boldsymbol{s} = \mathrm{d}. \tag{3.4}$$

The local limit of $\mathcal{L}_\delta$ is denoted as $\mathcal{L}_0$ when $\delta \to 0$. We are interested in particular cases where $\mathcal{L}_0 = \Delta$, such that eq. (3.2) goes to

$$\begin{cases} -\mathcal{L}_0 u = f, & \text{in } \Omega, \\ u = 0, & \text{on } \partial\Omega. \end{cases} \tag{3.5}$$

We proceed to define some functional spaces. Define a space on Ω_δ with zero volumetric constraint on $\Omega_{\mathcal{I}}$,

$$L_c^2(\Omega_\delta) := \{u \in L^2(\Omega_\delta) \mid u = 0 \text{ on } \Omega_{\mathcal{I}}\}.$$

The natural energy space associated with eq. (3.2) is given by

$$\mathcal{S}_\delta := \left\{ u \in L_c^2(\Omega_\delta) : \int_{\Omega_\delta} \int_{\Omega_\delta} \rho_\delta(|\boldsymbol{y} - \boldsymbol{x}|)|u(\boldsymbol{y}) - u(\boldsymbol{x})|^2 d\boldsymbol{y} d\boldsymbol{x} < \infty \right\}.$$

The nonlocal diffusion problem as described in eq. (3.2) is well-posed and uniformly stable. We give the following the result without proof and the details can be found in [80].

Lemma 3.1.1. ***(Uniform stability)*** *Assume $\delta \in (0, \delta_0]$ for some $\delta_0 > 0$. The bilinear form $(-\mathcal{L}_\delta u, u)$ is an inner product and for any $u \in \mathcal{S}_\delta$, we have*

$$|(-\mathcal{L}_\delta u, u)| \geq C \|u\|^2_{L^2(\Omega_\delta)},$$

where C is a constant that only depends on Ω and δ_0.

3.2 RK collocation method

In this section, we introduce the RK collocation method and some notations. We emphasize that some notations may be subjected to change throughout this dissertation but they are made clear and stay consistent in each chapter. For instance, ϵ is denoted as the RK support size in Chapter 2 but we use a as the notation for the

RK support size in this chapter. Since functions in the solution space $\mathcal{S}_\delta$ are zero on the boundary layer $\Omega_{\mathcal{I}}$, we can extend functions in $\mathcal{S}_\delta$ trivially to $\mathbb{R}^{\mathrm{d}}$ and work on the whole space instead. We define $\square$ to be a rectilinear Cartesian grid on $\mathbb{R}^{\mathrm{d}}$, namely

$$\square := \{\boldsymbol{x}_{\boldsymbol{k}} := \boldsymbol{k} \odot \boldsymbol{h} \mid \boldsymbol{k} \in \mathbb{Z}^{\mathrm{d}}\},$$

where $\boldsymbol{k} = (k_1, \ldots, k_{\mathrm{d}})$, $\boldsymbol{h} = (h_1, \ldots, h_{\mathrm{d}})$ consists of discretization parameters in each dimension and $\odot$ denotes component-wise multiplication, i.e.,

$$\boldsymbol{k} \odot \boldsymbol{h} = (k_1 h_1, \ldots, k_{\mathrm{d}} h_{\mathrm{d}}).$$

Sometime we also write the j-th component of $\boldsymbol{x}_{\boldsymbol{k}}$ by x_{k_j}, which is equal to $k_j h_j$ by definition. We introduce a component-wise division symbol $\oslash$:

$$\boldsymbol{k} \oslash \boldsymbol{h} = \left(\frac{k_1}{h_1}, \ldots, \frac{k_{\mathrm{d}}}{h_{\mathrm{d}}}\right).$$

It is noted that the grid size h_j can vary for different j. For instance, in two dimension, rectangular grids are allowed, i.e., Figure 3.1. Nonetheless, we assume the grid $\square$ is quasi-uniform such that $\boldsymbol{h}$ can also be written as

$$\boldsymbol{h} = h_{\max} \hat{\boldsymbol{h}}\,, \tag{3.6}$$

with $\hat{\boldsymbol{h}}$ being a fixed vector with the maximum component being 1 and the minimum component being bounded below.

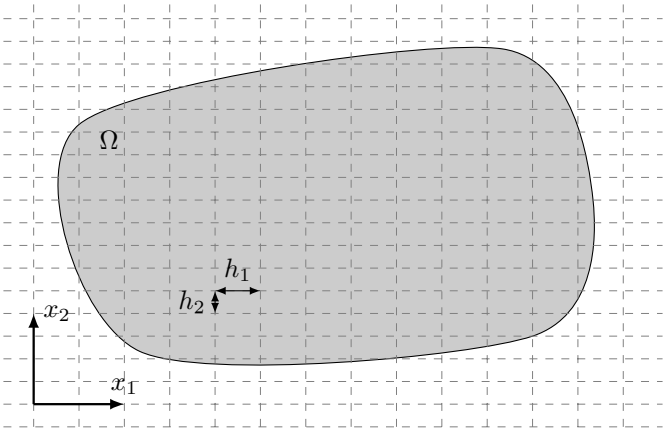

Figure 3.1: The dashed lines form the grid for the RK collocation method .

For any scalar function $u(\boldsymbol{x}) \in C^0(\mathbb{R})$, we define the restriction to $\square$ by

$$r^h u := (u(\boldsymbol{x}_{\boldsymbol{k}}))_{\boldsymbol{k}\in\mathbb{Z}^{\mathrm{d}}}, \tag{3.7}$$

and the restriction to $(\square \cap \Omega)$ as

$$r^h_\Omega u := (u(\boldsymbol{x}_{\boldsymbol{k}})), \quad \boldsymbol{x}_{\boldsymbol{k}} \in (\square \cap \Omega). \tag{3.8}$$

For any sequence $(u_{\boldsymbol{k}})_{\boldsymbol{k}\in\mathbb{Z}^{\mathrm{d}}}$ on $\mathbb{R}$, the RK interpolant operator is given as

$$i^h(u_{\boldsymbol{k}}) := \sum_{\boldsymbol{k}\in\mathbb{Z}^{\mathrm{d}}} \Psi_{\boldsymbol{k}}(\boldsymbol{x}) u_{\boldsymbol{k}},$$

where $\Psi_{\boldsymbol{k}}(\boldsymbol{x})$ is the RK basis function as defined in eq. (2.13) and we will discuss more details on how to choose the RK support size shortly. Denote by $S(\square)$ the trial space equipped with the RK basis $\Psi_{\boldsymbol{k}}(\boldsymbol{x})$ on $\square$, i.e., $S(\square) = \mathrm{span}\{\Psi_{\boldsymbol{k}}(\boldsymbol{x}) \mid \boldsymbol{k} \in \mathbb{Z}^{\mathrm{d}}\}$. Then we let

$$\Pi^h := i^h r^h$$

be the interpolation projector mapping from $C(\mathbb{R}^{\mathrm{d}})$ to $S(\square)$. For $j = 1, \ldots, \mathrm{d}$, we denote $u_j(\boldsymbol{x}) : \mathbb{R}^{\mathrm{d}} \to \mathbb{R}$ the j-th component of a vector field $\boldsymbol{u}(\boldsymbol{x}) = [u_1(\boldsymbol{x}), \ldots, u_{\mathrm{d}}(\boldsymbol{x})]^T$ and denote $(u_{j,\boldsymbol{k}})$ the j-th component of the vector sequence

$$(\boldsymbol{u}_{\boldsymbol{k}}) = [(u_{1,\boldsymbol{k}})_{\boldsymbol{k}\in\mathbb{Z}^{\mathrm{d}}}, \ldots, (u_{\mathrm{d},\boldsymbol{k}})_{\boldsymbol{k}\in\mathbb{Z}^{\mathrm{d}}}]^T.$$

Therefore, we can write

$$\Pi^h \boldsymbol{u} := [\Pi^h u_1, \ldots, \Pi^h u_{\mathrm{d}}]^T,$$

where $\Pi^h u_j(\boldsymbol{x})$ is the RK approximation of $u_j(\boldsymbol{x})$,

$$\Pi^h u_j(\boldsymbol{x}) = \sum_{\boldsymbol{k}\in\mathbb{Z}^{\mathrm{d}}} \Psi_{\boldsymbol{k}}(\boldsymbol{x}) u_j(\boldsymbol{x}_{\boldsymbol{k}}).$$

We proceed to recall the construction of the RK basis function as discussed in Chapter 2. Apart from that is discussed in subsection 2.1.2, we choose $\boldsymbol{\phi}_{\boldsymbol{a}}(\boldsymbol{x} - \boldsymbol{y})$,

which is the tensor product of kernel functions in each dimension with support $\boldsymbol{a}$, as the kernel function defined in eq. (2.3), i.e.

$$\boldsymbol{\phi_a}(\boldsymbol{x}-\boldsymbol{y}) \equiv \prod_{j=1}^{\mathrm{d}} \phi_{a_j}(x_j - y_j) = \prod_{j=1}^{\mathrm{d}} \phi\left(\frac{|x_j - y_j|}{a_j}\right), \tag{3.9}$$

where $\phi_{a_j}(x_j)$ is the kernel function in the j-th dimension, a_j is the support size for $\phi_{a_j}(x_j)$ and $\phi(x)$ is called the window function. In this dissertation, we use the cubic B-spline function as the window function, i.e.,

$$\phi(x) = \begin{cases} \frac{2}{3} - 4x^2 + 4x^3, & 0 \le x \le \frac{1}{2}, \\ \frac{4}{3}(1-x)^3, & \frac{1}{2} \le x \le 1, \\ 0, & \text{otherwise.} \end{cases} \tag{3.10}$$

Then the moment defined in eq. (2.17) becomes

$$\boldsymbol{m_\alpha}(\boldsymbol{x}) = \sum_{\boldsymbol{k}\in\mathbb{Z}^{\mathrm{d}}} \boldsymbol{\phi_a}(\boldsymbol{x}-\boldsymbol{x_k})(\boldsymbol{x}-\boldsymbol{x_k})^{\boldsymbol{\alpha}} = \prod_{j=1}^{\mathrm{d}} m_{\alpha_j}(x_j). \tag{3.11}$$

where $\boldsymbol{x} = (x_1, \ldots, x_{\mathrm{d}})$, $\boldsymbol{x_k} = (x_{k_1}, \ldots, x_{k_{\mathrm{d}}})$, and $m_{\alpha_j}(x_j)$ is the moment in the j-th dimension given by

$$m_{\alpha_j}(x_j) = \sum_{k_j\in\mathbb{Z}} \phi_{a_j}(x_j - x_{k_j})(x_j - x_{k_j})^{\alpha_j}. \tag{3.12}$$

In the rest of the dissertation, we assume the reproducing condition eq. (2.15) is satisfied with $p = 1$, therefore we call our method the linear RK approximation and the RK basis function is referred as the linear RK basis. If the RK support size is chosen properly, it is shown that the linear RK approximation has synchronized convergence as in [73, 74], a phenomenon where the convergence rates of higher-order error norms and lower-order error norms are of the same order.

Remark 3.2.1. *Choose the RK support as $\boldsymbol{a} = a_0\boldsymbol{h}$, where a_0 is an even number, the linear RK basis function becomes a rescaling of the cubic B-spline function, see [70],*

and the RK approximation has synchronized convergence for L^2, H^1 and H^2 error norm, as shown in [73]. For the simplicity of presentation, we assume $a_0 = 2$ in the paper but the analysis also works for general even number a_0.

Let $a_0 = 2$ be the parameter described in Remark 3.2.1, then the linear RK basis function can be written, see [70], as

$$\Psi_{\boldsymbol{k}}(\boldsymbol{x}) = \boldsymbol{\phi_a}(\boldsymbol{x} - \boldsymbol{x_k}) = \prod_{j=1}^{\mathrm{d}} \phi_{a_j}(x_j - x_{k_j})\,. \tag{3.13}$$

Another consequence of this choice of support size is that the one-dimensional moments up to the third order are independent of x_j, and more precisely

$$m_0(x_j) = 1, \quad m_1(x_j) = 0, \quad m_2(x_j) = \frac{h_j^2}{3}, \quad m_3(x_j) = 0\,, \tag{3.14}$$

for $j = 1, \ldots, \mathrm{d}$. From the one-dimensional moment, we can derive useful properties of the multi-dimensional moment which are summarized in the following lemma.

Lemma 3.2.2. *The multi-dimensional moments satisfy the following properties,*

(i) $\boldsymbol{m_0} = 1$ *and* $\boldsymbol{m_\alpha} = 0$ *for* $|\boldsymbol{\alpha}| = 1$ or 3,

(ii) $\boldsymbol{m_\alpha} = 0$ or $m_2(x_j)$ *for* $|\boldsymbol{\alpha}| = 2$ *and* $j = 1, \ldots, \mathrm{d}$,

Proof. By writing out the multi-index $\boldsymbol{\alpha}$ and from eqs. (3.11) and (3.14), the desired properties follow. □

We use the above discussed RK approximation (eq. (3.13)) and collocate the nonlocal models on the grid $\square$. In this chapter, we apply the RK collocation method for the nonlocal diffusion models; the collocation scheme is formulated as follows. Find a function $u \in S\,(\square \cap \Omega)$ such that

$$-\mathcal{L}_\delta u(\boldsymbol{x_k}) = f(\boldsymbol{x_k}), \quad \boldsymbol{x_k} \in (\square \cap \Omega), \tag{3.15}$$

where $S(\square \cap \Omega)$ is defined as

$$S(\square \cap \Omega) := \left\{ u = \sum_{\boldsymbol{k} \in \mathbb{Z}^{\mathrm{d}}} \Psi_{\boldsymbol{k}} u_{\boldsymbol{k}} \,\middle|\, u_{\boldsymbol{k}} = 0 \text{ for such } \boldsymbol{k} \text{ that } \boldsymbol{x}_{\boldsymbol{k}} \notin (\square \cap \Omega) \right\}.$$

Alternatively, eq. (3.15) can also be written as

$$-r_{\Omega}^{h} \mathcal{L}_{\delta} u = r_{\Omega}^{h} f \,,$$

where r_{Ω}^{h} is the restriction operator given in eq. (3.8).

Remark 3.2.3. *With the assumption in Remark 3.2.1, the RK basis has support size of $2h_j$ in the j-th dimension. So the support of $u \in S(\square \cap \Omega)$ is not fully contained in Ω but in a larger domain given as*

$$\widehat{\Omega} = (-2h_1, 1 + 2h_1) \times \cdots \times (-2h_{\mathrm{d}}, 1 + 2h_{\mathrm{d}}).$$

3.3 Convergence analysis of the RK collocation method for nonlocal diffusion

In this section, we show the convergence of the RK collocation for the nonlocal diffusion, which is also the method used in [95] without a convergence proof. The concern for convergence is that the numerical scheme should converge to the nonlocal problem for a fixed δ, and to the correct local problem as δ and grid size $h_{\max}$ both go to zero. So the proposed RK collocation scheme is an AC scheme proposed in [111].

3.3.1 Stability

In this subsection, we provide the stability proof of our method. The key idea is to compare the RK collocation scheme with the Galerkin scheme using Fourier analysis. Similar strategies have been developed in [28].

First, define a norm in the space of sequences by

$$|(u_{\boldsymbol{k}})_{\boldsymbol{k} \in \mathbb{Z}^{\mathrm{d}}}|_h := \|i^h(u_{\boldsymbol{k}})\|_{L^2(\mathbb{R}^{\mathrm{d}})} \,. \tag{3.16}$$

If a sequence $(u_{\boldsymbol{k}})$ is only defined for $\boldsymbol{k}$ in a subset of $\mathbb{Z}^{\mathrm{d}}$, then one can always use zero extension for $(u_{\boldsymbol{k}})$ so that it is defined for all $\boldsymbol{k} \in \mathbb{Z}^{\mathrm{d}}$. Then without further explanation, $|(u_{\boldsymbol{k}})|_h$ is always understood as (3.16) with the zero extension being used. The main theorem in this subsection is now given as follows.

Theorem 3.3.1. ***(Stability I)*** *For any $\delta \in (0, \delta_0]$ and $u \in S(\square \cap \Omega)$, we have*

$$\left|r_{\Omega}^{h}(-\mathcal{L}_{\delta} u)\right|_h \geq C\|u\|_{L^2(\mathbb{R}^{\mathrm{d}})},$$

where C is a constant that only depends on Ω and δ_0.

The proof of Theorem 3.3.1 is shown at the end of this subsection, however two more lemmas are introduced before showing the proof. Let $(\cdot\,,\cdot)_{l^2}$ be the l^2 norm associated inner product, namely,

$$((u_{\boldsymbol{k}}),(v_{\boldsymbol{k}}))_{l^2} := \prod_{j=1}^{\mathrm{d}} h_j \sum_{\boldsymbol{k}\in\mathbb{Z}^{\mathrm{d}}} u_{\boldsymbol{k}}\overline{v_{\boldsymbol{k}}}.$$

For Fourier series defined on $\boldsymbol{Q} = (-\pi, \pi)^{\mathrm{d}}$,

$$\widetilde{u}(\boldsymbol{\xi}) := \sum_{\boldsymbol{k}\in\mathbb{Z}^{\mathrm{d}}} e^{-i\boldsymbol{k}\cdot\boldsymbol{\xi}} u_{\boldsymbol{k}}, \tag{3.17}$$

where

$$u_{\boldsymbol{k}} = (2\pi)^{-\mathrm{d}} \int_{\boldsymbol{Q}} e^{i\boldsymbol{k}\cdot\boldsymbol{\xi}} \widetilde{u}(\boldsymbol{\xi}) d\boldsymbol{\xi}.$$

The nonlocal diffusion operator $\mathcal{L}_\delta$ defines two discrete sesquilinear forms:

$$(i^h(u_{\boldsymbol{k}}), -\mathcal{L}_\delta i^h(v_{\boldsymbol{k}})) = \sum_{\boldsymbol{k},\boldsymbol{k'}\in\mathbb{Z}^{\mathrm{d}}} u_{\boldsymbol{k}}(\Psi_{\boldsymbol{k}}, -\mathcal{L}_\delta \Psi_{\boldsymbol{k'}})\overline{v_{\boldsymbol{k'}}}, \tag{3.18}$$

and

$$((u_{\boldsymbol{k}}), -r^h \mathcal{L}_\delta i^h(v_{\boldsymbol{k}}))_{l^2} = \prod_{j=1}^{\mathrm{d}} h_j \sum_{\boldsymbol{k},\boldsymbol{k'}\in\mathbb{Z}^{\mathrm{d}}} u_{\boldsymbol{k}}(-\mathcal{L}_\delta \Psi_{\boldsymbol{k'}})(\boldsymbol{x}_{\boldsymbol{k}})\overline{v_{\boldsymbol{k'}}}. \tag{3.19}$$

The inner product $(\cdot\,,\cdot)$ in eq. (3.18) is the standard L^2 inner product. Equation (3.18) defines a quadratic form corresponding to the Galerkin method, meanwhile, the quadratic form eq. (3.19) corresponds to the collocation method. Moreover, the stiffness matrix for the collocation scheme eq. (3.15) can be considered as a finite section of the infinite Toeplitz matrix induced by eq. (3.19). Before applying the Fourier analysis to eqs. (3.18) and (3.19), we study the Fourier symbol of the nonlocal diffusion operator $\mathcal{L}_\delta$ first. Take $u \in \mathcal{S}_\delta$, $\widehat{u}(\boldsymbol{\xi})$ is the Fourier transform of $u(\boldsymbol{x})$ defined by

$$\widehat{u}(\boldsymbol{\xi}) := \int_{\mathbb{R}^{\mathrm{d}}} e^{-i\boldsymbol{x}\cdot\boldsymbol{\xi}} u(\boldsymbol{x}) d\boldsymbol{x}.$$

The Fourier transform of the nonlocal diffusion operator $\mathcal{L}_\delta$ is given as

$$\begin{aligned}
-\widehat{\mathcal{L}_\delta u}(\boldsymbol{\xi}) &= -\int_{\mathbb{R}^{\mathrm{d}}} e^{-i\boldsymbol{x}\cdot\boldsymbol{\xi}} \int_{B_\delta} \rho_\delta(|\boldsymbol{s}|)(u(\boldsymbol{x}+\boldsymbol{s}) - u(\boldsymbol{x})) d\boldsymbol{s} d\boldsymbol{x}, \\
&= -\int_{B_\delta} \int_{\mathbb{R}^{\mathrm{d}}} \rho_\delta(|\boldsymbol{s}|)(u(\boldsymbol{x}+\boldsymbol{s}) - u(\boldsymbol{x})) e^{-i\boldsymbol{x}\cdot\boldsymbol{\xi}} d\boldsymbol{x} d\boldsymbol{s}, \\
&= \int_{B_\delta} \rho_\delta(|\boldsymbol{s}|)(1 - e^{i\boldsymbol{s}\cdot\boldsymbol{\xi}}) \widehat{u}(\boldsymbol{\xi}) d\boldsymbol{s}, \\
&= \lambda_\delta(\boldsymbol{\xi}) \widehat{u}(\boldsymbol{\xi}),
\end{aligned}$$

where $\lambda_\delta(\boldsymbol{\xi})$ is the Fourier symbol of $\mathcal{L}_\delta$,

$$\lambda_\delta(\boldsymbol{\xi}) = \int_{B_\delta} \rho_\delta(|\boldsymbol{s}|)(1 - e^{i\boldsymbol{s}\cdot\boldsymbol{\xi}}) d\boldsymbol{s} = \int_{B_\delta} \rho_\delta(|\boldsymbol{s}|)(1 - \cos(\boldsymbol{s}\cdot\boldsymbol{\xi})) d\boldsymbol{s}. \tag{3.20}$$

More discussions on the spectral analysis of the nonlocal diffusion operator can be found in [40]. From eq. (3.20), it is obvious that $\lambda_\delta(\boldsymbol{\xi})$ is real and non-negative. Now, we give a comparison of the two quadratic forms eqs. (3.18) and (3.19) using Fourier analysis.

Lemma 3.3.2. *Let $\widetilde{u}(\boldsymbol{\xi})$ and $\widetilde{v}(\boldsymbol{\xi})$ be the Fourier series of the sequences $(u_{\boldsymbol{k}}), (v_{\boldsymbol{k}}) \in l^1(\mathbb{Z}^{\mathrm{d}})$ respectively. Then*

(i) $(i^h(u_{\boldsymbol{k}}), -\mathcal{L}_\delta i^h(v_{\boldsymbol{k}})) = (2\pi)^{-\mathrm{d}} \int_{\boldsymbol{Q}} \widetilde{u}(\boldsymbol{\xi}) \overline{\widetilde{v}(\boldsymbol{\xi})} \lambda_G(\delta, \boldsymbol{h}, \boldsymbol{\xi}) d\boldsymbol{\xi},$

(ii) $((u_{\boldsymbol{k}}), -r^h \mathcal{L}_\delta i^h(v_{\boldsymbol{k}}))_{l^2} = (2\pi)^{-\mathrm{d}} \int_{\boldsymbol{Q}} \widetilde{u}(\boldsymbol{\xi})\overline{\widetilde{v}(\boldsymbol{\xi})}\lambda_C(\delta, \boldsymbol{h}, \boldsymbol{\xi}) d\boldsymbol{\xi}$,

(iii) $\lambda_C(\delta, \boldsymbol{h}, \boldsymbol{\xi}) \geq C\lambda_G(\delta, \boldsymbol{h}, \boldsymbol{\xi})$, *for* C *independent of* $\delta, \boldsymbol{h}$ *and* $\boldsymbol{\xi}$,

and λ_G *and* λ_C *are given by*

$$\lambda_G(\delta, \boldsymbol{h}, \boldsymbol{\xi}) = 2^{8\mathrm{d}} \sum_{\boldsymbol{r}\in\mathbb{Z}^{\mathrm{d}}} \lambda_\delta\left((\boldsymbol{\xi} + 2\pi\boldsymbol{r}) \oslash \boldsymbol{h}\right) \prod_{j=1}^{\mathrm{d}} h_j \left(\frac{\sin(\xi_j/2)}{\xi_j + 2\pi r_j}\right)^8, \tag{3.21}$$

$$\lambda_C(\delta, \boldsymbol{h}, \boldsymbol{\xi}) = 2^{4\mathrm{d}} \sum_{\boldsymbol{r}\in\mathbb{Z}^{\mathrm{d}}} \lambda_\delta\left((\boldsymbol{\xi} + 2\pi\boldsymbol{r}) \oslash \boldsymbol{h}\right) \prod_{j=1}^{\mathrm{d}} h_j \left(\frac{\sin(\xi_j/2)}{\xi_j + 2\pi r_j}\right)^4. \tag{3.22}$$

Proof. The inverse Fourier transform of $\widehat{\mathcal{L}_\delta u}(\boldsymbol{\xi})$ is given by

$$-\mathcal{L}_\delta u(\boldsymbol{x}) = (2\pi)^{-\mathrm{d}} \int_{\mathbb{R}^{\mathrm{d}}} e^{i\boldsymbol{x}\cdot\boldsymbol{\xi}} \lambda_\delta(\boldsymbol{\xi})\widehat{u}(\boldsymbol{\xi}) d\boldsymbol{\xi}.$$

By Parseval's identity, we arrive at

$$\begin{aligned}
(\Psi_{\boldsymbol{k}}, -\mathcal{L}_\delta \Psi_{\boldsymbol{k}'}) &= (2\pi)^{-\mathrm{d}} \int_{\mathbb{R}^{\mathrm{d}}} \widehat{\Psi_{\boldsymbol{k}}}(\boldsymbol{\xi})\overline{\lambda_\delta(\boldsymbol{\xi})}\overline{\widehat{\Psi_{\boldsymbol{k}'}}(\boldsymbol{\xi})} d\boldsymbol{\xi}, \\
&= (2\pi)^{-\mathrm{d}} \int_{\mathbb{R}^{\mathrm{d}}} e^{i(\boldsymbol{x}_{\boldsymbol{k}'} - \boldsymbol{x}_{\boldsymbol{k}})\cdot\boldsymbol{\xi}} \lambda_\delta(\boldsymbol{\xi}) \widehat{\Psi_{\boldsymbol{0}}}^2(\boldsymbol{\xi}) d\boldsymbol{\xi}, \\
&= (2\pi)^{-\mathrm{d}} \int_{\boldsymbol{Q}} e^{i(\boldsymbol{k}' - \boldsymbol{k})\cdot\boldsymbol{\xi}} \lambda_G(\delta, \boldsymbol{h}, \boldsymbol{\xi}) d\boldsymbol{\xi}.
\end{aligned}$$

where we have used eq. (3.13) and the Fourier transform of the cubic B-spline function eq. (3.10) is given by

$$\widehat{\phi}(\xi) = \frac{1}{2}\left(\frac{\sin(\xi/4)}{\xi/4}\right)^4.$$

Hence, we have the Fourier transform of the RK basis function as

$$\widehat{\Psi_{\boldsymbol{0}}}(\boldsymbol{\xi}) = \prod_{j=1}^{\mathrm{d}} \phi\left(\frac{x_j}{2h_j}\right)\widehat{\ }(\xi_j) = \prod_{j=1}^{\mathrm{d}} h_j \left(\frac{\sin(h_j\xi_j/2)}{(h_j\xi_j/2)}\right)^4.$$

Therefore, by eq. (3.17) we obtain the Galerkin form eq. (3.18) as

$$\begin{aligned}(i^h(u_{\boldsymbol{k}}), -\mathcal{L}_\delta i^h(v_{\boldsymbol{k}})) &= (2\pi)^{-\mathrm{d}} \sum_{\boldsymbol{k},\boldsymbol{k'}\in\mathbb{Z}^{\mathrm{d}}} u_{\boldsymbol{k}}\overline{v_{\boldsymbol{k'}}} \int_{\boldsymbol{Q}} e^{i(\boldsymbol{k'}-\boldsymbol{k})\cdot\boldsymbol{\xi}}\lambda_G(\delta,\boldsymbol{h},\boldsymbol{\xi})d\boldsymbol{\xi},\\ &= (2\pi)^{-\mathrm{d}} \int_{\boldsymbol{Q}} \widetilde{u}(\boldsymbol{\xi})\overline{\widetilde{v}(\boldsymbol{\xi})}\lambda_G(\delta,\boldsymbol{h},\boldsymbol{\xi})d\boldsymbol{\xi}\,.\end{aligned}$$

Next, following the same procedure, we arrive at the collocation matrix expressed as

$$\begin{aligned}-\mathcal{L}_\delta \Psi_{\boldsymbol{k'}}(\boldsymbol{x}_{\boldsymbol{k}}) &= (2\pi)^{-\mathrm{d}} \int_{\mathbb{R}^d} e^{i\boldsymbol{x}_{\boldsymbol{k}}\cdot\boldsymbol{\xi}}\lambda_\delta(\boldsymbol{\xi})\widehat{\Psi_{\boldsymbol{k'}}}(\boldsymbol{\xi})d\boldsymbol{\xi},\\ &= (2\pi)^{-\mathrm{d}} \int_{\mathbb{R}^{\mathrm{d}}} e^{i(\boldsymbol{x}_{\boldsymbol{k}}-\boldsymbol{x}_{\boldsymbol{k'}})\cdot\boldsymbol{\xi}}\lambda_\delta(\boldsymbol{\xi})\widehat{\Psi_{\boldsymbol{0}}}(\boldsymbol{\xi})d\boldsymbol{\xi},\\ &= (2\pi)^{-\mathrm{d}} \int_{\boldsymbol{Q}} e^{i(\boldsymbol{k}-\boldsymbol{k'})\cdot\boldsymbol{\xi}}\lambda_C(\delta,\boldsymbol{h},\boldsymbol{\xi})d\boldsymbol{\xi}\,.\end{aligned}$$

Therefore, the collocation form eq. (3.19) is written as

$$\begin{aligned}((u_{\boldsymbol{k}}), -r^h\mathcal{L}_\delta i^h(v_{\boldsymbol{k}}))_{l^2} &= (2\pi)^{-\mathrm{d}} \sum_{\boldsymbol{k},\boldsymbol{k'}\in\mathbb{Z}^{\mathrm{d}}} u_{\boldsymbol{k}}\overline{v_{\boldsymbol{k'}}} \int_{\boldsymbol{Q}} e^{i(\boldsymbol{k'}-\boldsymbol{k})\cdot\boldsymbol{\xi}}\lambda_C(\delta,\boldsymbol{h},\boldsymbol{\xi})d\boldsymbol{\xi},\\ &= (2\pi)^{-\mathrm{d}} \int_{\boldsymbol{Q}} \widetilde{u}(\boldsymbol{\xi})\overline{\widetilde{v}(\boldsymbol{\xi})}\lambda_C(\delta,\boldsymbol{h},\boldsymbol{\xi})d\boldsymbol{\xi}.\end{aligned}$$

This finishes the proof of (ii).

With (i) and (ii) being established, it is easy to see (iii) by the fact that $\lambda_\delta(\boldsymbol{\xi})$ is non-negative and $0 \le \widehat{\Psi_{\boldsymbol{0}}}(\boldsymbol{\xi}) \le 1$. □

Remark 3.3.3. *$\lambda_C(\boldsymbol{\xi})$ defined in (3.22) is in fact the same as the Fourier representation of the Galerkin scheme with basis function defined by the tensor product of linear B-splines. This shows the equivalence of some special RK collocation schemes with certain non-standard Galerkin schemes.*

We need the following lemma that says the $|\cdot|_h$ norm defined through the RK basis and discrete l^2 norm are equivalent.

Lemma 3.3.4. *The following two norms are equivalent, i.e., there exist two constants $C_1, C_2 > 0$ independent of h, such that*

$$C_1\|u\|_{l^2(\mathbb{R}^{\mathrm{d}})} \le |(u_{\boldsymbol{k}})_{\boldsymbol{k}\in\mathbb{Z}^{\mathrm{d}}}|_h \le C_2\|u\|_{l^2(\mathbb{R}^{\mathrm{d}})}.$$

Proof. First, from Parsevel's identity, we can write the l^2 norm as

$$\begin{aligned}\|u\|^2_{l^2(\mathbb{R}^{\mathrm{d}})} &= \prod_{j=1}^{\mathrm{d}} h_j \sum_{\boldsymbol{k}\in\mathbb{Z}^d} u_{\boldsymbol{k}}\overline{u_{\boldsymbol{k}}},\\ &= (2\pi)^{-\mathrm{d}} \prod_{j=1}^{\mathrm{d}} h_j \int_{\boldsymbol{Q}} \widetilde{u}^2(\boldsymbol{\xi}) d\boldsymbol{\xi}.\end{aligned}$$

Then, similar to the proof of Lemma 3.3.2 (i), by replacing the nonlocal diffusion operator with the identity operator, we obtain

$$|(u_{\boldsymbol{k}})_{\boldsymbol{k}\in\mathbb{Z}^{\mathrm{d}}}|_h^2 = (i^h(u_{\boldsymbol{k}}), i^h(u_{\boldsymbol{k}})) = (2\pi)^{-\mathrm{d}} \prod_{j=1}^{\mathrm{d}} h_j \int_{\boldsymbol{Q}} \lambda^h(\boldsymbol{\xi})\widetilde{u}^2(\boldsymbol{\xi}) d\boldsymbol{\xi},$$

where $\lambda^h(\boldsymbol{\xi})$ is continuous and strictly positive,

$$\lambda^h(\boldsymbol{\xi}) = 2^{8\mathrm{d}} \sum_{\boldsymbol{r}\in\mathbb{Z}^{\mathrm{d}}} \prod_{j=1}^{\mathrm{d}} \left(\frac{\sin(\xi_j/2)}{\xi_j + 2\pi r_j}\right)^8.$$

Thus, $\lambda^h(\boldsymbol{\xi})$ is bounded above and below on $\boldsymbol{Q}$. Therefore, we complete the proof. □

Proof of of Theorem 3.3.1. For all sequences $(u_{\boldsymbol{k}}), (v_{\boldsymbol{k}})$, we derive via the Cauchy-Schwartz inequality and Lemma 3.3.4

$$\begin{aligned}|((u_{\boldsymbol{k}}), (v_{\boldsymbol{k}}))_{l^2}| &= \prod_{j=1}^{\mathrm{d}} h_j \left|\sum_{\boldsymbol{k}\in\mathbb{Z}^{\mathrm{d}}} u_{\boldsymbol{k}}\overline{v_{\boldsymbol{k}}}\right|,\\ &\le \left(\prod_{j=1}^{\mathrm{d}} h_j \sum_{\boldsymbol{k}\in\mathbb{Z}^{\mathrm{d}}} |u_{\boldsymbol{k}}|^2\right)^{1/2} \left(\prod_{j=1}^{\mathrm{d}} h_j \sum_{\boldsymbol{k}\in\mathbb{Z}^{\mathrm{d}}} |v_{\boldsymbol{k}}|^2\right)^{1/2},\\ &\le C|(u_{\boldsymbol{k}})|_h \cdot |(v_{\boldsymbol{k}})|_h.\end{aligned} \tag{3.23}$$

Finally, for $u \in S(\square \cap \Omega)$ we may write $u = i^h(u_{\boldsymbol{k}})$ by definition, and thus we have

$$\begin{aligned} |(u_{\boldsymbol{k}})|_h \cdot \left|r_\Omega^h(-\mathcal{L}_\delta u)\right|_h &\geq C\left|((u_{\boldsymbol{k}}), r_\Omega^h(-\mathcal{L}_\delta u))_{l^2}\right|, \\ &= C\left|((u_{\boldsymbol{k}}), r^h(-\mathcal{L}_\delta i^h(u_{\boldsymbol{k}})))_{l^2}\right|, \\ &\geq C\left|(i^h(u_{\boldsymbol{k}}), (-\mathcal{L}_\delta i^h(u_{\boldsymbol{k}})))\right|, \\ &\geq C\|u\|^2_{L^2(\mathbb{R}^{\mathrm{d}})}. \end{aligned}$$

The first line is a result of eq. (3.23) and the second line is by the definition of $S(\square\cap\Omega)$. Lemma 3.3.2 (iii) shows the third line and the fourth line is the stability given by Lemma 3.1.1 since $u \in S(\square \cap \Omega) \subset \mathcal{S}_\delta$. □

3.3.2 Consistency

In this subsection, we discuss uniform consistency of the RK collocation method for the nonlocal diffusion models. The truncation error has a uniform bound independent of the nonlocal scaling parameter δ. Combining the stability result in subsection 3.3.1 and the truncation error analysis to be presented shortly, we show that the RK collocation method is convergent. The asymptotic compatibility of the method is based on one important property of RK approximation – the synchronized convergence property of the linear RK approximation. Synchronized convergence means the convergence rates measured by higher-order error norms are of the same order as the ones measured by lower-order error norms. The linear RK approximation has the synchronized convergence is a long-known fact [73, 74] and we provide the statement in Lemma 3.3.6 without proof.

Another important property of the collocation scheme is the quadratic exactness which plays a crucial role in showing the uniform consistency of many numerical methods on nonlocal diffusion models [110, 37]. Even though Lemma 3.3.5 is not

needed in the consistency proof, we still present it here to show that the RK collocation scheme also has this property.

Lemma 3.3.5. ***(Quadratic Exactness)*** *For quadratic polynomials in* $\mathbb{R}^{\mathrm{d}}$ *as* $u(\boldsymbol{x}) = \boldsymbol{x}^{\boldsymbol{\alpha}}$, $|\boldsymbol{\alpha}| = 2$, *we have*

$$\sum_{|\boldsymbol{\alpha}|=2} \mathcal{L}_\delta \Pi^h \boldsymbol{x}^{\boldsymbol{\alpha}} = \sum_{|\boldsymbol{\alpha}|=2} \mathcal{L}_\delta \boldsymbol{x}^{\boldsymbol{\alpha}} = \mathrm{d}.$$

Proof. Let $\boldsymbol{x} = (x_1, x_2, \ldots, x_{\mathrm{d}})$ and $\boldsymbol{\alpha} = (\alpha_1, \alpha_2, \ldots, \alpha_{\mathrm{d}})$. From the definition of the nonlocal diffusion operator and the first-order polynomial reproduction property of the RK approximation, it is easy to see that

$$\sum_{|\boldsymbol{\alpha}|\leq 1} \mathcal{L}_\delta \Pi^h \boldsymbol{x}^{\boldsymbol{\alpha}} = \sum_{|\boldsymbol{\alpha}|\leq 1} \mathcal{L}_\delta \boldsymbol{x}^{\boldsymbol{\alpha}} = 0.$$

Then it is sufficient to show the cases when $|\boldsymbol{\alpha}| = 2$. We observe that for quadratic polynomials,

$$\sum_{|\boldsymbol{\alpha}|=2} \Pi^h \boldsymbol{x}^{\boldsymbol{\alpha}} = \sum_{|\boldsymbol{\alpha}|=2} \left[\boldsymbol{m}_{\boldsymbol{\alpha}}(\boldsymbol{x}) + \boldsymbol{x}^{\boldsymbol{\alpha}}\right]. \tag{3.24}$$

There are only two cases for $|\boldsymbol{\alpha}| = 2$. The first case is that there exist $i, j \in \{1, 2, \cdots \mathrm{d}\}$ and $i \neq j$ such that $\alpha_i = \alpha_j = 1$. In this case

$$\begin{aligned}\Pi^h \boldsymbol{x}^{\boldsymbol{\alpha}} &= \sum_{\boldsymbol{k}\in\mathbb{Z}^{\mathrm{d}}} \Psi_{\boldsymbol{k}}(\boldsymbol{x})(\boldsymbol{x}_{\boldsymbol{k}})^{\boldsymbol{\alpha}} = \sum_{\boldsymbol{k}\in\mathbb{Z}^{\mathrm{d}}} \Psi_{\boldsymbol{k}}(\boldsymbol{x}) x_{k_i} x_{k_j} \\ &= \sum_{k_i\in\mathbb{Z}} \sum_{k_j\in\mathbb{Z}} \phi_{a_i}(x_i - x_{k_i})\phi_{a_j}(x_j - x_{k_j}) x_{k_i} x_{k_j} = x_i x_j\,,\end{aligned}$$

where $\Psi_{\boldsymbol{k}}(\boldsymbol{x})$ is given by eq. (3.13). The second case is that there exists $j \in \{1, 2, \cdots \mathrm{d}\}$ with $\alpha_j = 2$, then

$$\Pi^h \boldsymbol{x}^{\boldsymbol{\alpha}} = \sum_{\boldsymbol{k}\in\mathbb{Z}^{\mathrm{d}}} \Psi_{\boldsymbol{k}}(\boldsymbol{x}) x_{k_j}^2 = \sum_{\boldsymbol{k}\in\mathbb{Z}^{\mathrm{d}}} \Psi_{\boldsymbol{k}}(\boldsymbol{x}) \left(x_{k_j}^2 - 2x_j x_{k_j} + 2x_j^2\right) = m_2(x_j) + x_j^2\,.$$

In both cases, we have eq. (3.24). From Lemma 3.2.2 and eq. (3.14), for $|\boldsymbol{\alpha}| = 2$, $\boldsymbol{m}_{\boldsymbol{\alpha}}(\boldsymbol{x})$ is a constant which does not depend on $\boldsymbol{x}$, thus

$$\sum_{|\boldsymbol{\alpha}|=2} \mathcal{L}_\delta \boldsymbol{m}_{\boldsymbol{\alpha}}(\boldsymbol{x}) = 0.$$

Therefore we have completed the proof. □

We remark that although the RK shape function eq. (3.13) can only reproduce linear polynomials, eq. (3.24) is the key for the RK collocation method to satisfy the quadratic exactness condition. In order to show convergence, we need another property (synchronized convergence) of the RK approximation with carefully chosen window function and support sizes. The result was first developed in [73] with approximation error measured by Sobolev norms. It is natural that the synchronized convergence is also valid pointwise under a stronger regularity assumption for the approximated function. Here we present the result without proof and readers should see [73, 74] for more details.

Lemma 3.3.6. ***(Synchronized Convergence)*** *Assume $u(\boldsymbol{x}) \in C^4(\mathbb{R}^{\mathrm{d}})$ and $\Pi^h u$ is the RK interpolation with the shape function given by eq. (3.13). $\Pi^h u$ has synchronized convergence, namely*

$$\left|D^{\boldsymbol{\alpha}}(\Pi^h u - u)\right|_\infty \leq C|u^{(|\boldsymbol{\alpha}|+2)}|_\infty h_{\max}^2, \quad \text{for } |\boldsymbol{\alpha}| = 0, 1, 2,$$

where C is a generic constant independent of $h_{\max}$.

Here and in the rest of the paper, we adopt the following notations for a function $u \in C^n(\mathbb{R}^{\mathrm{d}})$,

$$|u|_\infty = \sup_{\boldsymbol{x}\in\mathbb{R}^{\mathrm{d}}} |u(\boldsymbol{x})|, \text{ and } |u^{(l)}|_\infty = \sup_{|\boldsymbol{\beta}|=l} \sup_{\boldsymbol{y}\in\mathbb{R}^{\mathrm{d}}} |D^{\boldsymbol{\beta}} u(\boldsymbol{y})| \ (1 \leq l \leq n).$$

Now we are ready to present the truncation error analysis of the RK collocation method for the nonlocal diffusion models.

Lemma 3.3.7. ***(Uniform consistency)*** *Assume $u(\boldsymbol{x}) \in C^4(\mathbb{R}^{\mathrm{d}})$, then*

$$\left|r^h \mathcal{L}_\delta \Pi^h u - r^h \mathcal{L}_\delta u\right|_h \leq C h_{\max}^2 |u^{(4)}|_\infty,$$

where C is independent of $h_{\max}$ and δ.

Proof. For any $\boldsymbol{x} \in \mathbb{R}^{\mathrm{d}}$, we define the interpolation error of $u(\boldsymbol{x})$ as

$$E(\boldsymbol{x}) = \Pi^h u(\boldsymbol{x}) - u(\boldsymbol{x}). \tag{3.25}$$

Restricting to the grid $\square$, the truncation error is given by

$$\left|\mathcal{L}_\delta \left(\Pi^h u - u\right)(\boldsymbol{x_k})\right| = \left|\int_{B_\delta} \rho_\delta(|\boldsymbol{s}|)\left(E(\boldsymbol{x_k}+\boldsymbol{s}) - E(\boldsymbol{x_k})\right) d\boldsymbol{s}\right|. \tag{3.26}$$

Using Lemma 3.3.6 on $E = \Pi^h u - u$, we have

$$\begin{aligned} |E(\boldsymbol{x_k}+\boldsymbol{s}) + E(\boldsymbol{x_k}-\boldsymbol{s}) - 2E(\boldsymbol{x})| &\leq C|\boldsymbol{s}|^2 \max_{|\boldsymbol{\alpha}|=2} \left|D^{\boldsymbol{\alpha}} E\right|_\infty \\ &\leq C|\boldsymbol{s}|^2 |u^{(4)}|_\infty h_{\max}^2 . \end{aligned} \tag{3.27}$$

Now combing eqs. (3.26) and (3.27), and by the symmetry of the kernel ρ_δ, we arrive at

$$\left|\mathcal{L}_\delta \left(\Pi^h u - u\right)(\boldsymbol{x_k})\right| \leq C h_{\max}^2 |u^{(4)}|_\infty .$$

where C is a generic constant, independent of $h_{\max}$ and δ. Finally, the proof is finished by interpolating the truncation error. $\square$

The convergence theorem is now presented as a result of the stability (Theorem 3.3.1) and consistency (Lemma 3.3.7). We will show first that the numerical solution converges to the nonlocal solution for fixed δ as mesh size decreases, and then the convergence to the local solution as δ and mesh size both decrease to zero.

Theorem 3.3.8. ***(Uniform Convergence to nonlocal solution)*** *For a fixed $\delta \in (0, \delta_0]$, assume the nonlocal exact solution u^δ is sufficiently smooth, i.e., $u^\delta \in C^4(\overline{\Omega_\delta})$.*

Moreover, assume $|u^{\delta(4)}|_\infty$ *is uniformly bounded for every* δ*. Let* $u^{\delta,h}$ *be the numerical solution of the collocation scheme eq. (3.15). Then,*

$$\|u^\delta - u^{\delta,h}\|_{L^2(\Omega)} \leq Ch_{\max}^2,$$

where C *is independent of* $h_{\max}$ *and* δ*.*

Proof. Notice that since $u^\delta = 0$ on $\Omega_\mathcal{I}$ and $u^\delta \in C^4(\overline{\Omega_\delta})$, we can extend u^δ to $\mathbb{R}^\mathrm{d}$ by zero such that $u^\delta \in C^4(\mathbb{R}^\mathrm{d})$. From the RK collocation scheme eq. (3.15) and the nonlocal equation eq. (3.2), we have

$$-r_\Omega^h \mathcal{L}_\delta u^{\delta,h} = r_\Omega^h f = -r_\Omega^h \mathcal{L}_\delta u^\delta \,.$$

Combining Theorem 3.3.1, Lemma 3.3.7 and the above equation, we obtain

$$\begin{aligned}
\|\Pi^h u^\delta - u^{\delta,h}\|_{L^2(\mathbb{R}^\mathrm{d})} &\leq C \left| r_\Omega^h \mathcal{L}_\delta \left(\Pi^h u^\delta - u^{\delta,h} \right) \right|_h , \\
&\leq C \left| r_\Omega^h \mathcal{L}_\delta \Pi^h u^\delta - r_\Omega^h \mathcal{L}_\delta u^{\delta,h} \right|_h , \\
&\leq C \left| r_\Omega^h \mathcal{L}_\delta \Pi^h u^\delta - r_\Omega^h \mathcal{L}_\delta u^{\delta} \right|_h , \\
&\leq Ch_{\max}^2 \,.
\end{aligned}$$

Finally, from the triangle inequality, we arrive at

$$\|u^\delta - u^{\delta,h}\|_{L^2(\mathbb{R}^\mathrm{d})} \leq \|u^\delta - \Pi^h u^\delta\|_{L^2(\mathbb{R}^\mathrm{d})} + \|\Pi^h u^\delta - u^{\delta,h}\|_{L^2(\mathbb{R}^\mathrm{d})} \leq Ch_{\max}^2.$$

where we have used the approximation property of the RK approximation. □

Next, we show that the convergence of the RK collocation scheme to the correct local limit model is indeed uniform and is independent of δ. We start by bounding the truncation error between the collocation scheme and the local limit of the nonlocal model.

Lemma 3.3.9. ***(Discrete model error I)*** *Assume $u(\boldsymbol{x}) \in C^4(\mathbb{R}^{\mathrm{d}})$, then*

$$\left|r^h \mathcal{L}_\delta \Pi^h u - r^h \mathcal{L}_0 u\right|_h \leq C|u^{(4)}|_\infty (h_{\max}^2 + \delta^2),$$

where C is independent of $h_{\max}$ and δ.

Proof. From Lemma 3.3.7 and the continuum property of the nonlocal operators, we have

$$\begin{aligned}\left|r^h \mathcal{L}_\delta \Pi^h u - r^h \mathcal{L}_0 u\right|_h &\leq \left|r^h \mathcal{L}_\delta \Pi^h u - r^h \mathcal{L}_\delta u\right|_h + \left|r^h \mathcal{L}_\delta u - r^h \mathcal{L}_0 u\right|_h, \\ &\leq C|u^{(4)}|_\infty (h_{\max}^2 + \delta^2),,\end{aligned}$$

□

Combining Theorem 3.3.1 and Lemma 3.3.9, we have uniform convergence (asymptotic compatibility) to the local limit.

Theorem 3.3.10. ***(Asymptotic compatibility)*** *Assume the local exact solution u^0 is sufficiently smooth, i.e., $u^0 \in C^4(\overline{\Omega_{\delta_0}})$. For any $\delta \in (0, \delta_0]$, $u^{\delta,h}$ is the numerical solution of the collocation scheme eq. (3.15), then,*

$$\|u^0 - u^{\delta,h}\|_{L^2(\Omega)} \leq C(h_{\max}^2 + \delta^2).$$

Proof. The proof is similar to Theorem 3.3.8. Note that we also assume $u^0(\boldsymbol{x}) = 0$ for $\boldsymbol{x}$ outside of Ω. First, recall the collocation equation and its local limit,

$$-r_\Omega^h \mathcal{L}_\delta u^{\delta,h} = r_\Omega^h f = -r_\Omega^h \mathcal{L}_0 u^0 .$$

Then, from Theorem 3.3.1, Lemma 3.3.9 and the above equation, we obtain

$$
\begin{aligned}
\|\Pi^h u^0 - u^{\delta,h}\|_{L^2(\mathbb{R}^{\mathrm{d}})} &\leq C \left| r_\Omega^h \mathcal{L}_\delta \left(\Pi^h u^0 - u^{\delta,h} \right) \right|_h , \\
&\leq C \left| r_\Omega^h \mathcal{L}_\delta \Pi^h u^0 - r_\Omega^h \mathcal{L}_\delta u^{\delta,h} \right|_h , \\
&\leq C \left| r_\Omega^h \mathcal{L}_\delta \Pi^h u^0 - r_\Omega^h \mathcal{L}_0 u^0 \right|_h , \\
&\leq C h_{\max}^2 .
\end{aligned}
$$

Finally, we finish the proof by applying the triangle inequality

$$
\|u^0 - u^{\delta,h}\|_{L^2(\mathbb{R}^{\mathrm{d}})} \leq \|u^0 - \Pi^h u^0\|_{L^2(\mathbb{R}^{\mathrm{d}})} + \|\Pi^h u^0 - u^{\delta,h}\|_{L^2(\mathbb{R}^{\mathrm{d}})} \leq C(h_{\max}^2 + \delta^2).
$$

□

3.4 Numerical example

To validate the convergence analysis in the previous sections, we consider a numerical example in two dimensions. Using the manufactured solution $u(x_1, x_2) = x_1^2(1 - x_1^2) + x_2^2(1 - x_2^2)$ to calculate the right-hand side of eqs. (3.2) and (3.5), we obtain,

$$
f_0(\boldsymbol{x}) = 12(x_1^2 + x_2^2) - 4 \text{ and } f_\delta(\boldsymbol{x}) = f_0(\boldsymbol{x}) + 2\delta^2.
$$

and impose the corresponding values of $u(\boldsymbol{x})$ on $\Omega_{\mathcal{I}}$ such that the exact value to the local limit matches on Ω. Let $\Omega = (0, 1)^2$ and for a fixed δ, we investigate the convergence rate of the RK collocation scheme in section 3.3 for the following nonlocal equation

$$
\begin{cases}
-\mathcal{L}_\delta u(\boldsymbol{x}) = f_\delta(\boldsymbol{x}), & \boldsymbol{x} \in \Omega, \\
u(\boldsymbol{x}) = x_1^2(1 - x_1^2) + x_2^2(1 - x_2^2), & \boldsymbol{x} \in \Omega_{\mathcal{I}} ,
\end{cases}
\tag{3.28}
$$

since the exact solution of (3.28) is given. The nonlocal kernel is chosen as $\rho_\delta(|\boldsymbol{s}|) = \frac{4}{\pi\delta^4}$. To verify the asymptotic compatibility of our scheme where δ also goes zero,

we replace the right hand side f_δ of (3.28) with f_0, and test the convergence of the numerical solution of the following nonlocal diffusion problem

$$\begin{cases} -\mathcal{L}_\delta u(\boldsymbol{x}) = f_0(\boldsymbol{x}), & \boldsymbol{x} \in \Omega, \\ u(\boldsymbol{x}) = x_1^2(1-x_1^2) + x_2^2(1-x_2^2), & \boldsymbol{x} \in \Omega_{\mathcal{I}}, \end{cases} \tag{3.29}$$

to the solution of the local problem given by

$$\begin{cases} -\Delta u(\boldsymbol{x}) = f_0(\boldsymbol{x}), & \boldsymbol{x} \in \Omega, \\ u(\boldsymbol{x}) = 0, & \boldsymbol{x} \in \partial\Omega. \end{cases}$$

We apply the collocation scheme analyzed in section 3.3 and investigate their convergence properties. We choose the discretization parameter as $h_1 = 2h_2$ (so $h_{\max} = h_1$), and then study the convergence of the numerical solution to the nonlocal solution eq. (3.28) and local solution eq. (3.29). Note that we assume the nonlocal integration is evaluated exactly using high-order Gauss quadrature points. The distribution of the Gauss quadrature points in the horizon is shown in Figure 3.2 and more details are discussed in [95].

Convergence profiles are shown in Figure 3.3. We investigate the convergence behaviour when the nonlocal length scale δ is coupled with discretization parameter $h_{\max}$ in various ways. When δ is fixed, the numerical solution converges to the nonlocal solution at a second-order convergence rate. When both δ and $h_{\max}$ go to zero, the numerical solution converges to the local limit. When δ goes to zero faster ($\delta = h_{\max}^2$) and at the same rate as $h_{\max}$, ($\delta = h_{\max}$), the convergence is of second order. When δ approaches zero slower than $h_{\max}$, ($\delta = \sqrt{h_{\max}}$), we observe first-order convergence rate. The numerical examples agree with Theorem 3.3.10 and this verifies that the RK collocation method is asymptotically compatible.

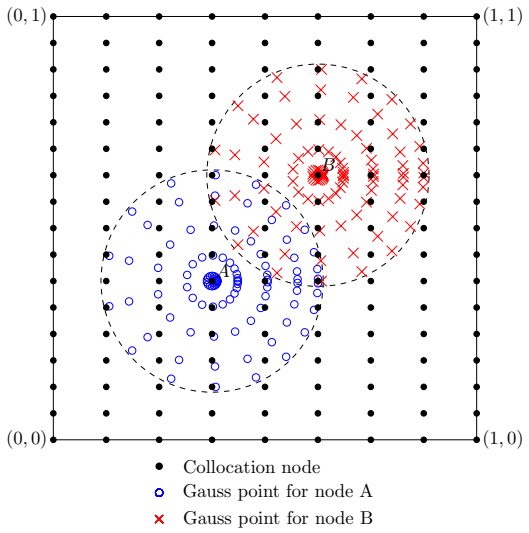

Figure 3.2: Meshfree discretization of a two-dimensional unit square domain with integration points within the neighborhood of each node. The dashed lines represent the limits of the neighborhoods of nodes A and B.

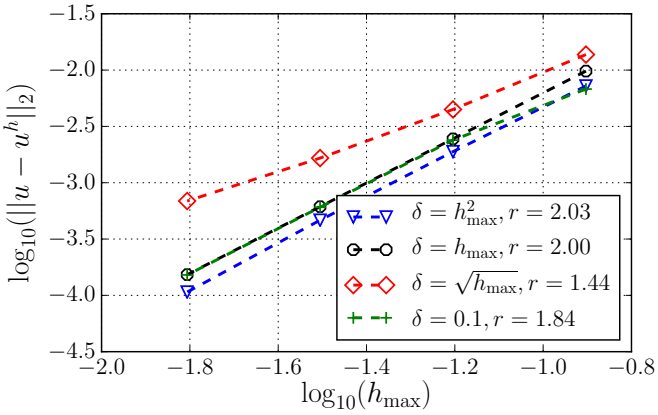

Figure 3.3: Convergence profiles using the RK collocation method.

Chapter 4

Quasi-discrete nonlocal diffusion

The RK collocation method for the nonlocal diffusion model as introduced in Chapter 3 is AC, but it is not practical in the sense that it is rather difficult to exactly evaluate the integral in the nonlocal diffusion operator, especially if the nonlocal kernel is singular. In [95], two Gauss quadrature schemes are investigated and high-order Gauss quadrature rules are necessary for both schemes to obtain algebraic convergence. Section 3.4 also discussed more details of one Gauss quadrature scheme.

To mitigate this computational complexity, in this chapter[1] we introduce a new nonlocal diffusion operator where the integral is replaced by finite summation of point evaluations in the horizon. We call it the quasi-discrete nonlocal diffusion operator. Whenever the local limit is concerned, it is much easier to use the quasi-discrete nonlocal operator than to use Gauss quadrature rules for integration. A similar technique has been proposed in [113] utilizing an optimization construction which admits interpretation as a generalized moving least squares (GMLS) process. We additionally illustrate a connection between the proposed technique and the GMLS process. Then, we show that the numerical solution of the RK collocation for the quasi-discrete nonlocal diffusion converges to the solution of local equation as δ and mesh size $h_{\max}$ both approach zero. The theoretical results are then validated using numerical experiments.

[1] This chapter is a part of [71]. The author's contribution includes theoretical derivation and conducting numerical experiments.

This chapter is organized as follows. A quasi-discrete nonlocal diffusion operator is developed in section 4.1. Convergence analysis of the RK collocation for the quasi-discrete nonlocal diffusion is presented in section 4.2. Section 4.3 gives numerical examples to verify our analysis.

4.1 Quasi-discrete nonlocal operators

4.1.1 Quasi-discrete nonlocal diffusion

For each $\boldsymbol{x}$, we use a finite number of quadrature points in the δ-neighborhood of $\boldsymbol{x}$ to approximation the integral in eq. (3.1). Assume $u(\boldsymbol{x}) \in C^0(\Omega_\delta)$, we define the quasi-discrete nonlocal diffusion operator $\mathcal{L}_\delta^\epsilon$ as

$$\mathcal{L}_\delta^\epsilon u(\boldsymbol{x}) = 2 \sum_{\boldsymbol{s} \in B_\delta^\epsilon(\mathbf{0})} \omega_\delta(\boldsymbol{s}) \rho_\delta(|\boldsymbol{s}|)(u(\boldsymbol{x}+\boldsymbol{s}) - u(\boldsymbol{x})), \quad \forall\, \boldsymbol{x} \in \Omega \tag{4.1}$$

where $\omega_\delta(\boldsymbol{s})$ is the quadrature weight at the quadrature point $\boldsymbol{s}$ and $B_\delta^\epsilon(\mathbf{0})$ is a finite collection of symmetric quadrature points $\boldsymbol{s}$ in the ball of radius δ about $\mathbf{0}$. We use the notation B_δ^ϵ to denote $B_\delta^\epsilon(\mathbf{0})$ for the rest of the dissertation. The superscript ϵ can be seen as the smallest distance between neighboring quadrature points and ϵ is independent of the spatial discretization applied to u later in section 4.2. We assume that the number of points in B_δ^ϵ, N_d, is a fixed number which only depends on the dimension, d, and N_d will be specified later. This effectively means that the ratio ϵ/δ is a fixed number. An example of quadrature points in the horizon of a given point $\boldsymbol{x} \in \Omega \subset \mathbb{R}^2$ is shown in Figure 4.1.

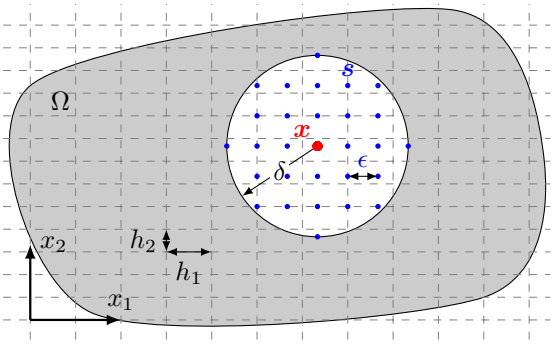

Figure 4.1: Quadrature points (blue dots) are shown in the horizon of $\boldsymbol{x} \in \Omega$. The dashed lines form the grid for the RK collocation scheme that will be applied later in section 4.2. $\boldsymbol{x}$ is not necessarily the grid point. The quadrature points are independent of the collocation points on the grid.

Note that although the evaluation of $\mathcal{L}_\delta^\epsilon u(\boldsymbol{x})$ only needs a finite summation, it is actually a continuous function in $\boldsymbol{x}$, and thus it bears the name of quasi-discrete nonlocal operator. Next we impose the conditions on $\mathcal{L}_\delta^\epsilon$ so that the numerical solution converges to the correct local limit. Recall the nonlocal kernel $\rho_\delta(|\boldsymbol{s}|)$ introduced in section 3.1 has a bounded second-order moment as in eq. (3.4). Therefore, the nonlocal diffusion operator $\mathcal{L}_\delta$ acting on constant, linear and quadratic polynomials has the following results

$$\mathcal{L}_\delta \boldsymbol{x}^0 = 0; \quad \mathcal{L}_\delta \boldsymbol{x}^{\boldsymbol{\alpha}} = 0, \text{ for } |\boldsymbol{\alpha}| = 1; \quad \sum_{|\boldsymbol{\alpha}|=2} \mathcal{L}_\delta \boldsymbol{x}^{\boldsymbol{\alpha}} = 2\mathrm{d}. \tag{4.2}$$

We proceed to design quadrature weights $\omega_\delta(\boldsymbol{s})$ such that $\mathcal{L}_\delta^\epsilon$ satisfies the same conditions as eq. (4.2),

$$\mathcal{L}_\delta^\epsilon \boldsymbol{x}^0 = 0; \quad \mathcal{L}_\delta^\epsilon \boldsymbol{x}^{\boldsymbol{\alpha}} = 0, \text{ for } |\boldsymbol{\alpha}| = 1; \quad \sum_{|\boldsymbol{\alpha}|=2} \mathcal{L}_\delta^\epsilon \boldsymbol{x}^{\boldsymbol{\alpha}} = 2\mathrm{d}. \tag{4.3}$$

There are many ways to design the quadrature weights $\omega_\delta(\boldsymbol{s})$. We present two approaches, one is using the RK approximation developed in [94] and the other is in the framework of GMLS as in [113]. We modify the RK approach and emphasize the

positivity of the weights in the following subsection. The convergence analysis shown in section 4.2 works for both the RK approach and the GMLS framework.

4.1.2 Quadrature weights using the RK approximation

Note that eq. (4.3) can be seen as a reproducing condition for polynomials up to second order. We can thus solve for the quadrature weights ω_δ under the same framework presented in Chapter 2. Due to the scaling of the nonlocal kernel $\rho_\delta(|\boldsymbol{s}|)$ as shown in eq. (3.3), $\omega_\delta(\boldsymbol{s})$ has the following scaling

$$\omega_\delta(\boldsymbol{s}) = \delta^{\mathrm{d}}\omega\left(\frac{\boldsymbol{s}}{\delta}\right),$$

where $\omega(\boldsymbol{s})$ is the quadrature weight at $\boldsymbol{s} \in B_1^{\epsilon_1}$ and $\epsilon_1 = \epsilon/\delta$ by scaling. $B_1^{\epsilon_1}$ is a finite collection of quadrature points in the unit ball. Since we assume that the number of points in the set B_δ^ϵ is fixed, this implies ϵ_1 is a fixed number. We next present the construction of $\omega(\boldsymbol{s})$ in $B_1^{\epsilon_1}$ so that for a general horizon δ, $\omega_\delta(\boldsymbol{s})$ can be obtained by rescaling. Without loss of generality, we assume $\boldsymbol{x} = \boldsymbol{0}$ in eq. (4.1). If we define

$$f(\boldsymbol{s}) = \rho(\boldsymbol{s})(u(\delta\boldsymbol{s}) - u(\boldsymbol{0})) \tag{4.4}$$

the problem is then equivalent to finding out the weights $\omega(\boldsymbol{s})$ such that

$$\sum_{\boldsymbol{s}\in B_1^{\epsilon_1}} \omega(\boldsymbol{s}) f(\boldsymbol{s}) d\boldsymbol{s} = \int_{B_1} f(\boldsymbol{s}) d\boldsymbol{s}\,, \tag{4.5}$$

where f is taken from a certain finite dimensional space. Condition eq. (4.3) is now interpreted as eq. (4.5) for f in the form of eq. (4.4) where u is taken from the space of polynomials up to second order. Notice that for u being a constant function, f is identically zero and eq. (4.5) is satisfied trivially. Therefore we only need to consider eq. (4.5) for

$$f(\boldsymbol{s}) = \rho(\boldsymbol{s})V(\boldsymbol{s}),\ \text{where } V(\boldsymbol{s}) = \boldsymbol{s}^{\boldsymbol{\alpha}}, 1 \le |\boldsymbol{\alpha}| \le 2. \tag{4.6}$$

Now we use a similar approach as the RK approximation presented in subsection 2.1.2 to find the weights. Define

$$\omega(\boldsymbol{s}) = C(\boldsymbol{s})\phi(|\boldsymbol{s}|), \tag{4.7}$$

where ϕ is taken to be the cubic B-spline function eq. (3.10) and $C(\boldsymbol{s})$ is the correction function that takes the form

$$C(\boldsymbol{s}) = \hat{\boldsymbol{H}}^T(\boldsymbol{s})\boldsymbol{b}, \tag{4.8}$$

where $\hat{\boldsymbol{H}}(\boldsymbol{s}) = [\{\boldsymbol{s}^{\boldsymbol{\alpha}}\}_{1\leq|\boldsymbol{\alpha}|\leq 2}]^T$ and $\boldsymbol{b}$ is a constant vector to be determined. For example, in two dimensions we have

$$\hat{\boldsymbol{H}}(\boldsymbol{s}) = [s_1, s_2, s_1^2, s_1 s_2, s_2^2]^T.$$

Substituting eqs. (4.6)–(4.8) into eq. (4.5), we obtain the following system for $\boldsymbol{b}$:

$$\widetilde{\boldsymbol{M}}\boldsymbol{b} = \widetilde{\boldsymbol{H}}_{\mathrm{d}}, \tag{4.9}$$

where $\widetilde{\boldsymbol{M}}$ is the moment matrix given by

$$\widetilde{\boldsymbol{M}} = \sum_{\boldsymbol{s}\in B_1^{\epsilon 1}} \hat{\boldsymbol{H}}(\boldsymbol{s})\rho(|\boldsymbol{s}|)\phi(|\boldsymbol{s}|)\hat{\boldsymbol{H}}^T(\boldsymbol{s}). \tag{4.10}$$

and $\widetilde{\boldsymbol{H}}_{\mathrm{d}}$ is the constant vector consisting the right hand side of eq. (4.3) when taking $f(\boldsymbol{s}) = \rho(\boldsymbol{s})\hat{\boldsymbol{H}}(\boldsymbol{s})$. For example, for $\mathrm{d} = 2$

$$\widetilde{\boldsymbol{H}}_2 = [0, 0, 1, 0, 1]^T.$$

We note that each entry of the moment matrix is given by

$$\widetilde{m}_{\alpha_1\ldots\alpha_d} = \sum_{\boldsymbol{s}\in B_1^{\epsilon 1}} \boldsymbol{s}^{\boldsymbol{\alpha}}\rho(|\boldsymbol{s}|)\phi(|\boldsymbol{s}|) \text{ for } \boldsymbol{\alpha} = (\alpha_1, \ldots, \alpha_d) \text{ and } 2 \leq |\boldsymbol{\alpha}| \leq 4\,. \tag{4.11}$$

For example, in two dimensions, eq. (4.9) has the explicit form

$$\begin{bmatrix} \widetilde{m}_{20} & \widetilde{m}_{11} & \widetilde{m}_{30} & \widetilde{m}_{21} & \widetilde{m}_{12} \\ \widetilde{m}_{11} & \widetilde{m}_{02} & \widetilde{m}_{21} & \widetilde{m}_{12} & \widetilde{m}_{03} \\ \widetilde{m}_{30} & \widetilde{m}_{21} & \widetilde{m}_{40} & \widetilde{m}_{31} & \widetilde{m}_{22} \\ \widetilde{m}_{21} & \widetilde{m}_{12} & \widetilde{m}_{31} & \widetilde{m}_{22} & \widetilde{m}_{13} \\ \widetilde{m}_{12} & \widetilde{m}_{03} & \widetilde{m}_{22} & \widetilde{m}_{13} & \widetilde{m}_{04} \end{bmatrix} \begin{bmatrix} b_{10} \\ b_{01} \\ b_{20} \\ b_{11} \\ b_{02} \end{bmatrix} = \begin{bmatrix} 0 \\ 0 \\ 1 \\ 0 \\ 1 \end{bmatrix}, \tag{4.12}$$

where $\boldsymbol{b} = [b_{10}, b_{01}, b_{20}, b_{11}, b_{02}]^T$.

If $\widetilde{\boldsymbol{M}}$ is invertible, then we have

$$\omega(\boldsymbol{s}) = \phi(|\boldsymbol{s}|)\hat{\boldsymbol{H}}^T(\boldsymbol{s})\widetilde{\boldsymbol{M}}^{-1}\widetilde{\boldsymbol{H}}_{\mathrm{d}}. \tag{4.13}$$

Otherwise, the inversion must be interpreted in a reasonable way. From eq. (4.13), it is unknown if the weights are strictly non-negative. Then, under the symmetry assumptions of quadrature points, we have a simple procedure to find a set of positive weights without the inversion of the moment matrix. It turns out the positivity of the weights $\omega(\boldsymbol{s})$ is critical for the stability of the numerical method.

Let us assume that the quadrature points are symmetrically distributed. More specially, we require the discrete set B_δ^ϵ to be invariant under reflection about axis as well as 90° rotation with respect to origin (in 2D) or axis (in 3D). Note that we could make this assumption because the quadrature points are completely decoupled from the collocation points, as shown in Figure 4.1. This assumption implies that $N_{\mathrm{d}} \geq 2\mathrm{d}$. Mathematically, the symmetry assumption allows us to see that the moment $\widetilde{m}_{\alpha_1 \ldots \alpha_{\mathrm{d}}} = 0$ if α_j $(j \in \{1, \ldots, \mathrm{d}\})$ is an odd number, and $\widetilde{m}_{\alpha_1 \ldots \alpha_{\mathrm{d}}}$ equals $\widetilde{m}_{\beta_1 \ldots \beta_{\mathrm{d}}}$ if $(\beta_1, \ldots, \beta_{\mathrm{d}})$ is a reordering of $(\alpha_1, \ldots, \alpha_{\mathrm{d}})$. Therefore, we see immediately from eq. (4.12) that

$$b_{10} = b_{01} = b_{11} = 0,$$

and the system eq. (4.12) is reduced to

$$\begin{aligned} \widetilde{m}_{40} b_{20} + \widetilde{m}_{22} b_{02} &= 1, \\ \widetilde{m}_{22} b_{20} + \widetilde{m}_{04} b_{02} &= 1. \end{aligned} \tag{4.14}$$

Notice that $\widetilde{m}_{40} = \widetilde{m}_{04}$ by the symmetry assumption and eq. (4.14) may have multiple solutions if $\widetilde{m}_{40} = \widetilde{m}_{22}$. We can at least find one solution by adding another constraint $b_{20} = b_{02}$. Then we obtain

$$b_{20} = b_{02} = \frac{1}{\widetilde{m}_{22} + \widetilde{m}_{40}}. \tag{4.15}$$

Substituting eqs. (2.4) and (4.15) into eq. (4.7), we arrive at an explicit expression of the quadrature weights

$$\omega(\boldsymbol{s}) = \frac{\phi(|\boldsymbol{s}|)}{\widetilde{m}_{22} + \widetilde{m}_{40}} |\boldsymbol{s}|^2. \tag{4.16}$$

In general, the weights are written as

$$\omega(\boldsymbol{s}) = \begin{cases} \dfrac{\phi(|\boldsymbol{s}|)}{\widetilde{m}_4} |\boldsymbol{s}|^2, & \mathrm{d} = 1, \\ \dfrac{\phi(|\boldsymbol{s}|)}{(\mathrm{d}-1)\widetilde{m}_{220\ldots0} + \widetilde{m}_{40\ldots0}} |\boldsymbol{s}|^2, & \mathrm{d} \geq 2. \end{cases}$$

By inspection of eq. (4.16), it is also easy to see that $\omega(\boldsymbol{s})$ only depends on $|\boldsymbol{s}|$. Therefore we have

$$\omega(\boldsymbol{s}) = \omega(|\boldsymbol{s}|).$$

4.1.3 Quadrature weights using GMLS

The way to construct weights using RK approximation as shown in subsection 4.1.2 can be seen as a special case of a GMLS quadrature discussed in [113]. This type of RKPM/MLS duality exists in the literature in many forms; while the classical RKPM and MLS shape functions are well-known to be equivalent under certain conditions as discussed in [17], more recent techniques such as the implicit gradient RKPM and GMLS approximation of derivatives are similarly identical, see [54, 85]. As discussed in [94], we show that a similar parallel holds for RKPM and GMLS nonlocal quadrature rules for completeness.

We state the GMLS problem as follows. Given a collection of points $B_1^{\epsilon_1}$,

we define the collection of quadrature weights $\boldsymbol{\omega}^T = \{\omega(\boldsymbol{s})\}_{\boldsymbol{s}\in B_1^{\epsilon_1}}$ via the equality constrained optimization problem:

$$\frac{1}{2}\underset{\omega\in\mathbb{R}^{N_\mathrm{d}}}{argmin} \sum_{\boldsymbol{s}\in B_1^{\epsilon_1}} \omega^2(\boldsymbol{s})\frac{1}{W(|\boldsymbol{s}|)} \tag{4.17}$$

$$\text{s.t.} \sum_{\boldsymbol{s}\in B_1^{\epsilon_1}} f(\boldsymbol{s})\omega(\boldsymbol{s}) = \int_{B_1} f(\boldsymbol{s})d\boldsymbol{s},\ \forall f \in \mathbf{V},$$

where $\mathbf{V}$ denotes a Banach space of integrands to be integrated exactly, and $W(r)$ is a radially symmetric positive weight function supported on B_1. Here we select $\mathbf{V}$ as the space of functions in the form of eq. (4.6). The solution to eq. (4.17) is then given explicitly by the saddle point problem

$$\begin{bmatrix} \boldsymbol{W}^{-1} & (\hat{\boldsymbol{H}}\boldsymbol{\rho})^T \\ \hat{\boldsymbol{H}}\boldsymbol{\rho} & \mathbf{0} \end{bmatrix} \begin{bmatrix} \boldsymbol{\omega} \\ \boldsymbol{\lambda} \end{bmatrix} = \begin{bmatrix} 0 \\ \widetilde{\boldsymbol{H}}_\mathrm{d} \end{bmatrix}, \tag{4.18}$$

where $\boldsymbol{\lambda} \in \mathbb{R}^{\dim(\mathbf{V})}$ denotes a vector of Lagrange multipliers used to enforce the constraint, $\boldsymbol{W}$ denotes a $N_\mathrm{d}\times N_\mathrm{d}$ diagonal matrix with diagonal entries $\{W(|\boldsymbol{s}|)\}_{\boldsymbol{s}\in B_1^{\epsilon_1}}$, $\hat{\boldsymbol{H}}$ denotes a $\dim(\boldsymbol{V})\times N_\mathrm{d}$ rectangular matrix with column vectors $\left\{\hat{\boldsymbol{H}}(\boldsymbol{s})\right\}_{\boldsymbol{s}\in B_1^{\epsilon_1}}$, and $\boldsymbol{\rho}$ denotes a $N_\mathrm{d}\times N_\mathrm{d}$ diagonal matrix with diagonal entries $\{\rho(|\boldsymbol{s}|)\}_{\boldsymbol{s}\in B_1^{\epsilon_1}}$. Solution of this system yields the following expression for the quadrature weights

$$\begin{aligned} \boldsymbol{\omega} &= \boldsymbol{W}(\hat{\boldsymbol{H}}\boldsymbol{\rho})^T\left((\hat{\boldsymbol{H}}\boldsymbol{\rho})\boldsymbol{W}(\hat{\boldsymbol{H}}\boldsymbol{\rho})^T\right)^{-1}\widetilde{\boldsymbol{H}}_\mathrm{d}, \\ &= \boldsymbol{W}\boldsymbol{\rho}\hat{\boldsymbol{H}}^T\left(\hat{\boldsymbol{H}}\boldsymbol{\rho}\boldsymbol{W}\boldsymbol{\rho}\hat{\boldsymbol{H}}^T\right)^{-1}\widetilde{\boldsymbol{H}}_\mathrm{d}. \end{aligned} \tag{4.19}$$

If we let $W(|\boldsymbol{s}|)\rho(|\boldsymbol{s}|) = \phi(|\boldsymbol{s}|)$, a direct comparison to eq. (4.13) reveal that the two are algebraically equivalent, depending upon how the matrix inverse is handled. In [113], the authors used a pseudo-inverse to handle the lack of uniqueness in the resulting solution.

There are several consequences for this equivalence. First, it reveals that the lack of invertibility of the moment matrix $\widetilde{\boldsymbol{M}}$ in eq. (4.10) may be interpreted as a non-unique solution to eq. (4.17), meaning that there are multiple choices of quadrature weights providing the desired reproduction properties. From the construction in the previous section, we know that at least one of those solutions corresponds to positive quadrature weights. We may thus add an inequality constraint to eq. (4.17) to enforce positivity, due to the existence of a non-empty feasible set. This is in contrast to existing literature [113], whereby no guarantees were made regarding positivity of quadrature weights. Of course, this result holds only for uniform grids, and future work may focus on whether such results hold for general quasi-uniform particle distributions in which [113] is applied.

In light of this GMLS/RK equivalence, the stability analysis in subsequent sections will apply equally to these previous works, and existing error analysis in the literature related to GMLS approaches likewise may be applied to the current scheme, under appropriate assumptions. Thus, the substantial literature pursuing both RK and MLS as platforms for establishing asymptotic compatibility are effectively equivalent.

4.1.4 Truncation error of the quasi-discrete nonlocal operator

We have constructed a quasi-discrete nonlocal diffusion operator using meshfree integration and we next study the associated truncation error.

Lemma 4.1.1. *Assume $u \in C^4(\mathbb{R}^{\mathrm{d}})$, then for any $\boldsymbol{x} \in \mathbb{R}^{\mathrm{d}}$,*

$$|\mathcal{L}_\delta^\epsilon u(\boldsymbol{x}) - \mathcal{L}_\delta u(\boldsymbol{x})| \leq C\delta^2 |u^{(4)}|_\infty.$$

Proof. Using Taylor's theorem, we have

$$u(\boldsymbol{x}+\boldsymbol{s})+u(\boldsymbol{x}-\boldsymbol{s})-2u(\boldsymbol{x})=2\sum_{|\boldsymbol{\alpha}|=2}\boldsymbol{s}^{\boldsymbol{\alpha}}\frac{D^{\boldsymbol{\alpha}}u(\boldsymbol{x})}{\boldsymbol{\alpha}!}+\sum_{|\boldsymbol{\beta}|=4}\boldsymbol{s}^{\boldsymbol{\beta}}\frac{R_{\boldsymbol{\beta}}(\boldsymbol{y})}{\boldsymbol{\beta}!}, \tag{4.20}$$

where $|R_{\boldsymbol{\beta}}(\boldsymbol{y})|\leq C|u^{(4)}|_\infty$. Therefore, for any point $\boldsymbol{x}\in\mathbb{R}^{\mathrm{d}}$,

$$\begin{aligned}
|\mathcal{L}_\delta^\epsilon u(\boldsymbol{x})-\mathcal{L}_\delta u(\boldsymbol{x})| &= \left|\sum_{|\boldsymbol{\alpha}|=2}\frac{D^{\boldsymbol{\alpha}}u(\boldsymbol{x})}{\boldsymbol{\alpha}!}\left(\sum_{\boldsymbol{s}\in B_\delta^\epsilon}\omega_\delta(\boldsymbol{s})\rho_\delta(|\boldsymbol{s}|)\boldsymbol{s}^{\boldsymbol{\alpha}}-\int_{B_\delta}\rho_\delta(|\boldsymbol{s}|)\boldsymbol{s}^{\boldsymbol{\alpha}}d\boldsymbol{s}\right)\right.\\
&\quad\left.+\sum_{|\boldsymbol{\beta}|=4}\frac{1}{2\boldsymbol{\beta}!}\left(\sum_{\boldsymbol{s}\in B_\delta^\epsilon}\omega_\delta(\boldsymbol{s})\rho_\delta(|\boldsymbol{s}|)\boldsymbol{s}^{\boldsymbol{\beta}}R_{\boldsymbol{\beta}}(\boldsymbol{y})-\int_{B_\delta}\rho_\delta(|\boldsymbol{s}|)\boldsymbol{s}^{\boldsymbol{\beta}}R_{\boldsymbol{\beta}}(\boldsymbol{y})d\boldsymbol{s}\right)\right|\\
&\leq 0+C|u^{(4)}|_\infty\left(\sum_{|\boldsymbol{\beta}|=4}\frac{1}{2\boldsymbol{\beta}!}\sum_{\boldsymbol{s}\in B_\delta^\epsilon}\omega_\delta(\boldsymbol{s})\rho_\delta(|\boldsymbol{s}|)|\boldsymbol{s}|^4+\int_{B_\delta}\rho_\delta(|\boldsymbol{s}|)|\boldsymbol{s}|^4d\boldsymbol{s}\right)\\
&\leq C\delta^2|u^{(4)}|_\infty.
\end{aligned}$$

where we have used eqs. (4.3) and (4.20). □

Lemma 4.1.1 shows that if the quasi-discrete operator $\mathcal{L}_\delta^\epsilon$ satisfy the polynomial reproducing conditions eq. (4.3) up to the second order, then $\mathcal{L}_\delta^\epsilon$ is a second-order approximation of $\mathcal{L}_\delta$ in δ. For high order approximations, one could follow the same procedure to design weights such that the quasi-discrete operator satisfy high order polynomial reproducing conditions. However, the positivity of weights for high order approximations needs further investigation which is beyond the scope of this paper. We will see in the next section that the positivity of weights is crucial to guarantee the stability of numerical schemes applied to the quasi-discrete operator.

4.2 Convergence analysis of the RK collocation for the quasi-discrete nonlocal diffusion

In this section, we apply the RK collocation method introduced in section 3.2 to the quasi-discrete nonlocal diffusion operator defined in section 4.1. The RK

collocation scheme for the quasi-discrete operator is formulated as follows. Find a function $u \in S(\square \cap \Omega)$ such that

$$-\mathcal{L}_\delta^\epsilon u(\boldsymbol{x_k}) = f(\boldsymbol{x_k}), \quad \boldsymbol{x_k} \in (\square \cap \Omega). \tag{4.21}$$

Equivalently, eq. (4.21) is also written as

$$-r_\Omega^h \mathcal{L}_\delta^\epsilon u = r_\Omega^h f, \quad u \in S(\square \cap \Omega). \tag{4.22}$$

For practical reasons, in this section we assume $\delta = M_0 h_{\max}$, where $M_0 > 0$ is fixed and investigate the convergence behaviour of the numerical solution of the collocation scheme, obtaining results similar to section 3.3.

4.2.1 Stability

We first present the stability of the RK collocation scheme eq. (4.22) as follows.

Theorem 4.2.1. ***(Stability II)*** *For any $\delta \in (0, \delta_0]$ and $u \in S(\square \cap \Omega)$, we have*

$$\left| r_\Omega^h(-\mathcal{L}_\delta^\epsilon u) \right|_h \geq C \|u\|_{L^2(\mathbb{R}^d)},$$

where C is a constant that only depends on Ω, δ_0, and M_0.

The proof of this theorem is similar to Theorem 3.3.1 as long as we have the next lemma. Before presenting the Lemma, we need to first show the Fourier symbol of the quasi-discrete nonlocal diffusion operator $\mathcal{L}_\delta^\epsilon$,

$$\begin{aligned}
-\widehat{\mathcal{L}_\delta^\epsilon u}(\boldsymbol{\xi}) &= -\int_{\mathbb{R}^d} e^{-i\boldsymbol{x}\cdot\boldsymbol{\xi}} \sum_{\boldsymbol{s}\in B_\delta^\epsilon} \omega_\delta(\boldsymbol{s})\rho_\delta(\boldsymbol{s})(u(\boldsymbol{x}+\boldsymbol{s}) - u(\boldsymbol{x}))d\boldsymbol{x}, \\
&= \sum_{\boldsymbol{s}\in B_\delta^\epsilon} \omega_\delta(\boldsymbol{s})\rho_\delta(\boldsymbol{s}) \int_{\mathbb{R}^d} (u(\boldsymbol{x}) - u(\boldsymbol{x}+\boldsymbol{s}))e^{-i\boldsymbol{x}\cdot\boldsymbol{\xi}} d\boldsymbol{x}, \\
&= \sum_{\boldsymbol{s}\in B_\delta^\epsilon} \omega_\delta(\boldsymbol{s})\rho_\delta(\boldsymbol{s})(1 - e^{i\boldsymbol{s}\cdot\boldsymbol{\xi}})\widehat{u}(\boldsymbol{\xi}), \\
&= \lambda_\delta^\epsilon(\boldsymbol{\xi})\widehat{u}(\boldsymbol{\xi}),
\end{aligned}$$

where $\lambda_\delta^\epsilon(\boldsymbol{\xi})$ is the Fourier symbol of $\mathcal{L}_\delta^\epsilon$,

$$\lambda_\delta^\epsilon(\boldsymbol{\xi}) = \sum_{\boldsymbol{s}\in B_\delta^\epsilon} \omega_\delta(\boldsymbol{s})\rho_\delta(\boldsymbol{s})(1-\cos(\boldsymbol{s}\cdot\boldsymbol{\xi})). \tag{4.23}$$

Since $\omega_\delta(\boldsymbol{s})$ is symmetric and non-negative, $\lambda_\delta^\epsilon(\boldsymbol{\xi})$ is real and non-negative. We obtain the Fourier representation of the collocation scheme as follows.

Lemma 4.2.2. *Let $\widetilde{u}(\boldsymbol{\xi})$ and $\widetilde{v}(\boldsymbol{\xi})$ be the Fourier series of the sequences $(u_{\boldsymbol{k}}), (v_{\boldsymbol{k}}) \in l^1(\mathbb{Z}^d)$ respectively. Then*

$$((u_{\boldsymbol{k}}), -r^h\mathcal{L}_\delta^\epsilon i^h(v_{\boldsymbol{k}}))_{l^2} = (2\pi)^{-\mathrm{d}}\int_{\boldsymbol{Q}} \widetilde{u}(\boldsymbol{\xi})\overline{\widetilde{v}(\boldsymbol{\xi})}\lambda_C^\epsilon(\delta,\boldsymbol{h},\boldsymbol{\xi})d\boldsymbol{\xi},$$

where λ_C^ϵ is defined as

$$\lambda_C^\epsilon(\delta,\boldsymbol{h},\boldsymbol{\xi}) = 2^{4\mathrm{d}}\sum_{\boldsymbol{r}\in\mathbb{Z}^{\mathrm{d}}} \lambda_\delta^\epsilon\left((\boldsymbol{\xi}+2\pi\boldsymbol{r})\oslash\boldsymbol{h}\right)\prod_{j=1}^{\mathrm{d}} h_j\left(\frac{\sin(\xi_j/2)}{\xi_j+2\pi r_j}\right)^4. \tag{4.24}$$

Moreover,

$$\lambda_C(\delta,\boldsymbol{h},\boldsymbol{\xi}) \le C\lambda_C^\epsilon(\delta,\boldsymbol{h},\boldsymbol{\xi}), \tag{4.25}$$

for some generic constant $C>0$.

Proof. The derivation of eq. (4.24) is similar to eq. (3.22), following the replacement of $\lambda_\delta(\boldsymbol{\xi}+2\pi\boldsymbol{r})$ by $\lambda_\delta^\epsilon(\boldsymbol{\xi}+2\pi\boldsymbol{r})$. We proceed to show eq. (4.25). By change of variables, we obtain

$$\lambda_\delta\left((\boldsymbol{\xi}+2\pi\boldsymbol{r})\oslash\boldsymbol{h}\right) = \frac{1}{\delta^2}\lambda_1\left(\delta(\boldsymbol{\xi}+2\pi\boldsymbol{r})\oslash\boldsymbol{h}\right)$$

and

$$\lambda_\delta^\epsilon\left((\boldsymbol{\xi}+2\pi\boldsymbol{r})\oslash\boldsymbol{h}\right) = \frac{1}{\delta^2}\lambda_1^{\epsilon_1}\left(\delta(\boldsymbol{\xi}+2\pi\boldsymbol{r})\oslash\boldsymbol{h}\right),$$

where

$$\lambda_1\left(\delta(\boldsymbol{\xi}+2\pi\boldsymbol{r})\oslash\boldsymbol{h}\right) = \int_{B_1}\rho(|\boldsymbol{s}|)\left(1-\cos\left(\delta\boldsymbol{s}\cdot\left((\boldsymbol{\xi}+2\pi\boldsymbol{r})\oslash\boldsymbol{h}\right)\right)\right)d\boldsymbol{s}$$

and

$$\lambda_1^{\epsilon_1}(\delta(\boldsymbol{\xi}+2\pi\boldsymbol{r})\oslash\boldsymbol{h}) = \sum_{\boldsymbol{s}\in B_1^{\epsilon_1}} \omega(|\boldsymbol{s}|)\rho(|\boldsymbol{s}|)\left(1-\cos\left(\delta\boldsymbol{s}\cdot((\boldsymbol{\xi}+2\pi\boldsymbol{r})\oslash\boldsymbol{h})\right)\right).$$

Let us decompose the set $\boldsymbol{Q}=(-\pi,\pi)^{\mathrm{d}}$ into $\boldsymbol{Q}_1$ and $\boldsymbol{Q}_2$,

$$\boldsymbol{Q}_1 := \{\boldsymbol{\xi}\in\boldsymbol{Q} : \frac{\delta|\boldsymbol{\xi}|}{h_{\min}} \le \pi\}, \text{ and } \boldsymbol{Q}_2 = \boldsymbol{Q}/\boldsymbol{Q}_1.$$

By the definition, if $\boldsymbol{\xi}\in\boldsymbol{Q}_1$, then

$$\left|\delta\boldsymbol{s}\cdot(\boldsymbol{\xi}\oslash\boldsymbol{h})\right| \le \frac{\delta|\boldsymbol{\xi}|}{h_{\min}} \le \pi\,.$$

First, by eq. (4.24), we observe that

$$\lambda_C^{\epsilon}(\delta,\boldsymbol{h},\boldsymbol{\xi}) \ge C\frac{1}{\delta^2}\lambda_1^{\epsilon_1}(\delta\boldsymbol{\xi}\oslash\boldsymbol{h})\prod_{j=1}^{\mathrm{d}} h_j\left(\frac{\sin(\xi_j/2)}{\xi_j}\right)^4.$$

Notice that there exists $C>0$ such that for $x\in(-\pi,\pi)$

$$1-\cos(x)\ge Cx^2\,.$$

Then, we have for $\boldsymbol{\xi}\in\boldsymbol{Q}_1$,

$$\begin{aligned}\lambda_1^{\epsilon_1}(\delta\boldsymbol{\xi}\oslash\boldsymbol{h}) &= \sum_{\boldsymbol{s}\in B_1^{\epsilon_1}}\omega(|\boldsymbol{s}|)\rho(|\boldsymbol{s}|)\left(1-\cos\left(\frac{\delta}{h_{\max}}\boldsymbol{s}\cdot\left(\boldsymbol{\xi}\oslash\hat{\boldsymbol{h}}\right)\right)\right),\\ &\ge C\left(\frac{\delta|\boldsymbol{\xi}|}{h_{\max}}\right)^2\sum_{\boldsymbol{s}\in B_1^{\epsilon_1}}\omega(|\boldsymbol{s}|)\rho(|\boldsymbol{s}|)|\boldsymbol{s}|^2\cos^2(\theta(\boldsymbol{s},\boldsymbol{\xi}\oslash\hat{\boldsymbol{h}})),\\ &\ge C|\boldsymbol{\xi}|^2,\end{aligned} \tag{4.26}$$

where we have used that $\boldsymbol{h}$ is quasi-uniform ($h_{\max}/h_{\min}$ is bounded above and below), C depends only on $M_0=\delta/h_{\max}$ and the set $B_1^{\epsilon_1}$ and $\theta=\theta(\boldsymbol{s},\boldsymbol{\xi}\oslash\hat{\boldsymbol{h}})$ is the angle between $\boldsymbol{s}$ and $\boldsymbol{\xi}\oslash\hat{\boldsymbol{h}}$. The last line of of eq. (4.26) comes from the following observation. For a fixed $\boldsymbol{\xi}\oslash\hat{\boldsymbol{h}}$, $\cos(\theta)=0$ only for the points $\boldsymbol{s}$ that lies in directions orthogonal to $\boldsymbol{\xi}\oslash\hat{\boldsymbol{h}}$. But from the symmetry assumption of the discrete set $B_1^{\epsilon_1}$ in

subsection 4.1.2, there are always $\boldsymbol{s} \in B_1^{\epsilon_1}$ such that $\boldsymbol{s}$ is not orthogonal to $\boldsymbol{\xi} \oslash \hat{\boldsymbol{h}}$. Therefore, for any nonzero $\boldsymbol{\xi} \in \boldsymbol{Q}_1$, the summation in the second line of eq. (4.26) is always a positive number. Then it has a positive lower bound since $\boldsymbol{Q}_1$ is a compact set. Now for $\boldsymbol{\xi} \in \boldsymbol{Q}_2$, we have $|\boldsymbol{\xi} \oslash \hat{\boldsymbol{h}}| \geq |\boldsymbol{\xi}| \geq \pi/M_0$, then

$$\begin{aligned} \lambda_1^{\epsilon_1}(\delta\boldsymbol{\xi} \oslash \boldsymbol{h}) &= \sum_{\boldsymbol{s} \in B_1^{\epsilon_1}} \omega(|\boldsymbol{s}|)\rho(|\boldsymbol{s}|)\left(1 - \cos\left(\frac{\delta}{h_{\max}}\boldsymbol{s} \cdot \left(\boldsymbol{\xi} \oslash \hat{\boldsymbol{h}}\right)\right)\right), \\ &= \sum_{\boldsymbol{s} \in B_1^{\epsilon_1}} \omega(|\boldsymbol{s}|)\rho(|\boldsymbol{s}|)\left(1 - \cos\left(M_0|\boldsymbol{s}||\boldsymbol{\xi} \oslash \hat{\boldsymbol{h}}|\cos(\theta(\boldsymbol{s}, \boldsymbol{\xi} \oslash \hat{\boldsymbol{h}}))\right)\right). \end{aligned} \tag{4.27}$$

As we have seen, for any fixed $\boldsymbol{\xi} \oslash \hat{\boldsymbol{h}}$, there always exists $\boldsymbol{s} \in B_1^{\epsilon_1}$ such that $\cos(\theta(\boldsymbol{s}, \boldsymbol{\xi} \oslash \hat{\boldsymbol{h}})) \neq 0$. However, $\lambda_1^{\epsilon_1}(\delta\boldsymbol{\xi} \oslash \boldsymbol{h})$ may still become zero if $\boldsymbol{s} \in B_1^{\epsilon_1}$ and $M_0|\boldsymbol{s}||\boldsymbol{\xi} \oslash \hat{\boldsymbol{h}}|\cos(\theta(\boldsymbol{s}, \boldsymbol{\xi} \oslash \hat{\boldsymbol{h}})) = 2k\pi$ for $k \in \mathbb{Z}^+$. If this happens, one can add another point $\tilde{\boldsymbol{s}} \in B_1^{\epsilon_1}$ in the same direction of $\boldsymbol{s}$ such that $|\boldsymbol{s}|/|\tilde{\boldsymbol{s}}|$ is an irrational number and thus $M_0|\tilde{\boldsymbol{s}}||\boldsymbol{\xi} \oslash \hat{\boldsymbol{h}}|\cos(\theta(\tilde{\boldsymbol{s}}, \boldsymbol{\xi} \oslash \hat{\boldsymbol{h}})) \neq 2k\pi$ for any $k \in \mathbb{Z}^+$. Therefore, for a proper choice of $B_1^{\epsilon_1}$ with $N_{\mathrm{d}} \geq 4\mathrm{d}$, we can always have $\lambda_1^{\epsilon_1}(\delta\boldsymbol{\xi} \oslash \boldsymbol{h}) \geq 0$ for $\boldsymbol{\xi} \in \boldsymbol{Q}_2$. Then since $\boldsymbol{Q}_2$ is a compact set, we have $\lambda_1^{\epsilon_1}(\delta\boldsymbol{\xi} \oslash \boldsymbol{h}) \geq C \geq |\boldsymbol{\xi}|^2$ for $\boldsymbol{\xi} \in \boldsymbol{Q}_2$. Now observe that for any nonzero $\boldsymbol{\xi} = (\xi_1, \ldots, \xi_{\mathrm{d}}) \in \boldsymbol{Q}$, we have

$$C_1 < \left(\frac{\sin(\xi_j/2)}{\xi_j}\right)^4 < C_2, \ j \in \{1, \ldots, \mathrm{d}\},$$

where $C_1, C_2 > 0$ are generic constants. Then we arrive at

$$\lambda_C^{\epsilon}(\delta, \boldsymbol{h}, \boldsymbol{\xi}) \geq C\left(\frac{|\boldsymbol{\xi}|}{\delta}\right)^2 \prod_{j=1}^{\mathrm{d}} h_j, \tag{4.28}$$

for $\boldsymbol{\xi} \in \boldsymbol{Q}$.

Next, use the fact that

$$1 - \cos(x) \leq x^2, \quad \text{for } x \geq 0,$$

to obtain, for any $\boldsymbol{r} \in \mathbb{Z}^{\mathrm{d}}$,

$$\begin{aligned}\lambda_1\left(\delta(\boldsymbol{\xi}+2\pi\boldsymbol{r}) \oslash \boldsymbol{h}\right) &\leq \int_{B_1} \rho(|\boldsymbol{s}|)\delta^2|\boldsymbol{s}|^2|(\boldsymbol{\xi}+2\pi\boldsymbol{r}) \oslash \boldsymbol{h}|^2 d\boldsymbol{s}, \\ &\leq C\left(\frac{\delta|(\boldsymbol{\xi}+2\pi\boldsymbol{r})|}{h_{\max}}\right)^2 \int_{B_1} \omega(|\boldsymbol{s}|)\rho(|\boldsymbol{s}|)|\boldsymbol{s}|^2 d\boldsymbol{s}, \\ &\leq C|(\boldsymbol{\xi}+2\pi\boldsymbol{r})|^2.\end{aligned}$$

Hence we have

$$\begin{aligned}&\sum_{\boldsymbol{r}\in\mathbb{Z}^{\mathrm{d}}} \lambda_1\left(\delta(\boldsymbol{\xi}+2\pi\boldsymbol{r}) \oslash \boldsymbol{h}\right) \prod_{j=1}^{\mathrm{d}} h_j \left(\frac{\sin(\xi_j/2)}{\xi_j+2\pi r_j}\right)^4 \\ &\leq C \sum_{\boldsymbol{r}\in\mathbb{Z}^{\mathrm{d}}} |\boldsymbol{\xi}+2\pi\boldsymbol{r}|^2 \prod_{j=1}^{\mathrm{d}} h_j \left(\frac{\sin(\xi_j/2)}{\xi_j+2\pi r_j}\right)^4, \\ &\leq C|\boldsymbol{\xi}|^4 \sum_{\boldsymbol{r}\in\mathbb{Z}^{\mathrm{d}}} |\boldsymbol{\xi}+2\pi\boldsymbol{r}|^2 \prod_{j=1}^{\mathrm{d}} h_j \left(\frac{1}{\xi_j+2\pi r_j}\right)^4 \\ &\leq C|\boldsymbol{\xi}|^4 \prod_{j=1}^{\mathrm{d}} h_j \sum_{\boldsymbol{r}\in\mathbb{Z}^{\mathrm{d}}} \prod_{j=1}^{\mathrm{d}} \frac{1}{|\xi_j+2\pi r_j|^2}, \\ &\leq C|\boldsymbol{\xi}|^2 \prod_{j=1}^{\mathrm{d}} h_j.\end{aligned}$$

Immediately, we have the following bound for $\lambda_C(\delta, \boldsymbol{h}, \boldsymbol{\xi})$ by

$$\lambda_C(\delta, \boldsymbol{h}, \boldsymbol{\xi}) \leq C\left(\frac{|\boldsymbol{\xi}|}{\delta}\right)^2 \prod_{j=1}^{\mathrm{d}} h_j. \tag{4.29}$$

Finally, eq. (4.25) is shown by combining eq. (4.28) and eq. (4.29). □

Proof of Theorem 4.2.1. By applying Lemma 4.2.2, the proof follows similarly to the proof of Theorem 3.3.1. □

4.2.2 Consistency

In this subsection, we establish the convergence of the RK scheme eq. (4.22) to the corresponding local problem as $h_{\max} \to 0$ with a fixed ratio between δ and h, i.e., $M_0 = \delta/h_{\max}$. We show first the discrete model error between the quasi-discrete nonlocal diffusion model and its local limit.

Lemma 4.2.3. ***(Discrete model error II)*** *Assume $u(\boldsymbol{x}) \in C^4(\mathbb{R}^{\mathrm{d}})$, then*

$$\left|r^h \mathcal{L}_\delta^\epsilon \Pi^h u - r^h \mathcal{L}_0 u\right|_h \leq C|u^{(4)}|_\infty (h_{\max}^2 + \delta^2).$$

Proof. In order to prove this Lemma, we need an intermediate result. Similar to the proof of Lemma 3.3.7, for $\boldsymbol{x_k} \in \square$ the quasi-discrete operator $\mathcal{L}_\delta^\epsilon$ acting on the RK approximation error eq. (3.25) is given as

$$\begin{aligned}\left|\mathcal{L}_\delta^\epsilon \Pi^h u(\boldsymbol{x_k}) - \mathcal{L}_\delta^\epsilon u(\boldsymbol{x_k})\right| &= \left|\sum_{\boldsymbol{s}\in B_\delta^\epsilon} \omega_\delta(\boldsymbol{s})\rho_\delta(\boldsymbol{s})\left(E(\boldsymbol{x_k}+\boldsymbol{s}) - E(\boldsymbol{x_k})\right)\right|, \\ &\leq Ch_{\max}^2 |u^{(4)}|_\infty \sum_{\boldsymbol{s}\in B_\delta^\epsilon} \omega_\delta(\boldsymbol{s})\rho_\delta(\boldsymbol{s})|\boldsymbol{s}|^2, \\ &\leq Ch_{\max}^2 |u^{(4)}|_\infty,\end{aligned} \tag{4.30}$$

Finally, by combining eq. (4.30) and Lemma 4.1.1 and using the RK interpolation, the discrete model error of collocation scheme is given as

$$\begin{aligned}\left|r^h \mathcal{L}_\delta^\epsilon \Pi^h u - r^h \mathcal{L}_0 u\right|_h &\leq \left|r^h \mathcal{L}_\delta^\epsilon \Pi^h u - r^h \mathcal{L}_\delta^\epsilon u\right|_h + \left|r^h \mathcal{L}_\delta^\epsilon u - r^h \mathcal{L}_\delta u\right|_h \\ &\quad + \left|r^h \mathcal{L}_\delta u - r^h \mathcal{L}_0 u\right|_h, \\ &\leq C(h_{\max}^2 + \delta^2 + \delta^2)|u^{(4)}|_\infty.\end{aligned}$$

□

Combining Theorem 4.2.1 and Lemma 4.2.3, the numerical solution of eq. (4.22) converges to its local limit.

Theorem 4.2.4. *Assume the local exact solution u^0 is sufficiently smooth, i.e., $u^0 \in C^4(\overline{\Omega_{\delta_0}})$. For any $\delta \in (0, \delta_0]$, let $u^{\delta,\epsilon,h}$ be the numerical solution of the collocation scheme with meshfree integration eq. (4.22) and fix the ratio between δ and $h_{\max}$. Then,*

$$\|u^0 - u^{\delta,\epsilon,h}\|_{L^2(\Omega)} \leq C(h_{\max}^2 + \delta^2).$$

Proof. Similar to the proof of Theorem 3.3.10, we first do a zero extension of u^0. The collocation equation is given by

$$-r_\Omega^h \mathcal{L}_\delta^\epsilon u^{\delta,\epsilon,h} = r_\Omega^h f = -r_\Omega^h \mathcal{L}_0 u^0 \,.$$

Combining the above equation, the stability result (Theorem 4.2.1) and the consistency result (Lemma 4.2.3), we obtain the following estimate

$$\begin{aligned}
\|\Pi^h u^0 - u^{\delta,\epsilon,h}\|_{L^2(\mathbb{R}^d)} &\leq C \left| r_\Omega^h \mathcal{L}_\delta^\epsilon \left(\Pi^h u^0 - u^{\delta,\epsilon,h} \right) \right|_h \,, \\
&\leq C \left| r_\Omega^h \mathcal{L}_\delta^\epsilon \Pi^h u^0 - r_\Omega^h \mathcal{L}_\delta^\epsilon u^{\delta,\epsilon,h} \right|_h \,, \\
&\leq C \left| r_\Omega^h \mathcal{L}_\delta^\epsilon \Pi^h u^0 - r_\Omega^h \mathcal{L}_0 u^0 \right|_h \,, \\
&\leq C h_{\max}^2 \,.
\end{aligned}$$

We complete the proof using the triangle inequality

$$\|u^0 - u^{\delta,\epsilon,h}\|_{L^2(\mathbb{R}^d)} \leq \|u^0 - \Pi^h u^0\|_{L^2(\mathbb{R}^d)} + \|\Pi^h u^0 - u^{\delta,\epsilon,h}\|_{L^2(\mathbb{R}^d)} \leq C(h_{\max}^2 + \delta^2).$$

□

4.3 Numerical example

As discussed in section 3.4, high-order Gauss quadrature rules are necessary to evaluate the integral for the RK collocation method, making the method computationally expensive. In practice, we sometimes couple grid size with horizon as $\delta = M_0 h_{\max}$ so that δ goes to 0 at the same rate as h approaches 0. Now, we use the RK collocation method for the quasi-discrete nonlocal diffusion as discussed in section 4.2 to solve eq. (3.29) and only study the convergence to the local limit. Convergence profiles are presented in Figure 4.2. We observe a second-order convergence

rate in agreement with Theorem 4.2.4. Therefore the RK collocation method for the quasi-discrete nonlocal diffusion converges to the correct local limit.

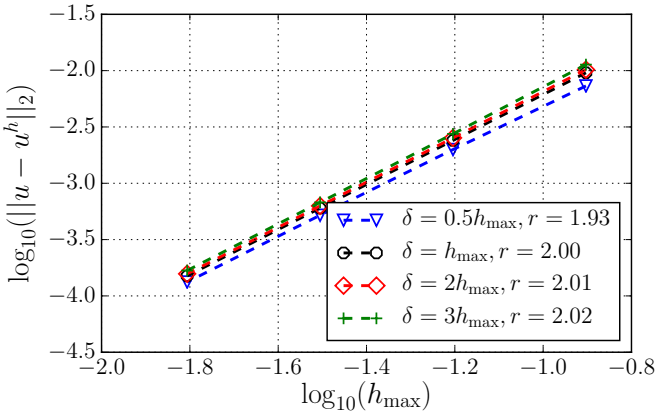

Figure 4.2: Convergence profiles using the RK collocation method for the quasi-discrete nonlocal diffusion.

Chapter 5

Peridynamic Navier equation

In this chapter[1], we extend the RK collocation framework developed for the nonlocal diffusion models (Chapters 3 and 4) to the peridynamic Navier equation. We first apply linear RK approximation on both displacements and dilatation, then back-substitute dilatation and solve the peridynamic Navier equation in a pure displacement form. The RK collocation scheme converges to the nonlocal limit and also to the local limit as the nonlocal interaction vanishes. Then we show the convergence analysis of the RK collocation method for the quasi-discrete peridynamic Navier equation to the correct local limit when the ratio of the nonlocal length scale and the discretization parameter is fixed. The analysis is carried out on a special family of rectilinear Cartesian grids for linear RK method with designated kernel with finite support. We also assume the Lamé parameters satisfy $\lambda \geq \mu$ to avoid adding extra constraints to the nonlocal kernel. Finally, numerical experiments are conducted to validate the theoretical results.

This chapter is organized as follows. In section 5.1, we introduce the peridynamic Navier equation with Dirichlet boundary conditions and also the quasi-discrete counterparts using finite summation of quadrature points to replace the integral. Moreover, we present the RK collocation scheme for peridynamic Navier equation. Section 5.2 discusses the convergence analysis of the RK collocation method for the

[1]This chapter is an adaption of [72]. The author's contribution includes theoretical derivation and conducting numerical experiments.

peridynamic Navier equation and shows that this RK collocation scheme is AC. Then the convergence analysis of the collocation method for the quasi-discrete peridynamic Navier equation is presented in section 5.3. Section 5.4 gives numerical examples to complement our theoretical analysis.

5.1 Peridynamic Navier equation

In this section, we first introduce some notations that are used throughout this chapter. The spatial dimension is denoted as d (2 or 3). An arbitrary point $\boldsymbol{x} \in \mathbb{R}^{\mathrm{d}}$ is expressed as $\boldsymbol{x} = (x_1, \ldots, x_{\mathrm{d}})$. A multi-index, $\boldsymbol{\alpha} = (\alpha_1, \ldots, \alpha_{\mathrm{d}})$, is a collection of d non-negative integers and its length is $|\boldsymbol{\alpha}| = \sum_{i=1}^{\mathrm{d}} \alpha_i$. As a consequence, we write $\boldsymbol{x}^{\boldsymbol{\alpha}} = x_1^{\alpha_1} \ldots x_{\mathrm{d}}^{\alpha_{\mathrm{d}}}$ for a given $\boldsymbol{\alpha}$. We let $\Omega \subset \mathbb{R}^{\mathrm{d}}$ be an open bounded domain then the corresponding interaction domain is defined as

$$\Omega_{\mathcal{I}} = \{\boldsymbol{x} \in \mathbb{R}^{\mathrm{d}} \backslash \Omega : \mathrm{dist}(\boldsymbol{x}, \Omega) \leq 2\delta\},$$

where δ is the nonlocal length scale and we denote $\Omega_\delta = \Omega \cup \Omega_{\mathcal{I}}$.

Next, we present the linearized state-based peridynamic Navier equation introduced in [107, 105], then use the quasi-discrete nonlocal operators as introduced in [71] to formulate the quasi-discrete counterparts. We differ in convention of the notations from nonlocal vector calculus developed in [36] which is more suited for variational formulation as in [34], but introduce a new notation for the bond-based peridynamics operator and adopt notations from [38, 39] for nonlocal divergence and gradient operators; these notations will alleviate the presentation for collocation method which will be introduced in the next section.

5.1.1 Nonlocal operators

The linearized state-based peridynamic Navier operator consists two parts: one is the bond-based peridynamic operator and the other is the composition of the nonlocal gradient and divergence operators. The bond-based peridynamic operator is defined, for a given vector-valued function $\boldsymbol{u}(\boldsymbol{x}) : \Omega_\delta \to \mathbb{R}^{\mathrm{d}}$, as

$$\mathcal{L}_\delta^B \boldsymbol{u}(\boldsymbol{x}) = \int_{\Omega_\delta} \rho_\delta(|\boldsymbol{y}-\boldsymbol{x}|) \frac{\boldsymbol{y}-\boldsymbol{x}}{|\boldsymbol{y}-\boldsymbol{x}|} \otimes \frac{\boldsymbol{y}-\boldsymbol{x}}{|\boldsymbol{y}-\boldsymbol{x}|} (\boldsymbol{u}(\boldsymbol{y}) - \boldsymbol{u}(\boldsymbol{x})) d\boldsymbol{y}, \quad \forall \boldsymbol{x} \in \Omega, \tag{5.1}$$

where $\rho_\delta(|\boldsymbol{y}-\boldsymbol{x}|)$ is the nonlocal kernel as defined in eq. (3.3). The weighted volume $m(\boldsymbol{x})$ is defined as

$$m(\boldsymbol{x}) = \int_{\Omega_\delta} \rho_\delta(|\boldsymbol{y}-\boldsymbol{x}|)|\boldsymbol{y}-\boldsymbol{x}|^2 d\boldsymbol{y}, \quad \forall \boldsymbol{x} \in \Omega. \tag{5.2}$$

From eqs. (3.3), (3.4), and (5.2), it is easy to see that $m(\boldsymbol{x}) = \mathrm{d}$. We remark that the weighted volume defined here as eq. (5.2) is a scaled form of the definition in [106, 105, 103]. Next, the nonlocal divergence operator $\mathcal{D}_\delta$ is defined as, see also [38, 39],

$$\mathcal{D}_\delta \boldsymbol{u}(\boldsymbol{x}) = \int_{\Omega_\delta} \rho_\delta(|\boldsymbol{y}-\boldsymbol{x}|)(\boldsymbol{y}-\boldsymbol{x}) \cdot (\boldsymbol{u}(\boldsymbol{y}) + \boldsymbol{u}(\boldsymbol{x})) d\boldsymbol{y}, \quad \forall \boldsymbol{x} \in \Omega,$$

and in the sense of principle value, $\mathcal{D}_\delta$ can also be written as

$$\mathcal{D}_\delta \boldsymbol{u}(\boldsymbol{x}) = \int_{\Omega_\delta} \rho_\delta(|\boldsymbol{y}-\boldsymbol{x}|)(\boldsymbol{y}-\boldsymbol{x}) \cdot (\boldsymbol{u}(\boldsymbol{y}) - \boldsymbol{u}(\boldsymbol{x})) d\boldsymbol{y}, \quad \forall \boldsymbol{x} \in \Omega. \tag{5.3}$$

Nonlocal dilatation $\theta(\boldsymbol{x})$ is defined from the nonlocal divergence operator

$$\theta(\boldsymbol{x}) = \frac{\mathrm{d}}{m(\boldsymbol{x})} \mathcal{D}_\delta \boldsymbol{u}(\boldsymbol{x}), \quad \forall \boldsymbol{x} \in \Omega, \tag{5.4}$$

Then, the nonlocal gradient operator $\mathcal{G}_\delta$ is defined by

$$\mathcal{G}_\delta \theta(\boldsymbol{x}) = \int_{\Omega_\delta} \rho_\delta(|\boldsymbol{y}-\boldsymbol{x}|)(\boldsymbol{y}-\boldsymbol{x})(\theta(\boldsymbol{y}) - \theta(\boldsymbol{x})) d\boldsymbol{y}, \quad \forall \boldsymbol{x} \in \Omega. \tag{5.5}$$

Finally, we have the linearized state-based peridynamic Navier operator,

$$\mathcal{L}_\delta^E \boldsymbol{u}(\boldsymbol{x}) = \frac{C_\alpha\,\mu}{m(\boldsymbol{x})}\mathcal{L}_\delta^B \boldsymbol{u}(\boldsymbol{x}) + \frac{C_\beta\,\mathrm{d}(\lambda-\mu)}{(m(\boldsymbol{x}))^2}\mathcal{G}_\delta\mathcal{D}_\delta \boldsymbol{u}(\boldsymbol{x}), \quad \forall \boldsymbol{x}\in\Omega, \tag{5.6}$$

where C_α and C_β are scaling parameters which will be given shortly, and λ and μ are Lamé parameters which are assumed constant in this work. The static peridynamic Navier equation with Dirichlet boundary condition can be formulated as

$$\begin{cases} -\mathcal{L}_\delta^E \boldsymbol{u} = \boldsymbol{f}, & \text{in } \Omega, \\ \quad \boldsymbol{u} = \boldsymbol{0}, & \text{on } \Omega_{\mathcal{I}}. \end{cases} \tag{5.7}$$

By introducing $p = (\lambda-\mu)\theta$, we can write eq. (5.7) into a mixed form, as follows,

$$\begin{cases} -\dfrac{C_\alpha\,\mu}{m(\boldsymbol{x})}\mathcal{L}_\delta^B \boldsymbol{u}(\boldsymbol{x}) - \dfrac{C_\beta}{m(\boldsymbol{x})}\mathcal{G}_\delta p(\boldsymbol{x}) = \boldsymbol{f}(\boldsymbol{x}), & \boldsymbol{x}\in\Omega, \\ \dfrac{\mathrm{d}\,(\lambda-\mu)}{m(\boldsymbol{x})}\mathcal{D}_\delta \boldsymbol{u}(\boldsymbol{x}) - p(\boldsymbol{x}) = 0, & \boldsymbol{x}\in\Omega, \\ \boldsymbol{u}(\boldsymbol{x}) = \boldsymbol{0}, & \boldsymbol{x}\in\Omega_{\mathcal{I}}. \end{cases} \tag{5.8}$$

The local limit of $\mathcal{L}_\delta^S$ is denoted as $\mathcal{L}_0^S$ when $\delta\to 0$ in [80]. We select $C_\alpha = 30, C_\beta = 3$ for 3D linear elasticity and $C_\alpha = 16, C_\beta = 2$ for 2D plane strain, then, for $\boldsymbol{u}\in C_0^\infty(\Omega;\mathbb{R}^{\mathrm{d}})$,

$$\mathcal{L}_0^S \boldsymbol{u}(\boldsymbol{x}) = \mu\mathrm{div}(\nabla \boldsymbol{u}(\boldsymbol{x})) + (\mu+\lambda)\nabla\mathrm{div}(\boldsymbol{u}(\boldsymbol{x})), \quad \forall \boldsymbol{x}\in\Omega,$$

and eq. (5.7) becomes

$$\begin{cases} -\mathcal{L}_0^S \boldsymbol{u} = \boldsymbol{f}_0, & \text{in } \Omega, \\ \quad \boldsymbol{u} = \boldsymbol{0}, & \text{on } \partial\Omega. \end{cases} \tag{5.9}$$

We define a space on Ω_δ with zero volumetric constraint on $\Omega_{\mathcal{I}}$,

$$L_c^2(\Omega_\delta;\mathbb{R}^{\mathrm{d}}) := \{\boldsymbol{u}\in L^2(\Omega_\delta;\mathbb{R}^{\mathrm{d}}) \mid \boldsymbol{u} = \boldsymbol{0} \text{ on } \Omega_{\mathcal{I}}\}.$$

The natural energy space associated with eq. (5.7) is given in [81] as

$$\mathcal{S}_\delta := \left\{ \boldsymbol{u}\in L_c^2(\Omega_\delta;\mathbb{R}^{\mathrm{d}}) : \int_{\Omega_\delta}\int_{\Omega_\delta} \rho_\delta(|\boldsymbol{y}-\boldsymbol{x}|)(\mathrm{Tr}(\mathcal{D}^*\boldsymbol{u})(\boldsymbol{y},\boldsymbol{x}))^2 d\boldsymbol{y}d\boldsymbol{x} < \infty \right\},$$

where $\mathrm{Tr}(\mathcal{D}^*\boldsymbol{u})$ is the trace of the operator $\mathcal{D}^*$ defined in [35, 81]:

$$\mathcal{D}^*\boldsymbol{u}(\boldsymbol{y},\boldsymbol{x}) := (\boldsymbol{u}(\boldsymbol{y}) - \boldsymbol{u}(\boldsymbol{x})) \otimes \frac{\boldsymbol{y}-\boldsymbol{x}}{|\boldsymbol{y}-\boldsymbol{x}|}.$$

The static peridynamic Navier equation eq. (5.7) is well-posed and uniformly stable as given in [81] and shown in the following theorem.

Theorem 5.1.1. *Assume $\delta \in (0, \delta_0]$ for some $\delta_0 > 0$. The bilinear form $(-\mathcal{L}_\delta^S \boldsymbol{u}, \boldsymbol{u})$ is an inner product and there exists a constant $C > 0$ which depends on δ_0, such that*

$$|(-\mathcal{L}_\delta^E \boldsymbol{u}, \boldsymbol{u})| \geq C\|\boldsymbol{u}\|^2_{L^2(\Omega_\delta;\mathbb{R}^{\mathrm{d}})}, \quad \forall\, \boldsymbol{u} \in \mathcal{S}_\delta.$$

5.1.2 Quasi-discrete nonlocal operators

As introduced in Chapter 4, we use a finite number of symmetric quadrature points $\boldsymbol{s}$ in the horizon to evaluate the integral such that the weighted volume defined in eq. (5.2) is exact,

$$m(\boldsymbol{x}) = \sum_{\boldsymbol{s}\in B_\delta^\epsilon} \omega_\delta(|\boldsymbol{s}|)\rho_\delta(|\boldsymbol{s}|)|\boldsymbol{s}|^2 = \mathrm{d}, \quad \forall \boldsymbol{x} \in \Omega, \tag{5.10}$$

where $\omega_\delta(|\boldsymbol{s}|)$ is the quadrature weight at the quadrature point $\boldsymbol{s}$. An example of quadrature points in the horizon of an arbitrary point $\boldsymbol{x} \in \Omega$ is shown in Figure 4.1. We have a discrete version of eq. (3.4) as,

$$\sum_{\boldsymbol{s}\in B_1^{\epsilon_1}} \omega(|\boldsymbol{s}|)\rho(|\boldsymbol{s}|)\boldsymbol{s}^2 = \mathrm{d}. \tag{5.11}$$

However, unlike the nonlocal diffusion in Chapter 4, eq. (5.11) is not sufficient for the peridynamic Navier equation and we will revisit the construction of quadrature weights at the end of this section.

For $\boldsymbol{u}(\boldsymbol{x}) \in C^0(\mathbb{R}^{\mathrm{d}}; \mathbb{R}^{\mathrm{d}})$, we can reformulate the quasi-discrete counter part of the nonlocal operators defined in the previous subsection. The quasi-discrete bond-

based peridynamic operator $\mathcal{L}^B_{\delta,\epsilon}$ is defined as

$$\mathcal{L}^B_{\delta,\epsilon}\boldsymbol{u}(\boldsymbol{x}) = \sum_{\boldsymbol{s}\in B^\epsilon_\delta} \omega_\delta(|\boldsymbol{s}|)\rho_\delta(|\boldsymbol{s}|)\frac{\boldsymbol{s}}{|\boldsymbol{s}|}\otimes\frac{\boldsymbol{s}}{|\boldsymbol{s}|}(\boldsymbol{u}(\boldsymbol{x}+\boldsymbol{s})-\boldsymbol{u}(\boldsymbol{x})), \quad \forall\, \boldsymbol{x}\in\Omega. \tag{5.12}$$

Similarly, the quasi-discrete nonlocal divergence operator $\mathcal{D}^\epsilon_\delta$ is formulated as ,

$$\mathcal{D}^\epsilon_\delta\boldsymbol{u}(\boldsymbol{x}) = \sum_{\boldsymbol{s}\in B^\epsilon_\delta} \omega_\delta(|\boldsymbol{s}|)\rho_\delta(|\boldsymbol{s}|)\,\boldsymbol{s}\cdot(\boldsymbol{u}(\boldsymbol{x}+\boldsymbol{s})-\boldsymbol{u}(\boldsymbol{x})), \quad \forall\, \boldsymbol{x}\in\Omega. \tag{5.13}$$

A direct consequence of the nonlocal divergence operator is the quasi-discrete nonlocal dilatation defined as

$$\theta^\epsilon(\boldsymbol{x}) = \frac{\mathrm{d}}{m(\boldsymbol{x})}\mathcal{D}^\epsilon_\delta\boldsymbol{u}(\boldsymbol{x}), \quad \forall\, \boldsymbol{x}\in\Omega. \tag{5.14}$$

We want to emphasize that θ^ϵ is a continuous function with respect to $\boldsymbol{x}$ and its definition differs from eq. (5.4). We also have the quasi-discrete nonlocal gradient operator,

$$\mathcal{G}^\epsilon_\delta\theta(\boldsymbol{x}) = \sum_{\boldsymbol{s}\in B^\epsilon_\delta} \omega_\delta(|\boldsymbol{s}|)\rho_\delta(|\boldsymbol{s}|)\,\boldsymbol{s}\,(\theta(\boldsymbol{x}+\boldsymbol{s})-\theta(\boldsymbol{x})), \quad \forall\, \boldsymbol{x}\in\Omega. \tag{5.15}$$

Finally, we arrive at the linearized state-based quasi-discrete peridynamic Navier operator as

$$\mathcal{L}^S_{\delta,\epsilon}\boldsymbol{u}(\boldsymbol{x}) = \frac{C_\alpha\mu}{m(\boldsymbol{x})}\mathcal{L}^B_{\delta,\epsilon}\boldsymbol{u}(\boldsymbol{x}) + \frac{C_\beta \mathrm{d}(\lambda-\mu)}{(m(\boldsymbol{x}))^2}\mathcal{G}^\epsilon_\delta\mathcal{D}^\epsilon_\delta\boldsymbol{u}(\boldsymbol{x}), \quad \forall\, \boldsymbol{x}\in\Omega, \tag{5.16}$$

and the static peridynamic Navier equation can be reformulated as

$$\begin{cases} -\mathcal{L}^S_{\delta,\epsilon}\boldsymbol{u} = \boldsymbol{f}, & \text{in } \Omega, \\ \quad\boldsymbol{u} = \boldsymbol{0}, & \text{on } \Omega_{\mathcal{I}}. \end{cases} \tag{5.17}$$

Similar to eq. (5.8), if we let $p = (\lambda-\mu)\theta^\epsilon$, we can write eq. (5.17) as

$$\begin{cases} -\dfrac{C_\alpha\,\mu}{m(\boldsymbol{x})}\mathcal{L}^B_{\delta,\epsilon}\boldsymbol{u}(\boldsymbol{x}) - \dfrac{C_\beta}{m(\boldsymbol{x})}\mathcal{G}^\epsilon_\delta\theta^\epsilon(\boldsymbol{x}) = \boldsymbol{f}(\boldsymbol{x}), & \boldsymbol{x}\in\Omega, \\ \dfrac{\mathrm{d}\,(\lambda-\mu)}{m(\boldsymbol{x})}\mathcal{D}^\epsilon_\delta\boldsymbol{u}(\boldsymbol{x}) - \theta^\epsilon(\boldsymbol{x}) = 0, & \boldsymbol{x}\in\Omega, \\ \boldsymbol{u}(\boldsymbol{x}) = \boldsymbol{0}, & \boldsymbol{x}\in\Omega_{\mathcal{I}}. \end{cases} \tag{5.18}$$

If, for $\boldsymbol{u}$ being any quadratic polynomials,

$$\mathcal{L}^S_{\delta,\epsilon}\boldsymbol{u} = \mathcal{L}^S_{\delta}\boldsymbol{u}, \tag{5.19}$$

the quasi-discrete peridynamic Navier operator $\mathcal{L}^S_{\delta,\epsilon}$ converges to $\mathcal{L}^S_0$ as δ goes to 0. Equation (5.19) is not guaranteed by eq. (5.11) but is fulfilled if the following is satisfied, i.e.,

$$\sum_{\boldsymbol{s}\in B_1^{\epsilon_1}} \omega(|\boldsymbol{s}|)\rho(|\boldsymbol{s}|)\frac{s_i^2 s_j^2}{|\boldsymbol{s}|^2} = \int_{\boldsymbol{s}\in B_1} \rho(|\boldsymbol{s}|)\frac{s_i^2 s_j^2}{|\boldsymbol{s}|^2} d\boldsymbol{s}, \tag{5.20}$$

for $i, j = 1, \ldots, \mathrm{d}$. It is easy to see that eq. (5.20) is bounded because of eq. (3.4) and eq. (5.20) is a reformulation of eq. (5.10) by adding more constraints.

5.1.3 RK collocation scheme

We apply RK approximation as discussed in eq. (3.13) on both $\boldsymbol{u}$ and θ, back-substitute θ into the first equation of eq. (5.8) and obtain

$$\mathcal{L}^S_{\delta}\Pi^h\boldsymbol{u} = \frac{C_\alpha\,\mu}{m(\boldsymbol{x})}\mathcal{L}^B_{\delta}\Pi^h\boldsymbol{u} + \frac{C_\beta \mathrm{d}\,(\lambda-\mu)}{(m(\boldsymbol{x}))^2}\mathcal{G}_\delta\Pi^h(\mathcal{D}_\delta\Pi^h\boldsymbol{u}).$$

Following a similar procedure, we arrive at

$$\mathcal{L}^S_{\delta,\epsilon}\Pi^h\boldsymbol{u} = \frac{C_\alpha\,\mu}{m(\boldsymbol{x})}\mathcal{L}^B_{\delta,\epsilon}\Pi^h\boldsymbol{u} + \frac{C_\beta \mathrm{d}\,(\lambda-\mu)}{(m(\boldsymbol{x}))^2}\mathcal{G}^\epsilon_\delta\Pi^h(\mathcal{D}^\epsilon_\delta\Pi^h\boldsymbol{u}).$$

Therefore the RK collocation scheme of eqs. (5.7) and (5.17) can be written in the following forms. Find a function $\boldsymbol{u} \in S(\square \cap \Omega; \mathbb{R}^{\mathrm{d}})$, such that

$$-r^h_\Omega\mathcal{L}^S_\delta\boldsymbol{u} = r^h_\Omega\boldsymbol{f}, \tag{5.21}$$

and

$$-r^h_\Omega\mathcal{L}^S_{\delta,\,\epsilon}\boldsymbol{u} = r^h_\Omega\boldsymbol{f}, \tag{5.22}$$

where for $\boldsymbol{u}$ in the trial space, we have abused the notations and let $\mathcal{L}^S_\delta\boldsymbol{u}$ and $\mathcal{L}^S_{\delta,\epsilon}\boldsymbol{u}$ represent,

$$\mathcal{L}^S_{\delta}\boldsymbol{u} = \frac{C_\alpha\,\mu}{m(\boldsymbol{x})}\mathcal{L}^B_{\delta}\boldsymbol{u} + \frac{C_\beta \mathrm{d}\,(\lambda-\mu)}{(m(\boldsymbol{x}))^2}\mathcal{G}_\delta\Pi^h(\mathcal{D}_\delta\boldsymbol{u}),$$

and

$$\mathcal{L}^S_{\delta,\epsilon}\boldsymbol{u} = \frac{C_\alpha\,\mu}{m(\boldsymbol{x})}\mathcal{L}^B_{\delta,\epsilon}\boldsymbol{u} + \frac{C_\beta \mathrm{d}\,(\lambda-\mu)}{(m(\boldsymbol{x}))^2}\mathcal{G}^\epsilon_\delta \Pi^h(\mathcal{D}^\epsilon_\delta \boldsymbol{u}).$$

We show the convergence analysis of the two collocation schemes in the next two sections.

5.2 Convergence analysis of RK collocation method for the peridynamic Navier equation

In this section, we show the convergence analysis of the RK collocation scheme eq. (5.21), which is used in [95] without any analysis. A convergence proof for nonlocal diffusion problems is provided in Chapters 3 and 4, and the analysis is extended to the peridynamic Navier equation in this chapter. The main objective is to show that the solution of the numerical scheme converges to the nonlocal problem for a fixed δ, and to the correct local problem as δ and grid size $h_{\max}$ both go to zero.

5.2.1 Stability

In this subsection, we show the stability analysis of the RK collocation method. We first define a norm in the space of sequences by

$$|(\boldsymbol{u}_{\boldsymbol{k}})_{\boldsymbol{k}\in\mathbb{Z}^{\mathrm{d}}}|_h := \|i^h(\boldsymbol{u}_{\boldsymbol{k}})\|_{L^2(\mathbb{R}^{\mathrm{d}};\mathbb{R}^{\mathrm{d}})}\ . \tag{5.23}$$

For a sequence $(\boldsymbol{u}_{\boldsymbol{k}})$ only defined for $\boldsymbol{k}$ being in a subset of $\mathbb{Z}^{\mathrm{d}}$, we can always extend $(\boldsymbol{u}_{\boldsymbol{k}})$ by zero to $\boldsymbol{k}\in\mathbb{Z}^{\mathrm{d}}$. Then without further explanation, $|(\boldsymbol{u}_{\boldsymbol{k}})|_h$ is always understood as (5.23) with zero extension. We next borrow the idea from [28, 71] and compare the RK collocation scheme with the Galerkin scheme using Fourier analysis.

Theorem 5.2.1. *For any $\delta\in(0,\delta_0]$, there exists a constant C that depends on Ω and δ_0, such that for $\boldsymbol{u}\in S(\square\cap\Omega;\mathbb{R}^{\mathrm{d}})$,*

$$|r^h_\Omega(-\mathcal{L}^S_\delta \boldsymbol{u})|_h \geq C\|\boldsymbol{u}\|_{L^2(\mathbb{R}^{\mathrm{d}};\mathbb{R}^{\mathrm{d}})}.$$

We need some intermediate results before proving Theorem 5.2.1. We define a scalar product in $l^2(\mathbb{Z}^{\mathrm{d}};\mathbb{C}^{\mathrm{d}})$,

$$\begin{aligned}((\boldsymbol{u_k}),(\boldsymbol{v_k}))_{l^2} &:= \sum_{\boldsymbol{k}\in\mathbb{Z}^{\mathrm{d}}} u_{1,\boldsymbol{k}}\overline{v_{1,\boldsymbol{k}}} + \ldots + \sum_{\boldsymbol{k}\in\mathbb{Z}^{\mathrm{d}}} u_{\mathrm{d},\boldsymbol{k}}\overline{v_{\mathrm{d},\boldsymbol{k}}} \\ &= \sum_{j=1}^{\mathrm{d}} \sum_{\boldsymbol{k}\in\mathbb{Z}^{\mathrm{d}}} u_{j,\boldsymbol{k}}\overline{v_{j,\boldsymbol{k}}}.\end{aligned}$$

The Fourier series of a vector-valued sequence $(\boldsymbol{u_k})$ is defined as

$$\widetilde{\boldsymbol{u}}(\boldsymbol{\xi}) = [\tilde{u}_1(\boldsymbol{\xi}),\ldots,\tilde{u}_{\mathrm{d}}(\boldsymbol{\xi})]^T$$

and the j-th component of $\widetilde{\boldsymbol{u}}(\boldsymbol{\xi})$ is

$$\tilde{u}_j(\boldsymbol{\xi}) := \sum_{\boldsymbol{k}\in\mathbb{Z}^{\mathrm{d}}} e^{-i\boldsymbol{k}\cdot\boldsymbol{\xi}} u_{j,\boldsymbol{k}},$$

where

$$u_{j,\boldsymbol{k}} = (2\pi)^{-\mathrm{d}} \int_{\boldsymbol{Q}} e^{i\boldsymbol{k}\cdot\boldsymbol{\xi}} \tilde{u}_j(\boldsymbol{\xi}) d\boldsymbol{\xi},$$

where $\boldsymbol{Q} := (-\pi,\pi)^{\mathrm{d}}$.

First, we present the Fourier symbol of the nonlocal operators $-\mathcal{L}_\delta^S$ in the next lemma. The Fourier transform of $\boldsymbol{u} \in S_\delta$ is defined by

$$\widehat{\boldsymbol{u}}(\boldsymbol{\xi}) := \int_{\mathbb{R}^{\mathrm{d}}} e^{-i\boldsymbol{x}\cdot\boldsymbol{\xi}} \boldsymbol{u}(\boldsymbol{x}) d\boldsymbol{x}.$$

Lemma 5.2.2. *The Fourier symbol of the operators $\mathcal{L}_\delta^B, \mathcal{G}_\delta, \mathcal{D}_\delta$ are given by*

$$-\widehat{\mathcal{L}_\delta^B \boldsymbol{u}}(\boldsymbol{\xi}) = \boldsymbol{M}_\delta^B(\boldsymbol{\xi})\widehat{\boldsymbol{u}}(\boldsymbol{\xi}), \tag{5.24}$$

$$\widehat{\mathcal{G}_\delta \theta}(\boldsymbol{\xi}) = i\boldsymbol{b}_\delta(\boldsymbol{\xi})\widehat{\theta}(\boldsymbol{\xi}), \tag{5.25}$$

$$\widehat{\mathcal{D}_\delta \boldsymbol{u}}(\boldsymbol{\xi}) = i\boldsymbol{b}_\delta^T(\boldsymbol{\xi})\widehat{\boldsymbol{u}}(\boldsymbol{\xi}), \tag{5.26}$$

where $\boldsymbol{M}_\delta^B(\boldsymbol{\xi})$ is a $\mathrm{d}\times\mathrm{d}$ matrix and $\boldsymbol{b}_\delta(\boldsymbol{\xi})$ is a vector. They are expressed as

$$\begin{aligned}\boldsymbol{M}_\delta^B(\boldsymbol{\xi}) &= \int_{B_\delta} \rho_\delta(|\boldsymbol{s}|)\frac{\boldsymbol{s}\otimes\boldsymbol{s}}{|\boldsymbol{s}|^2}(1-\cos(\boldsymbol{s}\cdot\boldsymbol{\xi}))d\boldsymbol{s}, \\ &= p_\delta(|\boldsymbol{\xi}|)\left(\boldsymbol{I}_{\mathrm{d}} - \vec{\boldsymbol{\xi}}\vec{\boldsymbol{\xi}}^T\right) + q_\delta(|\boldsymbol{\xi}|)\vec{\boldsymbol{\xi}}\vec{\boldsymbol{\xi}}^T,\end{aligned} \tag{5.27}$$

and

$$\boldsymbol{b}_\delta(\boldsymbol{\xi}) = \int_{B_\delta} \rho_\delta(|\boldsymbol{s}|)\boldsymbol{s}\sin(\boldsymbol{s}\cdot\boldsymbol{\xi})d\boldsymbol{s} = b_\delta(|\boldsymbol{\xi}|)\vec{\boldsymbol{\xi}}, \tag{5.28}$$

where $\boldsymbol{I}_{\mathrm{d}}$ *is the* d*-dimensional identity matrix,* $\vec{\boldsymbol{\xi}} = \dfrac{\boldsymbol{\xi}}{|\boldsymbol{\xi}|}$ *is the unit vector in the direction of* $\boldsymbol{\xi}$ *and the scalars* $p_\delta(|\boldsymbol{\xi}|), q_\delta(|\boldsymbol{\xi}|)$ *and* $b_\delta(|\boldsymbol{\xi}|)$ *are given by*

$$p_\delta(|\boldsymbol{\xi}|) = \int_{B_\delta} \rho_\delta(|\boldsymbol{s}|)\frac{s_1^2}{|\boldsymbol{s}|^2}(1-\cos(|\boldsymbol{\xi}|s_{\mathrm{d}}))d\boldsymbol{s}, \tag{5.29}$$

$$q_\delta(|\boldsymbol{\xi}|) = \int_{B_\delta} \rho_\delta(|\boldsymbol{s}|)\frac{s_{\mathrm{d}}^2}{|\boldsymbol{s}|^2}(1-\cos(|\boldsymbol{\xi}|s_{\mathrm{d}}))d\boldsymbol{s}, \tag{5.30}$$

$$b_\delta(|\boldsymbol{\xi}|) = \int_{B_\delta} \rho_\delta(|\boldsymbol{s}|)s_{\mathrm{d}}\sin(|\boldsymbol{\xi}|s_{\mathrm{d}})d\boldsymbol{s}. \tag{5.31}$$

Proof. The derivations of eqs. (5.24)–(5.26) follow directly from the definition of these nonlocal operators. The derivation of $\boldsymbol{b}_\delta(\boldsymbol{\xi})$ can be found in [39] and we follow the same strategy to show $\boldsymbol{M}_\delta^B(\boldsymbol{\xi})$,

$$\begin{aligned}
-\widehat{\mathcal{L}_\delta^B\boldsymbol{u}}(\boldsymbol{\xi}) &= -\int_{\mathbb{R}^{\mathrm{d}}} e^{-i\boldsymbol{x}\cdot\boldsymbol{\xi}}\int_{B_\delta}\rho_\delta(|\boldsymbol{s}|)\frac{\boldsymbol{s}\otimes\boldsymbol{s}}{|\boldsymbol{s}|^2}(\boldsymbol{u}(\boldsymbol{x}+\boldsymbol{s})-\boldsymbol{u}(\boldsymbol{x}))d\boldsymbol{s}d\boldsymbol{x},\\
&= -\int_{B_\delta}\int_{\mathbb{R}^3}\rho_\delta(|\boldsymbol{s}|)\frac{\boldsymbol{s}\otimes\boldsymbol{s}}{|\boldsymbol{s}|^2}(\boldsymbol{u}(\boldsymbol{x}+\boldsymbol{s})-\boldsymbol{u}(\boldsymbol{x}))e^{-i\boldsymbol{x}\cdot\boldsymbol{\xi}}d\boldsymbol{x}d\boldsymbol{s},\\
&= \int_{B_\delta}\rho_\delta(|\boldsymbol{s}|)\frac{\boldsymbol{s}\otimes\boldsymbol{s}}{|\boldsymbol{s}|^2}(1-e^{i\boldsymbol{s}\cdot\boldsymbol{\xi}})\widehat{\boldsymbol{u}}(\boldsymbol{\xi})d\boldsymbol{s},\\
&= \boldsymbol{M}_\delta^B(\boldsymbol{\xi})\widehat{\boldsymbol{u}}(\boldsymbol{\xi}),
\end{aligned}$$

where $\boldsymbol{M}_\delta^B(\boldsymbol{\xi})$ is given by the first line of eq. (5.27) and we have used the symmetry of the nonlocal kernel $\rho_\delta(|\boldsymbol{s}|)$.

We proceed to show the second line of eq. (5.27) only for $\mathrm{d}=3$ because the case $\mathrm{d}=2$ is similar. For any orthogonal matrix $\boldsymbol{\mathcal{R}}$, we have

$$\boldsymbol{M}_\delta^B(\boldsymbol{\xi}) = \boldsymbol{\mathcal{R}}^T\boldsymbol{M}_\delta^B(\boldsymbol{\mathcal{R}}\boldsymbol{\xi})\boldsymbol{\mathcal{R}}.$$

We let $\boldsymbol{\mathcal{R}}$ be the orthogonal matrix which rotates $\boldsymbol{\xi}$ to be aligned with $\boldsymbol{e}$, ($\boldsymbol{e}=(0,0,1)^T$), as

$$\boldsymbol{\mathcal{R}}\boldsymbol{\xi} = |\boldsymbol{\xi}|\boldsymbol{e}.$$

Then $\boldsymbol{\mathcal{R}}\boldsymbol{\xi}\cdot\boldsymbol{s} = |\boldsymbol{\xi}|s_3$ and we have

$$\boldsymbol{M}_\delta^B(\boldsymbol{\xi}) = \int_{B_\delta} \rho_\delta(|\boldsymbol{s}|)\frac{1-\cos(|\boldsymbol{\xi}|s_3)}{|\boldsymbol{s}|^2}\boldsymbol{\mathcal{R}}^T\boldsymbol{s}(\boldsymbol{\mathcal{R}}^T\boldsymbol{s})^T d\boldsymbol{s},$$

$\boldsymbol{\mathcal{R}}$ is the rotation matrix that rotates $\boldsymbol{\xi}$ by an angle of

$$\arccos\left(\boldsymbol{e}\cdot\frac{\boldsymbol{\xi}}{|\boldsymbol{\xi}|}\right) = \arccos\left(\frac{\xi_3}{|\boldsymbol{\xi}|}\right),$$

around the axis in the direction of

$$\frac{\boldsymbol{\xi}\times\boldsymbol{e}}{|\boldsymbol{\xi}\times\boldsymbol{e}|} = \frac{1}{\sqrt{\xi_1^2+\xi_2^2}}(\xi_2,-\xi_1,0).$$

$\boldsymbol{\mathcal{R}}$ can be explicitly constructed as

$$\boldsymbol{\mathcal{R}} = \begin{bmatrix} \frac{\xi_3}{|\boldsymbol{\xi}|}+\frac{\xi_2^2}{\xi_1^2+\xi_2^2}\left(1-\frac{\xi_3}{|\boldsymbol{\xi}|}\right) & \frac{-\xi_1\xi_2}{\xi_1^2+\xi_2^2}\left(1-\frac{\xi_3}{|\boldsymbol{\xi}|}\right) & -\frac{\xi_1}{|\boldsymbol{\xi}|} \\ \frac{-\xi_1\xi_2}{\xi_1^2+\xi_2^2}\left(1-\frac{\xi_3}{|\boldsymbol{\xi}|}\right) & \frac{\xi_3}{|\boldsymbol{\xi}|}+\frac{\xi_1^2}{\xi_1^2+\xi_2^2}\left(1-\frac{\xi_3}{|\boldsymbol{\xi}|}\right) & -\frac{\xi_2}{|\boldsymbol{\xi}|} \\ \frac{\xi_1}{|\boldsymbol{\xi}|} & \frac{\xi_2}{|\boldsymbol{\xi}|} & \frac{\xi_3}{|\boldsymbol{\xi}|} \end{bmatrix}. \tag{5.32}$$

Hence each component of $\boldsymbol{M}_\delta(\boldsymbol{\xi})$ is written as

$$\begin{aligned}[\boldsymbol{M}_\delta^B(\boldsymbol{\xi})]_{ik} &= \int_{B_\delta}\rho_\delta(|\boldsymbol{s}|)\frac{1-\cos(|\boldsymbol{\xi}|s_3)}{|\boldsymbol{s}|^2}\sum_{j=1}^3\mathcal{R}_{ji}s_j\sum_{l=1}^3\mathcal{R}_{lk}s_l\,d\boldsymbol{s}, \\ &= \int_{B_\delta}\rho_\delta(|\boldsymbol{s}|)\frac{1-\cos(|\boldsymbol{\xi}|s_3)}{|\boldsymbol{s}|^2}\sum_{j=1}^3\mathcal{R}_{ji}\mathcal{R}_{jk}s_j^2\,d\boldsymbol{s}, \quad \text{for } i,k=1,2,3,\end{aligned}$$

where $\mathcal{R}_{ij}$ is the component of $\boldsymbol{\mathcal{R}}$. We can rewrite the Fourier symbol $\boldsymbol{M}_\delta^B(\boldsymbol{\xi})$ as

$$\boldsymbol{M}_\delta^B(\boldsymbol{\xi}) = \int_{B_\delta}\rho_\delta(|\boldsymbol{s}|)\frac{1-\cos(|\boldsymbol{\xi}|s_3)}{|\boldsymbol{s}|^2}\boldsymbol{M}(\boldsymbol{\xi},\boldsymbol{s})\,d\boldsymbol{s}, \tag{5.33}$$

where each component of $\boldsymbol{M}(\boldsymbol{\xi},\boldsymbol{s})$ is given by

$$M_{ik} = \sum_{j=1}^3 R_{ji}R_{jk}s_j^2\,.$$

From eq. (5.32), we arrive at

$$\begin{aligned}\boldsymbol{M}(\boldsymbol{\xi},\boldsymbol{s}) &= \frac{1}{|\boldsymbol{\xi}|^2}\begin{bmatrix}(\xi_2^2+\xi_3^2)s_1^2+\xi_1^2s_3^2 & \xi_1\xi_2(s_3^2-s_1^2) & \xi_1\xi_3(s_3^2-s_1^2)\\ \xi_2\xi_1(s_3^2-s_1^2) & (\xi_1^2+\xi_3^2)s_1^2+\xi_2^2s_3^2 & \xi_2\xi_3(s_3^2-s_1^2)\\ \xi_3\xi_1(s_3^2-s_1^2) & \xi_3\xi_2(s_3^2-s_1^2) & (\xi_1^2+\xi_2^2)s_1^2+\xi_3^2s_3^2\end{bmatrix},\\ &= s_1^2\left(\boldsymbol{I}_3-\vec{\boldsymbol{\xi}}\vec{\boldsymbol{\xi}}^T\right)+s_3^2\vec{\boldsymbol{\xi}}\vec{\boldsymbol{\xi}}^T,\end{aligned} \tag{5.34}$$

where we have used the equivalence of s_1 and s_2 in the integrand. Substitute eq. (5.34) into eq. (5.33), we obtain the second line of eq. (5.27) and $p_\delta(|\boldsymbol{\xi}|)$ and $q_\delta(|\boldsymbol{\xi}|)$ as given in eqs. (5.29) and (5.30). □

With the establishment of the previous lemma, we obtain the Fourier symbol of the peridynamic Navier operator $-\mathcal{L}_\delta^S$.

Lemma 5.2.3. *The Fourier symbol of the peridynamic Navier operator $\mathcal{L}_\delta^S$ is given by*

$$-\widehat{\mathcal{L}_\delta^S\boldsymbol{u}}(\boldsymbol{\xi}) = \boldsymbol{M}_\delta^S(\boldsymbol{\xi})\widehat{\boldsymbol{u}}(\boldsymbol{\xi}), \tag{5.35}$$

where the Fourier symbol $\boldsymbol{M}_\delta^S(\boldsymbol{\xi})$ is a $\mathrm{d}\times\mathrm{d}$ matrix and consists of two parts,

$$\boldsymbol{M}_\delta^S(\boldsymbol{\xi}) = \boldsymbol{M}_\delta^B(\boldsymbol{\xi}) + \boldsymbol{M}_\delta^D(\boldsymbol{\xi}), \tag{5.36}$$

where

$$\boldsymbol{M}_\delta^B(\boldsymbol{\xi}) = \frac{C_\mu}{\delta^2}p_1(\delta|\boldsymbol{\xi}|)\left(\boldsymbol{I}_\mathrm{d}-\vec{\boldsymbol{\xi}}\vec{\boldsymbol{\xi}}^T\right)+\frac{C_\mu}{\delta^2}q_1(\delta|\boldsymbol{\xi}|)\vec{\boldsymbol{\xi}}\vec{\boldsymbol{\xi}}^T, \tag{5.37}$$

and

$$\boldsymbol{M}_\delta^D(\boldsymbol{\xi}) = \frac{C_{\lambda,\mu}}{\delta^2}\left(b_1(\delta|\boldsymbol{\xi}|)\right)^2\vec{\boldsymbol{\xi}}\vec{\boldsymbol{\xi}}^T, \tag{5.38}$$

where $C_\mu = C_\alpha\mu/\mathrm{d}$ and $C_{\lambda,\mu} = C_\beta(\lambda-\mu)$ are material dependent constants and the scalars $p_1(|\boldsymbol{\xi}|), q_1(|\boldsymbol{\xi}|)$ and $b_1(|\boldsymbol{\xi}|)$ are given by

$$p_1(|\boldsymbol{\xi}|) = \int_{B_1}\rho(|\boldsymbol{s}|)\frac{s_1^2}{|\boldsymbol{s}|^2}(1-\cos(|\boldsymbol{\xi}|s_\mathrm{d}))d\boldsymbol{s}, \tag{5.39}$$

$$q_1(|\boldsymbol{\xi}|) = \int_{B_1} \rho(|\boldsymbol{s}|)\frac{s_{\mathrm{d}}^2}{|\boldsymbol{s}|^2}(1-\cos(|\boldsymbol{\xi}|s_{\mathrm{d}}))d\boldsymbol{s}, \tag{5.40}$$

$$b_1(|\boldsymbol{\xi}|) = \int_{B_1} \rho(|\boldsymbol{s}|)s_{\mathrm{d}}\sin(|\boldsymbol{\xi}|s_{\mathrm{d}})d\boldsymbol{s}. \tag{5.41}$$

Proof. Due to the scaling of the nonlocal kernel eq. (3.3), we can rewrite $p_\delta(|\boldsymbol{\xi}|)$, $q_\delta(|\boldsymbol{\xi}|)$ and $b_\delta(|\boldsymbol{\xi}|)$ as the following

$$p_\delta(|\boldsymbol{\xi}|) = \frac{p_1(\delta|\boldsymbol{\xi}|)}{\delta^2}, \tag{5.42}$$

$$q_\delta(|\boldsymbol{\xi}|) = \frac{q_1(\delta|\boldsymbol{\xi}|)}{\delta^2}, \tag{5.43}$$

$$b_\delta(|\boldsymbol{\xi}|) = \frac{b_1(\delta|\boldsymbol{\xi}|)}{\delta}, \tag{5.44}$$

where $p_1(\delta|\boldsymbol{\xi}|)$, $q_1(\delta|\boldsymbol{\xi}|)$ and $b_1(\delta|\boldsymbol{\xi}|)$ are given as in eqs. (5.39)–(5.41) respectively. Combing eqs. (5.24)–(5.26), we arrive at eq. (5.35). Substituting eqs. (5.42) and (5.43) into eq. (5.27), while, eq. (5.44) into eq. (5.28), we obtain eq. (5.36). □

From eq. (5.36), if $C_{\lambda,\mu} \geq 0$ we can see that the Fourier symbol $\boldsymbol{M}_\delta^S(\boldsymbol{\xi})$ is positive definite.

Lemma 5.2.4. *Assume $\lambda \geq \mu$, the Fourier symbol $\boldsymbol{M}_\delta^S(\boldsymbol{\xi})$ is positive definite for any $\boldsymbol{\xi} \neq \boldsymbol{0}$.*

Proof. By observation, $\boldsymbol{M}_\delta^S(\boldsymbol{\xi})$ is a real matrix. Moreover, from eqs. (5.39) and (5.40) we know that

$$p_1(\delta|\boldsymbol{\xi}|), q_1(\delta|\boldsymbol{\xi}|) > 0, \qquad \text{for } \delta|\boldsymbol{\xi}| \neq 0.$$

Without loss of generality, we let $\boldsymbol{v}$ be a unit vector so $|\boldsymbol{v}^T\vec{\boldsymbol{\xi}}| \leq |\boldsymbol{v}|$ because $|\vec{\boldsymbol{\xi}}| = 1$.

Then, we have

$$\begin{aligned}
\delta^2 \boldsymbol{v}^T \boldsymbol{M}_\delta^S(\boldsymbol{\xi})\boldsymbol{v} &\geq C_\mu p_1(\delta|\boldsymbol{\xi}|)\boldsymbol{v}^T\left(\boldsymbol{I}_{\mathrm{d}} - \vec{\boldsymbol{\xi}}\vec{\boldsymbol{\xi}}^T\right)\boldsymbol{v} \\
&\quad + \left[C_\mu q_1(\delta|\boldsymbol{\xi}|) + C_{\lambda,\mu}\left(b_1(\delta|\boldsymbol{\xi}|)\right)^2\right]\boldsymbol{v}^T\vec{\boldsymbol{\xi}}\vec{\boldsymbol{\xi}}^T\boldsymbol{v}, \\
&= C_\mu p_1(\delta|\boldsymbol{\xi}|)\left(|\boldsymbol{v}|^2 - |\boldsymbol{v}^T\vec{\boldsymbol{\xi}}|^2\right) \\
&\quad + \left[C_\mu q_1(\delta|\boldsymbol{\xi}|) + C_{\lambda,\mu}\left(b_1(\delta|\boldsymbol{\xi}|)\right)^2\right]|\boldsymbol{v}^T\vec{\boldsymbol{\xi}}|^2, \\
&> 0,
\end{aligned}$$

where we have used the assumption that $C_{\lambda,\mu} = \lambda - \mu \geq 0$. □

Remark 5.2.5. *In order to show the positive definiteness of $\boldsymbol{M}_\delta^S$ for more general λ and μ, we need more details on the nonlocal kernel ($\rho(|\boldsymbol{s}|)$) which is beyond the scope of this dissertation and we assume $\lambda \geq \mu$ to avoid such discussion. For materials that satisfy such constraint, the Poisson ratio ν has to be in $[0.25, 0.5)$. However, the well-posedness of eq. (5.7) proved in [81] infers that $\boldsymbol{M}_\delta^S$ is positive definite even without this assumption.*

The peridynamic Navier operator $\mathcal{L}_\delta^S$ defines two discrete sesquilinear forms:

$$\left(i^h(\boldsymbol{u}_{\boldsymbol{k}}), -\mathcal{L}_\delta^S i^h(\boldsymbol{v}_{\boldsymbol{k}})\right) = \sum_{j,\,j'=1}^{\mathrm{d}} \sum_{\boldsymbol{k},\,\boldsymbol{k'}\in\mathbb{Z}^{\mathrm{d}}} u_{j,\,\boldsymbol{k}}\left((\Psi_{\boldsymbol{k}}), -\mathcal{L}_\delta^S(\Psi_{\boldsymbol{k'}})\right)\overline{v_{j',\,\boldsymbol{k'}}}\,, \tag{5.45}$$

and

$$\left((\boldsymbol{u}_{\boldsymbol{k}}), -r^h\mathcal{L}_\delta^S i^h(\boldsymbol{v}_{\boldsymbol{k}})\right)_{l^2} = \prod_{j=1}^{\mathrm{d}} h_j \sum_{j,j'=1}^{\mathrm{d}} \sum_{\boldsymbol{k},\boldsymbol{k'}\in\mathbb{Z}^{\mathrm{d}}} u_{j,\,\boldsymbol{k}}\left(-\mathcal{L}_\delta^S(\Psi_{\boldsymbol{k'}})\right)(\boldsymbol{x}_{\boldsymbol{k}})\overline{v_{j',\,\boldsymbol{k'}}}\,. \tag{5.46}$$

Equation (5.45) defines a quadratic form corresponding to the Galerkin method, meanwhile, eq. (5.46) corresponds to the collocation method. The two quadratic forms eqs. (5.45) and (5.46) are compared as follows and the proof is similar to Lemma 3.3.2.

Lemma 5.2.6. *Let $\widetilde{\boldsymbol{u}}(\boldsymbol{\xi})$ and $\widetilde{\boldsymbol{v}}(\boldsymbol{\xi})$ be the Fourier series of the sequences $(\boldsymbol{u_k}), (\boldsymbol{v_k}) \in l^1(\mathbb{Z}^{\mathrm{d}}; \mathbb{C}^{\mathrm{d}})$ respectively and the RK interpolation of two sequences is expressed as $i^h(\boldsymbol{u_k}) = [i^h(u_{1,\boldsymbol{k}}), \ldots, i^h(u_{\mathrm{d},\boldsymbol{k}})]^T$ and $i^h(\boldsymbol{v_k}) = \left[i^h(v_{1,\boldsymbol{k}}), \ldots, i^h(v_{\mathrm{d},\boldsymbol{k}})\right]^T$. Then*

(i) $\left(i^h(\boldsymbol{u_k}), -\mathcal{L}_\delta^S i^h(\boldsymbol{v_k})\right) = (2\pi)^{-\mathrm{d}} \displaystyle\int_{\boldsymbol{Q}} \widetilde{\boldsymbol{u}}(\boldsymbol{\xi}) \cdot \boldsymbol{M}_G(\delta, \boldsymbol{h}, \boldsymbol{\xi}) \overline{\widetilde{\boldsymbol{v}}(\boldsymbol{\xi})} d\boldsymbol{\xi},$

(ii) $\left((\boldsymbol{u_k}), -r^h \mathcal{L}_\delta^S i^h(\boldsymbol{v_k})\right)_{l^2} = (2\pi)^{-\mathrm{d}} \displaystyle\int_{\boldsymbol{Q}} \widetilde{\boldsymbol{u}}(\boldsymbol{\xi}) \cdot \boldsymbol{M}_C(\delta, \boldsymbol{h}, \boldsymbol{\xi}) \overline{\widetilde{\boldsymbol{v}}(\boldsymbol{\xi})} d\boldsymbol{\xi},$

(iii) There exists a constant $C > 0$ independent of $\delta, \boldsymbol{h}$ and $\boldsymbol{\xi}$ such that $\boldsymbol{M}_C(\delta, \boldsymbol{h}, \boldsymbol{\xi}) - C\boldsymbol{M}_G(\delta, \boldsymbol{h}, \boldsymbol{\xi})$ is positive definite for any $\boldsymbol{\xi} \neq \boldsymbol{0}$,

where $\boldsymbol{M}_G$ and $\boldsymbol{M}_C$ are defined as

$$\begin{aligned} \boldsymbol{M}_G(\delta, \boldsymbol{h}, \boldsymbol{\xi}) = {} & 2^{8\mathrm{d}} \sum_{\boldsymbol{r} \in \mathbb{Z}^{\mathrm{d}}} \boldsymbol{M}_\delta^B \left((\boldsymbol{\xi} + 2\pi\boldsymbol{r}) \oslash \boldsymbol{h}\right) \prod_{j=1}^{\mathrm{d}} h_j \left(\frac{\sin(\xi_j/2)}{\xi_j + 2\pi r_j}\right)^8 \\ & + 2^{8\mathrm{d}+4} \sum_{\boldsymbol{r} \in \mathbb{Z}^{\mathrm{d}}} \boldsymbol{M}_\delta^D \left((\boldsymbol{\xi} + 2\pi\boldsymbol{r}) \oslash \boldsymbol{h}\right) \prod_{j=1}^{\mathrm{d}} h_j \left(\frac{\sin(\xi_j/2)}{\xi_j + 2\pi r_j}\right)^{12}, \end{aligned} \tag{5.47}$$

$$\begin{aligned} \boldsymbol{M}_C(\delta, \boldsymbol{h}, \boldsymbol{\xi}) = {} & 2^{4\mathrm{d}} \sum_{\boldsymbol{r} \in \mathbb{Z}^{\mathrm{d}}} \boldsymbol{M}_\delta^B \left((\boldsymbol{\xi} + 2\pi\boldsymbol{r}) \oslash \boldsymbol{h}\right) \prod_{j=1}^{\mathrm{d}} h_j \left(\frac{\sin(\xi_j/2)}{\xi_j + 2\pi r_j}\right)^4 \\ & + 2^{4\mathrm{d}+4} \sum_{\boldsymbol{r} \in \mathbb{Z}^{\mathrm{d}}} \boldsymbol{M}_\delta^D \left((\boldsymbol{\xi} + 2\pi\boldsymbol{r}) \oslash \boldsymbol{h}\right) \prod_{j=1}^{\mathrm{d}} h_j \left(\frac{\sin(\xi_j/2)}{\xi_j + 2\pi r_j}\right)^8. \end{aligned} \tag{5.48}$$

Proof. The inverse Fourier transform of $\widehat{\mathcal{L}_\delta^S \boldsymbol{u}}(\boldsymbol{\xi})$ gives

$$-\mathcal{L}_\delta^S \boldsymbol{u}(\boldsymbol{x}) = (2\pi)^{-\mathrm{d}} \int_{\mathbb{R}^{\mathrm{d}}} e^{i\boldsymbol{x}\cdot\boldsymbol{\xi}} \boldsymbol{M}_\delta^S(\boldsymbol{\xi}) \widehat{\boldsymbol{u}}(\boldsymbol{\xi}) d\boldsymbol{\xi},$$

From Parseval's identity, we have

$$\begin{aligned}((\Psi_{\boldsymbol{k}}), -\mathcal{L}_\delta^S(\Psi_{\boldsymbol{k'}})) &= (2\pi)^{-\mathrm{d}} \int_{\mathbb{R}^{\mathrm{d}}} \left(\widehat{\Psi_{\boldsymbol{k}}}(\boldsymbol{\xi})\right) \overline{\boldsymbol{M}_\delta^S(\boldsymbol{\xi})} \overline{\left(\widehat{\Psi_{\boldsymbol{k'}}}(\boldsymbol{\xi})\right)} d\boldsymbol{\xi}, \\ &= (2\pi)^{-\mathrm{d}} \sum_{j,j'=1}^{\mathrm{d}} \int_{\mathbb{R}^{\mathrm{d}}} e^{i\left((\boldsymbol{x_{k'}})-(\boldsymbol{x_k})\right)\cdot\boldsymbol{\xi}} \left[\boldsymbol{M}_\delta^S(\boldsymbol{\xi})\right]_{jj'} \widehat{\Psi_{\boldsymbol{0}}}^2(\boldsymbol{\xi}) d\boldsymbol{\xi}, \\ &= (2\pi)^{-\mathrm{d}} \sum_{j,j'=1}^{\mathrm{d}} \int_{\boldsymbol{Q}} e^{i(\boldsymbol{k'}-\boldsymbol{k})\cdot\boldsymbol{\xi}} \left[\boldsymbol{M}_G(\delta, \boldsymbol{h}, \boldsymbol{\xi})\right]_{jj'} d\boldsymbol{\xi},\end{aligned}$$

where we have used eq. (3.13) and the Fourier transform of the RK shape function

$$\widehat{\Psi_{\boldsymbol{0}}}(\boldsymbol{\xi}) = \prod_{j=1}^{\mathrm{d}} \widehat{\phi\left(\frac{x_j}{2h_j}\right)}(\xi_j) = \prod_{j=1}^{\mathrm{d}} h_j \left(\frac{\sin(h_j\xi_j/2)}{h_j\xi_j/2}\right)^4,$$

where the Fourier transform of the cubic B-spline function is given as

$$\widehat{\phi}(\xi) = \frac{1}{2}\left(\frac{\sin(\xi/4)}{\xi/4}\right)^4.$$

Hence, the Galerkin form eq. (5.45) can be written as

$$\begin{aligned}&(i^h(\boldsymbol{u_k}), -\mathcal{L}_\delta^S i^h(\boldsymbol{v_k})) \\ &= (2\pi)^{-\mathrm{d}} \sum_{j,j'=1}^{\mathrm{d}} \sum_{\boldsymbol{k},\boldsymbol{k'}\in\mathbb{Z}^{\mathrm{d}}} u_{j,\boldsymbol{k}} \overline{v_{j',\boldsymbol{k'}}} \int_{\boldsymbol{Q}} e^{i(\boldsymbol{k'}-\boldsymbol{k})\cdot\boldsymbol{\xi}} \left[\boldsymbol{M}_G(\delta, h, \boldsymbol{\xi})\right]_{jj'} d\boldsymbol{\xi}, \\ &= (2\pi)^{-\mathrm{d}} \sum_{j,j'=1}^{\mathrm{d}} \int_{\boldsymbol{Q}} \widetilde{u_j}(\boldsymbol{\xi}) \overline{\widetilde{v_{j'}}(\boldsymbol{\xi})} \left[\boldsymbol{M}_G(\delta, \boldsymbol{h}, \boldsymbol{\xi})\right]_{jj'} d\boldsymbol{\xi},\end{aligned}$$

and we have proved (i).

Next, we use the same strategy to express the collocation matrix as

$$\begin{aligned}-\left[\mathcal{L}_\delta^S\left(\Psi_{\boldsymbol{k'}}\right)\right]_j(\boldsymbol{x_k}) &= (2\pi)^{-\mathrm{d}} \int_{\mathbb{R}^{\mathrm{d}}} e^{i\boldsymbol{x_k}\cdot\boldsymbol{\xi}} \boldsymbol{M}_\delta^S(\boldsymbol{\xi}) \left(\widehat{\Psi_{\boldsymbol{k'}}}(\boldsymbol{\xi})\right) d\boldsymbol{\xi}, \\ &= (2\pi)^{-\mathrm{d}} \int_{\mathbb{R}^{\mathrm{d}}} e^{i(\boldsymbol{x_k}-\boldsymbol{x_{k'}})\cdot\boldsymbol{\xi}} \boldsymbol{M}_\delta^S(\boldsymbol{\xi}) \left(\widehat{\Psi_{\boldsymbol{0}}}(\boldsymbol{\xi})\right) d\boldsymbol{\xi}, \\ &= (2\pi)^{-\mathrm{d}} \sum_{j'=1}^{\mathrm{d}} \int_{\boldsymbol{Q}} e^{i(\boldsymbol{k}-\boldsymbol{k'})\cdot\boldsymbol{\xi}} \left[\boldsymbol{M}_C(\delta, \boldsymbol{h}, \boldsymbol{\xi})\right]_{jj'} d\boldsymbol{\xi},\end{aligned}$$

then we arrive at the collocation form eq. (5.46) as

$$
\begin{aligned}
&\left((\boldsymbol{u_k}), -r^h\mathcal{L}_\delta^S i^h(\boldsymbol{v_{k'}})(\boldsymbol{x_k})\right)_{l^2} \\
&= (2\pi)^{-\mathrm{d}} \sum_{j,j'=1}^{\mathrm{d}} \sum_{\boldsymbol{k},\boldsymbol{k'}\in\mathbb{Z}^{\mathrm{d}}} u_{j,\boldsymbol{k}}\, \overline{v_{j',\boldsymbol{k'}}} \int_{\boldsymbol{Q}} e^{i(\boldsymbol{k'}-\boldsymbol{k})\cdot\boldsymbol{\xi}}\, \overline{[\boldsymbol{M}_C(\delta,\boldsymbol{h},\boldsymbol{\xi})]_{jj'}}\, d\boldsymbol{\xi}, \\
&= (2\pi)^{-\mathrm{d}} \sum_{j,j'=1}^{\mathrm{d}} \int_{\boldsymbol{Q}} \widetilde{u_j}(\boldsymbol{\xi})\overline{\widetilde{v_{j'}}(\boldsymbol{\xi})}\, [\boldsymbol{M}_C(\delta,\boldsymbol{h},\boldsymbol{\xi})]_{jj'}\, d\boldsymbol{\xi}.
\end{aligned}
$$

This finishes the proof of (ii). In addition, for any $\boldsymbol{\xi} \in \boldsymbol{Q}$, we have

$$
p_1\left(\delta|(\boldsymbol{\xi}+2\pi\boldsymbol{r})\oslash\boldsymbol{h}|\right)\prod_{j=1}^{\mathrm{d}}\left(\frac{\sin(\xi_j)}{(\xi_j+2\pi r_j)}\right)^4\left(1-C\left(\frac{\sin(\xi_j)}{\xi_j+2\pi r_j}\right)^4\right) > 0,
$$

for a generic $C > 0$, $\boldsymbol{\xi} \neq \boldsymbol{0}$, and $\boldsymbol{r} \in \mathbb{Z}^{\mathrm{d}}$. Following similar procedure as in Lemma 5.2.4, we can see (iii) immediately. □

Finally, we are ready to prove Theorem 5.2.1 using Lemma 5.2.6.

Proof of Theorem 5.2.1. For $\boldsymbol{u} = i^h(\boldsymbol{u_k}) \in S(\square \cap \Omega; \mathbb{R}^{\mathrm{d}})$, we have

$$
\begin{aligned}
|(\boldsymbol{u_k})|_h \cdot |r_\Omega^h(-\mathcal{L}_\delta^S\boldsymbol{u})|_h &\geq C|((\boldsymbol{u_k}), r_\Omega^h(-\mathcal{L}_\delta^S\boldsymbol{u}))_{l^2}|, \\
&= C|((\boldsymbol{u_k}), r^h(-\mathcal{L}_\delta^S i^h(\boldsymbol{u_k})))_{l^2}|, \\
&\geq C|(i^h(\boldsymbol{u_k}), (-\mathcal{L}_\delta^S i^h(\boldsymbol{u_k})))|, \\
&\geq C\|\boldsymbol{u}\|^2_{L^2(\mathbb{R}^{\mathrm{d}};\mathbb{R}^{\mathrm{d}})}.
\end{aligned}
$$

The first line comes from Cauchy-Schwartz inequality and the third line is an adaption of Lemma 3.3.4. □

5.2.2 Consistency

In this subsection, we first show the consistency analysis of the RK collocation method and then present the convergence result using the stability analysis in

subsection 5.2.1 and consistency. The RK collocation scheme converges to the non-local solution as grid size $h_{\max}$ goes to zero with a fixed δ and to its local limit as δ vanishes as δ and $h_{\max}$ both vanish. The most important ingredient for the proof of asymptotic compatibility of the collocation scheme is the synchronized convergence (Lemma 3.3.6). We study the truncation error of the RK collocation method for the peridynamic Navier equation. Here and for the rest of this section, we adopt the following notations for a vector-valued function $\boldsymbol{u} \in C^n(\mathbb{R}^{\mathrm{d}}; \mathbb{R}^{\mathrm{d}})$,

$$
\begin{aligned}
|\boldsymbol{u}|_\infty &= \sup_{1\le j\le \mathrm{d}} \sup_{\boldsymbol{x}\in\mathbb{R}^{\mathrm{d}}} |u_j(\boldsymbol{x})|, \text{ and} \\
|\boldsymbol{u}^{(l)}|_\infty &= \sup_{1\le j\le \mathrm{d}} \sup_{|\boldsymbol{\beta}|=l} \sup_{\boldsymbol{y}\in\mathbb{R}^{\mathrm{d}}} |D^{\boldsymbol{\beta}} u_j(\boldsymbol{y})|, \quad 1 \le l \le n.
\end{aligned}
$$

Lemma 5.2.7. ***(Uniform consistency)*** *Assume $\boldsymbol{u} \in C^4(\mathbb{R}^{\mathrm{d}}; \mathbb{R}^{\mathrm{d}})$, then*

$$
|r^h \mathcal{L}_\delta^S \Pi^h \boldsymbol{u} - r^h \mathcal{L}_\delta^S \boldsymbol{u}|_h \le C h_{\max}^2 |\boldsymbol{u}^{(4)}|_\infty,
$$

where C is independent of $h_{\max}$ and δ.

Proof. We first define the interpolation error of $u_j(\boldsymbol{x})$, for $\boldsymbol{x} \in \mathbb{R}^{\mathrm{d}}$, and $j = 1, \dots, \mathrm{d}$, as

$$
E_j(\boldsymbol{x}) = \Pi^h u_j(\boldsymbol{x}) - u_j(\boldsymbol{x}),
$$

then

$$
\boldsymbol{E}(\boldsymbol{x}) = [E_1(\boldsymbol{x}), \dots, E_{\mathrm{d}}(\boldsymbol{x})]^T.
$$

By restricting on the the grid point $\boldsymbol{x_k}$, for $i = 1, \dots, \mathrm{d}$, the truncation error of $\mathcal{L}_\delta^B$ is given as

$$
\begin{aligned}
\left| \left[\mathcal{L}_\delta^B \left(\Pi^h \boldsymbol{u} - \boldsymbol{u} \right) \right]_i (\boldsymbol{x_k}) \right| &= \left| \left[\mathcal{L}_\delta^B \boldsymbol{E} \right]_i (\boldsymbol{x_k}) \right|, \\
&= \left| \sum_{j=1}^{\mathrm{d}} \int_{B_\delta} \rho_\delta(|\boldsymbol{s}|) \frac{s_i s_j}{|\boldsymbol{s}|^2} \left(E_j(\boldsymbol{x_k} + \boldsymbol{s}) - E_j(\boldsymbol{x_k}) \right) d\boldsymbol{s} \right|.
\end{aligned} \tag{5.49}
$$

Next, using Lemma 3.3.6, we can bound the interpolation error as

$$\begin{aligned} |E_j(\boldsymbol{x_k}+\boldsymbol{s})+E_j(\boldsymbol{x_k}-\boldsymbol{s})-2E_j(\boldsymbol{x_k})| &\leq C|\boldsymbol{s}|^2 \max_{|\boldsymbol{\alpha}|=2} |D^{\boldsymbol{\alpha}} E_j(\boldsymbol{x})|_\infty \,, \\ &\leq C|\boldsymbol{s}|^2 |u_j^{(4)}|_\infty h_{\max}^2 \,. \end{aligned} \tag{5.50}$$

By combining eqs. (5.49) and (5.50), we have

$$\begin{aligned} \left|[\mathcal{L}_\delta^B \left(\Pi^h \boldsymbol{u}-\boldsymbol{u}\right)(\boldsymbol{x_k})]_i\right| &\leq C h_{\max}^2 \sum_{j=1}^{\mathrm{d}} |u_j^{(4)}|_\infty \int_{B_\delta} \rho_\delta(|\boldsymbol{s}|)|s_i||s_j| \, d\boldsymbol{s}, \\ &\leq C h_{\max}^2 \left|\boldsymbol{u}^{(4)}\right|_\infty , \end{aligned} \tag{5.51}$$

where we have used eq. (5.2) and $C > 0$ is a generic constant depending on the dimension d.

Next, we define the interpolation error of the scaled nonlocal dilatation as

$$\begin{aligned} E_\theta &= \Pi^h \mathcal{D}_\delta \Pi^h \boldsymbol{u} - \mathcal{D}_\delta \boldsymbol{u}, \\ &= \Pi^h (\mathcal{D}_\delta \Pi^h \boldsymbol{u} - \mathcal{D}_\delta \boldsymbol{u}) + \Pi^h \mathcal{D}_\delta \boldsymbol{u} - \mathcal{D}_\delta \boldsymbol{u}, \\ &= \Pi^h \mathcal{D}_\delta \boldsymbol{E} + (\Pi^h \theta - \theta), \end{aligned} \tag{5.52}$$

where we have used the definition of the nonlocal dilatation eq. (5.4). There are two RK interpolation projectors (Π^h) in the first line of eq. (5.52) because we apply the same RK approximation to $\boldsymbol{u}$ and θ, then substitute θ back to get a pure displacement form. The nonlocal gradient operator acting on E_θ can be bounded by

$$\begin{aligned} |[\mathcal{G}_\delta E_\theta(\boldsymbol{x_k})]_i| &= \left| \int_{B_\delta} \rho_\delta(|\boldsymbol{t}|) t_i \left(E_\theta(\boldsymbol{x_k}+\boldsymbol{t}) - E_\theta(\boldsymbol{x_k})\right) d\boldsymbol{t} \right| , \\ &\leq \max_{|\boldsymbol{\beta}|=1} \left|D^{\boldsymbol{\beta}} E_\theta\right| \int_{B_\delta} \rho_\delta(|\boldsymbol{t}|)|t_i||\boldsymbol{t}| \, d\boldsymbol{t} \,, \\ &\leq C \max_{|\boldsymbol{\beta}|=1} \left|D^{\boldsymbol{\beta}} E_\theta\right| , \\ &\leq C \max_{|\boldsymbol{\beta}|=1} \left|D^{\boldsymbol{\beta}} \Pi^h \mathcal{D}_\delta \boldsymbol{E}\right| + C \max_{|\boldsymbol{\beta}|=1} \left|D^{\boldsymbol{\beta}} (\Pi^h \theta - \theta)\right| , \end{aligned} \tag{5.53}$$

for $i = 1, \ldots, \mathrm{d}$. we can bound the first term in the last line of eq. (5.53) by

$$\begin{aligned}
\max_{|\boldsymbol{\beta}|=1} \left| D^{\boldsymbol{\beta}} \Pi^h \mathcal{D}_\delta \boldsymbol{E} \right| &= \max_{|\boldsymbol{\beta}|=1} \left| \sum_{j=1}^{\mathrm{d}} D^{\boldsymbol{\beta}} \Pi^h \int_{B_\delta} \rho_\delta(|\boldsymbol{s}|) s_j \left(E_j(\boldsymbol{x}+\boldsymbol{s}) - E_j(\boldsymbol{x}) \right) d\boldsymbol{s} \right|, \\
&\leq \sum_{j=1}^{\mathrm{d}} \int_{B_\delta} \rho_\delta(|\boldsymbol{s}|) |s_j| |\boldsymbol{s}| d\boldsymbol{s} \max_{|\boldsymbol{\alpha}|=|\boldsymbol{\beta}|=1} \left| D^{\boldsymbol{\beta}} \Pi^h D^{\boldsymbol{\alpha}} E_j(\boldsymbol{x}) \right|, \\
&\leq C h_{\max}^2 \left| \boldsymbol{u}^{(4)} \right|_\infty .
\end{aligned} \tag{5.54}$$

where the derivation of the second line to the last can be obtained by similar expansion of [74, eq. (36)] and the result of Lemma 2.3.1, and we have used Lemma 3.3.6. Next, we have the bound of the second term in the last line of eq. (5.53) as

$$\max_{|\boldsymbol{\beta}|=1} \left| D^{\boldsymbol{\beta}} (\Pi^h \theta - \theta) \right| \leq C |\theta^{(3)}|_\infty h_{\max}^2 . \tag{5.55}$$

Moreover, $|\theta^{(3)}|_\infty$ is bounded by

$$\begin{aligned}
|\theta^{(3)}|_\infty &= \max_{|\boldsymbol{\beta}|=3} \left| \sum_{j=1}^{\mathrm{d}} D^{\boldsymbol{\beta}} \int_{B_\delta} \rho_\delta(|\boldsymbol{s}|) s_j \left(u_j(\boldsymbol{x}+\boldsymbol{s}) - u_j(\boldsymbol{x}) \right) d\boldsymbol{s} \right|, \\
&\leq \sum_{j=1}^{\mathrm{d}} \int_{B_\delta} \rho_\delta(|\boldsymbol{s}|) |s_j| |\boldsymbol{s}| d\boldsymbol{s} \max_{|\boldsymbol{\alpha}|=4} |D^{\boldsymbol{\alpha}} u_j(\boldsymbol{x})| , \\
&\leq C \left| \boldsymbol{u}^{(4)} \right|_\infty .
\end{aligned} \tag{5.56}$$

By collecting eqs. (5.53)–(5.56), the truncation error of the composition of the nonlocal gradient and divergence operators is bounded as

$$\left| [(\mathcal{G}_\delta \Pi^h \mathcal{D}_\delta \Pi^h \boldsymbol{u} - \mathcal{G}_\delta \mathcal{D}_\delta \boldsymbol{u})(\boldsymbol{x}_{\boldsymbol{k}})]_i \right| \leq C h_{\max}^2 \left| \boldsymbol{u}^{(4)} \right|_\infty . \tag{5.57}$$

Finally, the proof is finished by combing eqs. (5.51) and (5.57). □

With stability Theorem 5.2.1 and consistency Lemma 5.2.7 of the RK collocation method, we can immediately show the convergence to the nonlocal solution.

Theorem 5.2.8. ***(Uniform Convergence to nonlocal solution)*** *For a fixed* $\delta \in (0, \delta_0]$, *assume the nonlocal exact solution* $\boldsymbol{u}^\delta$ *is sufficiently smooth, i.e.,* $\boldsymbol{u}^\delta \in$

$C^4(\overline{\Omega_\delta};\mathbb{R}^{\mathrm{d}})$. *Moreover, assume* $|\boldsymbol{u}^{\delta(4)}|_\infty$ *is uniformly bounded for every* δ. *Let* $\boldsymbol{u}^{\delta,h}$ *be the numerical solution of the collocation scheme eq. (5.21), then,*

$$\|\boldsymbol{u}^\delta - \boldsymbol{u}^{\delta,h}\|_{L^2(\Omega;\mathbb{R}^{\mathrm{d}})} \leq Ch^2_{\max},$$

where C *is independent of* $h_{\max}$ *and* δ.

Proof. First, we can extend $\boldsymbol{u}^\delta$ to $\mathbb{R}^{\mathrm{d}}$ by zero such that $\boldsymbol{u}^\delta \in C^4(\overline{\Omega_\delta};\mathbb{R}^{\mathrm{d}})$ because $\boldsymbol{u}^\delta = \boldsymbol{0}$ on $\Omega_{\mathcal{I}}$. Recall the nonlocal model eq. (5.7) and the collocation scheme eq. (5.21),

$$-r^h_\Omega \mathcal{L}^S_\delta \boldsymbol{u}^{\delta,h} = r^h_\Omega \boldsymbol{f} = -r^h_\Omega \mathcal{L}^S_\delta \boldsymbol{u}^\delta\,.$$

Then, gathering Theorem 5.2.1, Lemma 5.2.7 and the above equation, we have

$$\begin{aligned}
\|\Pi^h \boldsymbol{u}^\delta - \boldsymbol{u}^{\delta,h}\|_{L^2(\Omega;\mathbb{R}^{\mathrm{d}})} &\leq C\left|r^h_\Omega \mathcal{L}^S_\delta\left(\Pi^h \boldsymbol{u}^\delta - \boldsymbol{u}^{\delta,h}\right)\right|_h, \\
&\leq C\left|r^h_\Omega \mathcal{L}^S_\delta \Pi^h \boldsymbol{u}^\delta - r^h_\Omega \mathcal{L}^S_\delta \boldsymbol{u}^{\delta,h}\right|_h, \\
&\leq C\left|r^h_\Omega \mathcal{L}^S_\delta \Pi^h \boldsymbol{u}^\delta - r^h_\Omega \mathcal{L}^S_\delta \boldsymbol{u}^{\delta}\right|_h, \\
&\leq Ch^2_{\max}\,.
\end{aligned}$$

We finish the proof by applying the triangle inequality

$$\begin{aligned}
\|\boldsymbol{u}^\delta - \boldsymbol{u}^{\delta,h}\|_{L^2(\Omega;\mathbb{R}^{\mathrm{d}})} &\leq \|\boldsymbol{u}^\delta - \Pi^h \boldsymbol{u}^\delta\|_{L^2(\Omega;\mathbb{R}^{\mathrm{d}})} + \|\Pi^h \boldsymbol{u}^\delta - \boldsymbol{u}^{\delta,h}\|_{L^2(\Omega;\mathbb{R}^{\mathrm{d}})} \\
&\leq Ch^2_{\max}.
\end{aligned}$$

□

Before showing that the convergence of the RK collocation scheme to the local limit is independent of δ, we need the bound of truncation error between the collocation scheme and the local limit of the peridyanmic Navier model.

Lemma 5.2.9. ***(Asymptotic consistency I)*** *Assume* $\boldsymbol{u} \in C^4(\mathbb{R}^{\mathrm{d}}; \mathbb{R}^{\mathrm{d}})$*, then*

$$|r^h \mathcal{L}_\delta^S \Pi^h \boldsymbol{u} - r^h \mathcal{L}_0^S \boldsymbol{u}|_h \leq C |\boldsymbol{u}^{(4)}|_\infty (h_{\max}^2 + \delta^2),$$

where C *is independent of* $h_{\max}$ *and* δ*.*

Proof. From Lemma 5.2.7 and the continuous property of the nonlocal operators, we have

$$\begin{aligned} \left|r^h \mathcal{L}_\delta^S \Pi^h \boldsymbol{u} - r^h \mathcal{L}_0^S \boldsymbol{u}\right|_h &\leq \left|r^h \mathcal{L}_\delta^S \Pi^h \boldsymbol{u} - r^h \mathcal{L}_\delta^S \boldsymbol{u}\right|_h + \left|r^h \mathcal{L}_\delta^S \boldsymbol{u} - r^h \mathcal{L}_0^S \boldsymbol{u}\right|_h, \\ &\leq C \left|\boldsymbol{u}^{(4)}\right|_\infty (h_{\max}^2 + \delta^2). \end{aligned}$$

□

Combining Theorem 5.2.1 and Lemma 5.2.9, we have the uniform convergence (asymptotic compatibility) to the local limit. We leave out the proof of Theorem 5.2.10 for conciseness because it is similar to the proof of Theorem 5.2.8.

Theorem 5.2.10. ***(Asymptotic compatibility)*** *Assume the local exact solution* $\boldsymbol{u}^0$ *is sufficiently smooth, i.e.,* $\boldsymbol{u}^0 \in C^4(\overline{\Omega_\delta}; \mathbb{R}^{\mathrm{d}})$*. For any* $\delta \in (0, \delta_0]$*,* $\boldsymbol{u}^{\delta,h}$ *is the numerical solution of the collocation scheme eq. (5.21), then,*

$$\|\boldsymbol{u}^0 - \boldsymbol{u}^{\delta,h}\|_{L^2(\Omega; \mathbb{R}^{\mathrm{d}})} \leq C(h_{\max}^2 + \delta^2).$$

5.3 Convergence analysis of the RK collocation for the quasi-discrete peridynamic Navier equation

In practice, accurate evaluation of the integral in nonlocal models is computationally prohibitive especially if the nonlocal kernel is singular. This motivates us to use the quasi-discrete nonlocal models as introduced in subsection 5.1.2. It is practical to couple δ with grid size $h_{\max}$ because this results in a banded linear system.

Thus in this section, we assume $\delta = M_0 h_{\max}$ where $M_0 > 0$. As $h_{\max}$ goes to zero, so does δ and the quasi-discrete nonlocal operator converges to its local limit. We provide convergence analysis of the collocation scheme eq. (5.22) to its local limit.

5.3.1 Stability

We start with the stability of the collocation scheme eq. (5.22).

Theorem 5.3.1. *For any $\delta \in (0, \delta_0]$, there exists a generic constant C which depends on Ω, δ_0 and M_0, such that for $\boldsymbol{u} \in S(\square \cap \Omega; \mathbb{R}^{\mathrm{d}})$,*

$$|r_{\Omega}^{h}(-\mathcal{L}_{\delta,\epsilon}^{S}\boldsymbol{u})|_h \geq C\|\boldsymbol{u}\|_{L^2(\mathbb{R}^{\mathrm{d}};\mathbb{R}^{\mathrm{d}})}.$$

To prove Theorem 5.3.1, we need the Fourier symbol of the quasi-discrete peridynamic Navier operator $\mathcal{L}_{\delta,\epsilon}^{S}$ shown in Lemma 5.3.2. We present the lemma without proof because the proof follows similarly as Lemma 5.2.3 using the fact that the quadrature points are symmetric and the quadrature weights are positive [71].

Lemma 5.3.2. *The Fourier symbol of the quasi-discrete peridynamic Navier operator $\mathcal{L}_{\delta,\epsilon}^{S}$ is given by*

$$-\widehat{\mathcal{L}_{\delta,\epsilon}^{S}\boldsymbol{u}}(\boldsymbol{\xi}) = \boldsymbol{M}_{\delta,\epsilon}^{S}(\boldsymbol{\xi})\widehat{\boldsymbol{u}}(\boldsymbol{\xi}), \tag{5.58}$$

where the Fourier symbol $\boldsymbol{M}_{\delta,\epsilon}^{S}(\boldsymbol{\xi})$ is a $\mathrm{d} \times \mathrm{d}$ matrix and can be written as

$$\boldsymbol{M}_{\delta,\epsilon}^{S}(\boldsymbol{\xi}) = \boldsymbol{M}_{\delta,\epsilon}^{B}(\boldsymbol{\xi}) + \boldsymbol{M}_{\delta,\epsilon}^{D}(\boldsymbol{\xi}), \tag{5.59}$$

where

$$\boldsymbol{M}_{\delta,\epsilon}^{B}(\boldsymbol{\xi}) = \frac{C_\mu}{\delta^2} p_1^{\epsilon_1}(\delta|\boldsymbol{\xi}|)\left(\boldsymbol{I}_{\mathrm{d}} - \vec{\boldsymbol{\xi}}\vec{\boldsymbol{\xi}}^{T}\right) + \frac{C_\mu}{\delta^2} q_1^{\epsilon_1}(\delta|\boldsymbol{\xi}|)\vec{\boldsymbol{\xi}}\vec{\boldsymbol{\xi}}^{T}, \tag{5.60}$$

and

$$\boldsymbol{M}_{\delta,\epsilon}^{D}(\boldsymbol{\xi}) = \frac{C_{\lambda,\mu}}{\delta^2}\left(b_1^{\epsilon_1}(\delta|\boldsymbol{\xi}|)\right)^2 \vec{\boldsymbol{\xi}}\vec{\boldsymbol{\xi}}^{T}, \tag{5.61}$$

where the scalars $p_1^{\epsilon_1}(|\boldsymbol{\xi}|), q_1^{\epsilon_1}(|\boldsymbol{\xi}|)$ *and* $b_1^{\epsilon_1}(|\boldsymbol{\xi}|)$ *are given as follows*

$$p_1^{\epsilon_1}(|\boldsymbol{\xi}|) = \sum_{\boldsymbol{s}\in B_1^{\epsilon}} \omega(|\boldsymbol{s}|)\rho(|\boldsymbol{s}|)\frac{s_1^2}{|\boldsymbol{s}|^2}(1-\cos(|\boldsymbol{\xi}|s_{\mathrm{d}})), \tag{5.62}$$

$$q_1^{\epsilon_1}(|\boldsymbol{\xi}|) = \sum_{\boldsymbol{s}\in B_1^{\epsilon}} \omega(|\boldsymbol{s}|)\rho(|\boldsymbol{s}|)\frac{s_{\mathrm{d}}^2}{|\boldsymbol{s}|^2}(1-\cos(|\boldsymbol{\xi}|s_{\mathrm{d}})), \tag{5.63}$$

$$b_1^{\epsilon_1}(|\boldsymbol{\xi}|) = \sum_{\boldsymbol{s}\in B_1^{\epsilon}} \omega(|\boldsymbol{s}|)\rho(|\boldsymbol{s}|)s_{\mathrm{d}}\sin(|\boldsymbol{\xi}|s_{\mathrm{d}}). \tag{5.64}$$

From Lemma 5.3.2, we have the Fourier representation of the collocation scheme on the quasi-discrete peridynamic Navier operator as follows.

Lemma 5.3.3. *Let* $\widetilde{\boldsymbol{u}}(\boldsymbol{\xi})$ *and* $\widetilde{\boldsymbol{v}}(\boldsymbol{\xi})$ *be the Fourier series of the sequences* $(\boldsymbol{u_k}), (\boldsymbol{v_k}) \in l^1(\mathbb{Z}^{\mathrm{d}};\mathbb{C}^{\mathrm{d}})$ *respectively. Then*

$$((\boldsymbol{u_k}), -r^h\mathcal{L}_{\delta,\epsilon}^S i^h(\boldsymbol{v_k}))_{l^2} = (2\pi)^{-\mathrm{d}}\int_{\boldsymbol{Q}} \widetilde{\boldsymbol{u}}(\boldsymbol{\xi})\cdot \boldsymbol{M}_C^{\epsilon}(\delta,\boldsymbol{h},\boldsymbol{\xi})\overline{\widetilde{\boldsymbol{v}}(\boldsymbol{\xi})}d\boldsymbol{\xi}, \tag{5.65}$$

where $\boldsymbol{\lambda}_C^{\epsilon}$ *are defined as*

$$\begin{aligned}\boldsymbol{M}_C^{\epsilon}(\delta,\boldsymbol{h},\boldsymbol{\xi}) = {} & 2^{4\mathrm{d}}\sum_{\boldsymbol{r}\in\mathbb{Z}^{\mathrm{d}}} \boldsymbol{M}_{\delta,\epsilon}^B((\boldsymbol{\xi}+2\pi\boldsymbol{r})\oslash\boldsymbol{h})\prod_{j=1}^{\mathrm{d}} h_j\left(\frac{\sin(\xi_j/2)}{\xi_j+2\pi r_j}\right)^4 \\ & + 2^{4\mathrm{d}+4}\sum_{\boldsymbol{r}\in\mathbb{Z}^{\mathrm{d}}} \boldsymbol{M}_{\delta,\epsilon}^D((\boldsymbol{\xi}+2\pi\boldsymbol{r})\oslash\boldsymbol{h})\prod_{j=1}^{\mathrm{d}} h_j\left(\frac{\sin(\xi_j/2)}{\xi_j+2\pi r_j}\right)^8.\end{aligned} \tag{5.66}$$

Moreover, there exists $C>0$*, independent of* δ *and* $\boldsymbol{h}$ *such that,*

$$\boldsymbol{M}_C^{\epsilon}(\delta,\boldsymbol{h},\boldsymbol{\xi}) - C\boldsymbol{M}_C(\delta,\boldsymbol{h},\boldsymbol{\xi}) \tag{5.67}$$

is positive definite for any $\boldsymbol{\xi}\neq\boldsymbol{0}$*.*

Proof. The derivation of eq. (5.66) is similar to eq. (5.48), we can simply replace $\boldsymbol{M}_{\delta}^S(\boldsymbol{\xi}+2\pi\boldsymbol{r})$ with $\boldsymbol{M}_{\delta,\epsilon}^S(\boldsymbol{\xi}+2\pi\boldsymbol{r})$. The challenge is to show that eq. (5.67) is positive definite. First, we decompose the set $\boldsymbol{Q}=(-\pi,\pi)^{\mathrm{d}}$ into $\boldsymbol{Q}_1$ and $\boldsymbol{Q}_2$, where

$$\boldsymbol{Q}_1 := \{\boldsymbol{\xi}\in\boldsymbol{Q} : \frac{\delta|\boldsymbol{\xi}|}{h_{\min}}\leq\pi\} \text{ and } \boldsymbol{Q}_2 = \boldsymbol{Q}\backslash\boldsymbol{Q}_1,$$

thus for $\boldsymbol{\xi} \in \boldsymbol{Q}_1$,

$$|\delta s_{\mathrm{d}} \cdot (\boldsymbol{\xi} \oslash \boldsymbol{h})| \leq \frac{\delta|\boldsymbol{\xi}|}{h_{\min}} \leq \pi.$$

We recall that

$$p_1^{\epsilon_1}(\delta|\boldsymbol{\xi} \oslash \boldsymbol{h}|) = \sum_{\boldsymbol{s} \in B_1^{\epsilon_1}} \omega(|\boldsymbol{s}|)\rho(|\boldsymbol{s}|)\frac{s_1^2}{|\boldsymbol{s}|^2}\left(1 - \cos\left(\frac{\delta s_{\mathrm{d}}}{h_{\max}}|\boldsymbol{\xi} \oslash \hat{\boldsymbol{h}}|\right)\right),$$

and for $x \in (-\pi, \pi)$, there is $C > 0$ such that

$$1 - \cos(x) \geq Cx^2;$$

so for $\boldsymbol{\xi} \in \boldsymbol{Q}_1$, we obtain

$$p_1^{\epsilon_1}\left(\delta|\boldsymbol{\xi} \oslash \boldsymbol{h}|\right) \geq C\left(\frac{\delta|\boldsymbol{\xi}|}{h_{\max}}\right)^2 \sum_{\boldsymbol{s} \in B_1^{\epsilon}} \omega(|\boldsymbol{s}|)\rho(|\boldsymbol{s}|)\frac{s_1^2 s_{\mathrm{d}}^2}{|\boldsymbol{s}|^2} \geq C_p^{\epsilon}|\boldsymbol{\xi}|^2,$$

where we have used that $\boldsymbol{h}$ is quasi-uniform ($h_{\max}/h_{\min}$ is bounded above and below),

$$\sum_{\boldsymbol{s} \in B_1^{\epsilon_1}} \omega(|\boldsymbol{s}|)\rho(|\boldsymbol{s}|)\frac{s_1^2 s_{\mathrm{d}}^2}{|\boldsymbol{s}|^2} > 0,$$

is bounded below by eq. (5.20), and $C_p^{\epsilon_1}$ depends on M_0 and d, and $B_1^{\epsilon_1}$. It is easy to notice that $p_1^{\epsilon_1}(\delta|\boldsymbol{\xi} \oslash \boldsymbol{h}|) = 0$ if for all $\boldsymbol{s} \in B_1^{\epsilon_1}$, $M_0 s_{\mathrm{d}}|\boldsymbol{\xi} \oslash \hat{\boldsymbol{h}}| = 2k\pi$ for $k \in \mathbb{Z}^+$. If this happens, we can always add more points $\tilde{\boldsymbol{s}}$ to $B_1^{\epsilon_1}$ such that for a certain points $\boldsymbol{s}$ in the original set $B_1^{\epsilon_1}$, $|\boldsymbol{s}|/|\tilde{\boldsymbol{s}}|$ is an irrational number and thus $M_0\tilde{s_{\mathrm{d}}}|\boldsymbol{\xi} \oslash \hat{\boldsymbol{h}}| \neq 2k\pi$ for any $k \in \mathbb{Z}^+$. As a consequence, we can always choose $B_1^{\epsilon_1}$ such that $p_1^{\epsilon_1}\left(\delta|\boldsymbol{\xi} \oslash \boldsymbol{h}|\right)$ is nonzero; $p_1^{\epsilon_1}\left(\delta|\boldsymbol{\xi} \oslash \boldsymbol{h}|\right) \geq C \geq |\boldsymbol{\xi}|^2$ for $\boldsymbol{\xi} \in \boldsymbol{Q}_2$ because $\boldsymbol{Q}_2$ is compact. Moreover, for $\boldsymbol{\xi} \in \boldsymbol{Q}$, it is also true that

$$C_1 < \left(\frac{\sin(\xi_j/2)}{\xi_j}\right)^4 < C_2,$$

where $C_1, C_2 > 0$ are generic constants. Therefore, we have for $\boldsymbol{\xi} \in \boldsymbol{Q}$,

$$p_1^{\epsilon_1}\left(\delta|\boldsymbol{\xi} \oslash \boldsymbol{h}|\right)\prod_{j=1}^{3} h_j \left(\frac{\sin(\xi_j/2)}{\xi_j + 2\pi r_j}\right)^4 \geq C_p^{\epsilon_1}|\boldsymbol{\xi}|^2 \prod_{j=1}^{\mathrm{d}} h_j\,. \tag{5.68}$$

Similarly we can obtain

$$q_1^{\epsilon_1}\left(\delta|\boldsymbol{\xi}\oslash\boldsymbol{h}|\right)\prod_{j=1}^{\mathrm{d}}h_j\left(\frac{\sin(\xi_j/2)}{\xi_j+2\pi r_j}\right)^4\geq C_q^{\epsilon_1}|\boldsymbol{\xi}|^2\prod_{j=1}^{\mathrm{d}}h_j, \tag{5.69}$$

where $C_q^{\epsilon}>0$ is a generic constant. Combining eqs. (5.68) and (5.69), we have the bound for $\boldsymbol{\xi}\in\boldsymbol{Q}$,

$$\begin{aligned}\boldsymbol{M}_C^{\epsilon_1}(\delta,\boldsymbol{h},\boldsymbol{\xi})&\geq C_\mu\left(\frac{|\boldsymbol{\xi}|}{\delta}\right)^2\left\{C_p^{\epsilon_1}\left(\boldsymbol{I}_{\mathrm{d}}-\vec{\boldsymbol{\xi}}_{\boldsymbol{h}}\vec{\boldsymbol{\xi}}_{\boldsymbol{h}}^T\right)+C_q^{\epsilon_1}\vec{\boldsymbol{\xi}}_{\boldsymbol{h}}\vec{\boldsymbol{\xi}}_{\boldsymbol{h}}^T\right\}\prod_{j=1}^{\mathrm{d}}h_j\\&\geq\min\{C_p^{\epsilon_1},C_q^{\epsilon_1}\}C_\mu\left(\frac{|\boldsymbol{\xi}|}{\delta}\right)^2\prod_{j=1}^{\mathrm{d}}h_j\,\boldsymbol{I}_{\mathrm{d}}\geq C\left(\frac{|\boldsymbol{\xi}|}{\delta}\right)^2\prod_{j=1}^{\mathrm{d}}h_j\,\boldsymbol{I}_{\mathrm{d}},\end{aligned} \tag{5.70}$$

where $\boldsymbol{\xi}_{\boldsymbol{h}}=\boldsymbol{\xi}\oslash\boldsymbol{h}$ and we have ignored the terms for $\boldsymbol{r}\neq\boldsymbol{0}$ because they are non-negative positive definite.

Next, we use the fact that

$$1-\cos(x)\leq x^2\ \text{and}\ \sin(x)\leq x,\quad\text{for } x\geq 0,$$

to obtain, for any $\boldsymbol{r}\in\mathbb{Z}^{\mathrm{d}}$,

$$p_1\left(\delta|\left(\boldsymbol{\xi}+2\pi\boldsymbol{r}\right)\oslash\boldsymbol{h}|\right)\leq\left(\frac{\delta|\boldsymbol{\xi}+2\pi\boldsymbol{r}|}{h_{\max}}\right)^2\int_{B_1}\rho(|\boldsymbol{s}|)\frac{s_1^2s_{\mathrm{d}}^2}{|\boldsymbol{s}|^2}d\boldsymbol{s}\leq C|\boldsymbol{\xi}+2\pi\boldsymbol{r}|^2,$$

and similarly we also have

$$q_1\left(\delta|\left(\boldsymbol{\xi}+2\pi\boldsymbol{r}\right)\oslash\boldsymbol{h}|\right)\leq C|\boldsymbol{\xi}+2\pi\boldsymbol{r}|^2,\quad b_1\left(\delta|\left(\boldsymbol{\xi}+2\pi\boldsymbol{r}\right)\oslash\boldsymbol{h}|\right)\leq C|\boldsymbol{\xi}+2\pi\boldsymbol{r}|,$$

where we have used eq. (3.4). Hence we obtain

$$\begin{aligned}&p_1\left(\delta|\left(\boldsymbol{\xi}+2\pi\boldsymbol{r}\right)\oslash\boldsymbol{h}|\right)\prod_{j=1}^{\mathrm{d}}h_j\left(\frac{\sin(\xi_j/2)}{\xi_j+2\pi r_j}\right)^4\\&\leq C|\boldsymbol{\xi}+2\pi\boldsymbol{r})|^2\left(\frac{\sin(\boldsymbol{\xi}/2)}{\boldsymbol{\xi}+2\pi\boldsymbol{r}}\right)^4\prod_{j=1}^{\mathrm{d}}h_j\leq C_p\frac{|\boldsymbol{\xi}|^2}{|\boldsymbol{\xi}_{\boldsymbol{r}}|^2}\prod_{j=1}^{\mathrm{d}}h_j,\end{aligned} \tag{5.71}$$

where $\boldsymbol{\xi}_{\boldsymbol{r}} = \boldsymbol{\xi} + 2\pi\boldsymbol{r}$ and C_p is a generic constant. Similarly we also have

$$q_1\left(\delta|\left(\boldsymbol{\xi}+2\pi\boldsymbol{r}\right)\oslash\boldsymbol{h}|\right)\prod_{j=1}^{\mathrm{d}}h_j\left(\frac{\sin(\xi_j/2)}{\xi_j+2\pi r_j}\right)^4 \le C_q\frac{|\boldsymbol{\xi}|^2}{|\boldsymbol{\xi}_{\boldsymbol{r}}|^2}\prod_{j=1}^{\mathrm{d}}h_j \tag{5.72}$$

and

$$\left(b_1\left(\delta|\left(\boldsymbol{\xi}+2\pi\boldsymbol{r}\right)\oslash\boldsymbol{h}|\right)\right)^2\prod_{j=1}^{\mathrm{d}}h_j\left(\frac{\sin(\xi_j/2)}{\xi_j+2\pi r_j}\right)^8 \le C_b\frac{|\boldsymbol{\xi}|^2}{|\boldsymbol{\xi}_{\boldsymbol{r}}|^2}\prod_{j=1}^{\mathrm{d}}h_j, \tag{5.73}$$

where $C_q, C_b > 0$. By gathering eqs. (5.71)–(5.73) and letting $C_pC_\mu = C_qC_\mu + C_bC_{\lambda,\mu}$, we arrive at

$$\begin{aligned}
&\boldsymbol{M}_C(\delta,\boldsymbol{h},\boldsymbol{\xi})\\
&\le\left(\frac{|\boldsymbol{\xi}|}{\delta}\right)^2\sum_{\boldsymbol{r}\in\mathbb{Z}^{\mathrm{d}}}\frac{C_pC_\mu\left(\boldsymbol{I}_{\mathrm{d}}-\vec{\boldsymbol{\xi}}_{\boldsymbol{h},\boldsymbol{r}}\vec{\boldsymbol{\xi}}_{\boldsymbol{h},\boldsymbol{r}}^T\right)+C_qC_\mu\vec{\boldsymbol{\xi}}_{\boldsymbol{h},\boldsymbol{r}}\vec{\boldsymbol{\xi}}_{\boldsymbol{h},\boldsymbol{r}}^T+C_bC_{\lambda,\mu}\vec{\boldsymbol{\xi}}_{\boldsymbol{h},\boldsymbol{r}}\vec{\boldsymbol{\xi}}_{\boldsymbol{h},\boldsymbol{r}}^T}{|\boldsymbol{\xi}_{\boldsymbol{r}}|^2}\prod_{j=1}^{\mathrm{d}}h_j,\\
&\le C\left(\frac{|\boldsymbol{\xi}|}{\delta}\right)^2\prod_{j=1}^{\mathrm{d}}h_j\,\boldsymbol{I}_{\mathrm{d}},
\end{aligned} \tag{5.74}$$

where $\boldsymbol{\xi}_{\boldsymbol{h},\boldsymbol{r}} = \left(\boldsymbol{\xi}+2\pi\boldsymbol{r}\right)\oslash\boldsymbol{h}$.

Finally, eq. (5.67) is shown by combing eqs. (5.70) and (5.74). □

Proof of Theorem 5.3.1. By applying Lemma 5.3.3, the proof follows similarly to the proof of Theorem 5.2.1. □

5.3.2 Consistency

Before showing the discrete model error between $\mathcal{L}^S_{\delta,\epsilon}$ and $\mathcal{L}^S_0$, we need the truncation error between $\mathcal{L}^S_\delta$ and $\mathcal{L}^S_{\delta,\epsilon}$.

Lemma 5.3.4. *Assume $\boldsymbol{u}\in C^4(\mathbb{R}^{\mathrm{d}};\mathbb{R}^{\mathrm{d}})$, then for $i = 1,\dots,\mathrm{d}$,*

$$\left|\left[\mathcal{L}^S_{\delta,\epsilon}\boldsymbol{u}-\mathcal{L}^S_\delta\boldsymbol{u}\right]_i\right| \le C\delta^2|\boldsymbol{u}^{(4)}|_\infty.$$

Proof. Using Taylor's theorem, for $\boldsymbol{x}\in\mathbb{R}^{\mathrm{d}}$, $j = 1,\dots,\mathrm{d}$, and $\boldsymbol{s}\in B_\delta$ we have

$$u_j(\boldsymbol{x}+\boldsymbol{s})-u_j(\boldsymbol{x}) = \sum_{|\boldsymbol{\alpha}|=1,2}\boldsymbol{s}^{\boldsymbol{\alpha}}\frac{D^{\boldsymbol{\alpha}}u_j(\boldsymbol{x})}{\boldsymbol{\alpha}!}+\sum_{|\boldsymbol{\beta}|=3}\boldsymbol{s}^{\boldsymbol{\beta}}\frac{R_j^{\boldsymbol{\beta}}(\boldsymbol{y})}{\boldsymbol{\beta}!}. \tag{5.75}$$

and

$$u_j(\boldsymbol{x}+\boldsymbol{s})+u_j(\boldsymbol{x}-\boldsymbol{s})-2u_j(\boldsymbol{x})=2\sum_{|\boldsymbol{\alpha}|=2}\boldsymbol{s}^{\boldsymbol{\alpha}}\frac{D^{\boldsymbol{\alpha}}u_j(\boldsymbol{x})}{\boldsymbol{\alpha}!}+\sum_{|\boldsymbol{\beta}|=4}\boldsymbol{s}^{\boldsymbol{\beta}}\frac{R_j^{\boldsymbol{\beta}}(\boldsymbol{y})}{\boldsymbol{\beta}!}\,, \tag{5.76}$$

where $|R_j^{\boldsymbol{\beta}}(\boldsymbol{y})|\le C|u_j^{(4)}|_\infty$ and $\boldsymbol{y}$ depends on $\boldsymbol{x}$ and $\boldsymbol{s}$. First, we study the truncation error between $\mathcal{L}_\delta^B\boldsymbol{u}$ and $\mathcal{L}_{\delta,\epsilon}^B\boldsymbol{u}$, for $i=1,\dots,\mathrm{d}$,

$$\begin{aligned}
&\left|[\mathcal{L}_{\delta,\epsilon}^B\boldsymbol{u}(\boldsymbol{x})-\mathcal{L}_\delta^B\boldsymbol{u}(\boldsymbol{x})]_i\right|\\
&=\left|\sum_{j=1}^{\mathrm{d}}\sum_{|\boldsymbol{\alpha}|=2}\frac{D^{\alpha}u_j(\boldsymbol{x})}{\boldsymbol{\alpha}!}\left(\sum_{\boldsymbol{s}\in B_\delta^\epsilon}\omega_\delta(|\boldsymbol{s}|)\rho_\delta(|\boldsymbol{s}|)\frac{s_is_j}{|\boldsymbol{s}|^2}\boldsymbol{s}^{\boldsymbol{\alpha}}-\int_{B_\delta}\rho_\delta(|\boldsymbol{s}|)\frac{s_is_j}{|\boldsymbol{s}|^2}\boldsymbol{s}^{\boldsymbol{\alpha}}d\boldsymbol{s}\right)\right.\\
&\left.+\sum_{|\boldsymbol{\beta}|=4}\frac{1}{2\boldsymbol{\beta}!}\left(\sum_{\boldsymbol{s}\in B_\delta^\epsilon}\omega_\delta(|\boldsymbol{s}|)\rho_\delta(|\boldsymbol{s}|)\frac{s_is_j}{|\boldsymbol{s}|^2}\boldsymbol{s}^{\boldsymbol{\beta}}R_j^{\boldsymbol{\beta}}(\boldsymbol{y})-\int_{B_\delta}\rho_\delta(|\boldsymbol{s}|)\frac{s_is_j}{|\boldsymbol{s}|^2}\boldsymbol{s}^{\boldsymbol{\beta}}R_j^{\boldsymbol{\beta}}(\boldsymbol{y})d\boldsymbol{s}\right)\right|\\
&\le 0+\left|\boldsymbol{u}^{(4)}\right|_\infty\sum_{j=1}^{\mathrm{d}}\sum_{|\boldsymbol{\beta}|=4}\left(\sum_{\boldsymbol{s}\in B_\delta^\epsilon}\omega_\delta(|\boldsymbol{s}|)\rho_\delta(|\boldsymbol{s}|)\frac{|s_is_j|}{|\boldsymbol{s}|^2}|\boldsymbol{s}|^{\boldsymbol{\beta}}+\int_{B_\delta}\rho_\delta(|\boldsymbol{s}|)\frac{|s_is_j|}{|\boldsymbol{s}|^2}|\boldsymbol{s}|^{\boldsymbol{\beta}}d\boldsymbol{s}\right),\\
&\le C\delta^2\left|\boldsymbol{u}^{(4)}\right|_\infty,
\end{aligned} \tag{5.77}$$

where we have used eqs. (5.2), (5.11), (5.20), and (5.76).

Next, via eq. (5.75), the quasi-discrete nonlocal divergence operator $\mathcal{D}_\delta^\epsilon$ acting on $\boldsymbol{u}$ can be written as

$$\begin{aligned}
\mathcal{D}_\delta^\epsilon\boldsymbol{u}(\boldsymbol{x})&=\sum_{j=1}^{\mathrm{d}}\sum_{|\boldsymbol{\alpha}|=1,2}\frac{D^{\boldsymbol{\alpha}}u_j(\boldsymbol{x})}{\boldsymbol{\alpha}!}\sum_{\boldsymbol{s}\in B_\delta^\epsilon}\omega_\delta(|\boldsymbol{s}|)\rho_\delta(|\boldsymbol{s}|)s_j\boldsymbol{s}^{\boldsymbol{\alpha}}\\
&\quad+\sum_{j=1}^{\mathrm{d}}\sum_{|\boldsymbol{\beta}|=3}\frac{1}{\boldsymbol{\beta}!}\sum_{\boldsymbol{s}\in B_\delta^\epsilon}\omega_\delta(|\boldsymbol{s}|)\rho_\delta(|\boldsymbol{s}|)s_j\boldsymbol{s}^{\boldsymbol{\beta}}R_j^{\boldsymbol{\beta}}(\boldsymbol{y}),\\
&=\frac{m(\boldsymbol{x})}{\mathrm{d}}\sum_{j=1}^{\mathrm{d}}u_j'(\boldsymbol{x})+\sum_{j=1}^{\mathrm{d}}\sum_{|\boldsymbol{\beta}|=3}\frac{1}{\boldsymbol{\beta}!}\sum_{\boldsymbol{s}\in B_\delta^\epsilon}\omega_\delta(|\boldsymbol{s}|)\rho_\delta(|\boldsymbol{s}|)s_j\boldsymbol{s}^{\boldsymbol{\beta}}R_j^{\boldsymbol{\beta}}(\boldsymbol{y}),
\end{aligned} \tag{5.78}$$

where we denote $u_j'(\boldsymbol{x})=\dfrac{\mathrm{d}u_j(\boldsymbol{x})}{\mathrm{d}x_j}$ and we have used eq. (5.10). We immediately have

a similar result for $\mathcal{D}_\delta$,

$$\mathcal{D}_\delta \boldsymbol{u}(\boldsymbol{x}) = \frac{m(\boldsymbol{x})}{\mathrm{d}} \sum_{j=1}^{\mathrm{d}} u_j'(\boldsymbol{x}) + \sum_{j=1}^{\mathrm{d}} \sum_{|\boldsymbol{\beta}|=3} \frac{1}{\boldsymbol{\beta}!} \int_{B_\delta} \rho_\delta(|\boldsymbol{s}|) s_j \boldsymbol{s}^{\boldsymbol{\beta}} R_j^{\boldsymbol{\beta}}(\boldsymbol{y}) d\boldsymbol{s}. \tag{5.79}$$

Then, the truncation error between $\mathcal{G}_\delta^\epsilon \mathcal{D}_\delta^\epsilon \boldsymbol{u}$ and $\mathcal{G}_\delta \mathcal{D}_\delta \boldsymbol{u}$ is given by

$$\begin{aligned}
&|[\mathcal{G}_\delta^\epsilon \mathcal{D}_\delta^\epsilon \boldsymbol{u} - \mathcal{G}_\delta \mathcal{D}_\delta \boldsymbol{u}]_i(\boldsymbol{x})| \\
&= \Bigg| \frac{m(\boldsymbol{x})}{\mathrm{d}} \sum_{j=1}^{\mathrm{d}} \sum_{|\boldsymbol{\alpha}|=1,2} \frac{D^{\boldsymbol{\alpha}}(u_j')(\boldsymbol{x})}{\boldsymbol{\alpha}!} \left(\sum_{\boldsymbol{t} \in B_\delta^\epsilon} \omega_\delta(|\boldsymbol{t}|) \rho_\delta(|\boldsymbol{t}|) t_i \boldsymbol{t}^{\boldsymbol{\alpha}} - \int_{B_\delta} \rho_\delta(|\boldsymbol{t}|) t_i \boldsymbol{t}^{\boldsymbol{\alpha}} d\boldsymbol{t} \right) \\
&\quad + \frac{m(\boldsymbol{x})}{\mathrm{d}} \sum_{j=1}^{\mathrm{d}} \sum_{|\boldsymbol{\gamma}|=3} \frac{1}{\boldsymbol{\gamma}!} \left(\sum_{\boldsymbol{t} \in B_\delta^\epsilon} \omega_\delta(|\boldsymbol{t}|) \rho_\delta(|\boldsymbol{t}|) t_i \boldsymbol{t}^{\boldsymbol{\gamma}} \tilde{R}_j^{\boldsymbol{\gamma}}(\boldsymbol{z}) - \int_{B_\delta} \rho_\delta(|\boldsymbol{t}|) t_i \boldsymbol{t}^{\boldsymbol{\gamma}} \tilde{R}_j^{\boldsymbol{\gamma}}(\boldsymbol{z}) d\boldsymbol{t} \right) \\
&\quad + \sum_{j=1}^{\mathrm{d}} \sum_{|\boldsymbol{\beta}|=3} \frac{1}{\boldsymbol{\beta}!} \sum_{\boldsymbol{t} \in B_\delta^\epsilon} \omega_\delta(|\boldsymbol{t}|) \rho_\delta(|\boldsymbol{t}|) t_i \sum_{\boldsymbol{s} \in B_\delta^\epsilon} \omega_\delta(|\boldsymbol{s}|) \rho_\delta(|\boldsymbol{s}|) s_j \boldsymbol{s}^{\boldsymbol{\beta}} \left(R_j^{\boldsymbol{\beta}}(\boldsymbol{y} + \boldsymbol{t}) - R_j^{\boldsymbol{\beta}}(\boldsymbol{y}) \right) \\
&\quad - \sum_{j=1}^{\mathrm{d}} \sum_{|\boldsymbol{\beta}|=3} \frac{1}{\boldsymbol{\beta}!} \int_{B_\delta} \rho_\delta(|\boldsymbol{t}|) t_i \int_{B_\delta} \rho_\delta(|\boldsymbol{s}|) s_j \boldsymbol{s}^{\boldsymbol{\beta}} \left(R_j^{\boldsymbol{\beta}}(\boldsymbol{y} + \boldsymbol{t}) - R_j^{\boldsymbol{\beta}}(\boldsymbol{y}) \right) d\boldsymbol{s} d\boldsymbol{t} \Bigg|, \\
&\leq 0 + C \left(\sum_{j=1}^{\mathrm{d}} \sum_{|\boldsymbol{\gamma}|=3} \frac{\left|\boldsymbol{u}^{(4)}\right|_\infty}{\boldsymbol{\gamma}!} \sum_{\boldsymbol{t} \in B_\delta^\epsilon} \omega_\delta(|\boldsymbol{t}|) \rho_\delta(|\boldsymbol{t}|) |t_i| |\boldsymbol{t}^{\boldsymbol{\gamma}}| + \int_{B_\delta} \rho_\delta(|\boldsymbol{t}|) |t_i| |\boldsymbol{t}^{\boldsymbol{\gamma}}| d\boldsymbol{t} \right) \\
&\quad + \sum_{j=1}^{\mathrm{d}} \sum_{|\boldsymbol{\beta}|=3} \frac{\left|\boldsymbol{u}^{(4)}\right|_\infty}{\boldsymbol{\beta}!} \sum_{|\alpha|=1} \sum_{\boldsymbol{t} \in B_\delta^\epsilon} \omega_\delta(|\boldsymbol{t}|) \rho_\delta(|\boldsymbol{t}|) |t_i| |\boldsymbol{t}^{\boldsymbol{\alpha}}| \sum_{\boldsymbol{s} \in B_\delta^\epsilon} \omega_\delta(|\boldsymbol{s}|) \rho_\delta(|\boldsymbol{s}|) |s_j| \left|\boldsymbol{s}^{\boldsymbol{\beta}}\right| \\
&\quad + \sum_{j=1}^{\mathrm{d}} \sum_{|\boldsymbol{\beta}|=3} \frac{\left|\boldsymbol{u}^{(4)}\right|_\infty}{\boldsymbol{\beta}!} \sum_{|\alpha|=1} \int_{B_\delta} \omega_\delta(|\boldsymbol{t}|) \rho_\delta(|\boldsymbol{t}|) |t_i| |\boldsymbol{t}^{\boldsymbol{\alpha}}| d\boldsymbol{t} \int_{B_\delta} \omega_\delta(|\boldsymbol{s}|) \rho_\delta(|\boldsymbol{s}|) |s_j| \left|\boldsymbol{s}^{\boldsymbol{\beta}}\right| d\boldsymbol{s} \\
&\leq C\delta^2 |\boldsymbol{u}^{(4)}|_\infty.
\end{aligned} \tag{5.80}$$

where $\tilde{R}_j$ is the remainder by expanding u_j' as eq. (5.75) and we have used eqs. (5.78) and (5.79).

Equations (5.77) and (5.80) together complete the proof. □

Now, we present the discrete model error between the quasi-discrete nonlocal

peridynamic Navier equation and its local limit.

Lemma 5.3.5. ***(Asymptotic consistency II)*** *Assume* $\boldsymbol{u} \in C^4(\mathbb{R}^{\mathrm{d}}; \mathbb{R}^{\mathrm{d}})$*, then*

$$|r_\Omega^h \mathcal{L}_{\delta,\epsilon}^S \Pi^h \boldsymbol{u} - r_\Omega^h \mathcal{L}_0^S \boldsymbol{u}^0|_h \leq C|\boldsymbol{u}^{(4)}|_\infty (h_{\max}^2 + \delta^2).$$

Proof. In order to prove this Lemma, we need the following intermediate result

$$\left|r^h \mathcal{L}_{\delta,\epsilon}^S \Pi^h \boldsymbol{u} - r^h \mathcal{L}_{\delta,\epsilon}^S \boldsymbol{u}\right|_h \leq C h_{\max}^2 \left|\boldsymbol{u}^{(4)}\right|_\infty . \tag{5.81}$$

The proof of eq. (5.81) is similar to Lemma 5.2.7, following the replacement of the nonlocal operators with their quasi-discrete counterparts. By gathering eq. (5.81) and Lemma 5.3.4, the discrete model error of collocation scheme eq. (5.22) is given as

$$\begin{aligned}
\left|r^h \mathcal{L}_{\delta,\epsilon}^S \Pi^h \boldsymbol{u} - r^h \mathcal{L}_0^S \boldsymbol{u}\right|_h &\leq \left|r^h \mathcal{L}_{\delta,\epsilon}^S \Pi^h \boldsymbol{u} - r^h \mathcal{L}_{\delta,\epsilon}^S \boldsymbol{u}\right|_h + \left|r^h \mathcal{L}_{\delta,\epsilon}^S \boldsymbol{u} - r^h \mathcal{L}_\delta^S \boldsymbol{u}\right|_h \\
&\quad + \left|r^h \mathcal{L}_\delta^S \boldsymbol{u} - r^h \mathcal{L}_0^S \boldsymbol{u}\right|_h , \\
&\leq C \left|\boldsymbol{u}^{(4)}\right|_\infty (h_{\max}^2 + \delta^2 + \delta^2).
\end{aligned}$$

□

Combining Theorem 5.3.1 and Lemma 5.3.5, we follow the similar procedure as the proof Theorem 5.2.8 and show that the numerical solution of eq. (5.22) converges to its local limit.

Theorem 5.3.6. *Assume the local exact solution* $\boldsymbol{u}^0$ *is sufficiently smooth, i.e.,* $\boldsymbol{u}^0 \in C^4(\overline{\Omega}; \mathbb{R}^{\mathrm{d}})$*. For any* $\delta \in (0, \delta_0]$*, let* $\boldsymbol{u}^{\delta,\epsilon,h}$ *be the numerical solution of the collocation scheme eq. (5.22) and fix the ratio between* δ *and* $h_{\max}$*. Then,*

$$\|\boldsymbol{u}^0 - \boldsymbol{u}^{\delta,\epsilon,h}\|_{L^2(\Omega;\mathbb{R}^{\mathrm{d}})} \leq C(h_{\max}^2 + \delta^2).$$

5.4 Numerical example

In this section, we validate the convergence analysis in the previous sections by considering a numerical example in two dimension. We let the discretization parameter be $h_1 = 2h_2$ so the collocation grid has $h_{\max} = h_1$. Choosing the manufactured solution $\boldsymbol{u}(x_1, x_2) = [x_1^2(1-x_1^2) + x_2^2(1-x_2^2), 0]^T$, we obtain the right-hand side of eqs. (5.7) and (5.9) as

$$\boldsymbol{f}_\delta(\boldsymbol{x}) = \boldsymbol{f}_0(\boldsymbol{x}) - \left[\frac{18\lambda}{5}\delta^2,\, 0\right]^T$$

where

$$\boldsymbol{f}_0(\boldsymbol{x}) = -\left[2\lambda(1-6x_1+6x_2^2) + 6\mu(1-4x_1+4x_1^2-2x_2+2x_2^2),\, 0\right]^T.$$

We impose the corresponding values of $\boldsymbol{u}(\boldsymbol{x})$ on $\Omega_{\mathcal{I}}$ such that the exact value to the local limit matches on $\partial\Omega$. The nonlocal kernel is chosen as $\rho_\delta(|\boldsymbol{s}|) = \dfrac{3}{2\pi\delta^3|\boldsymbol{s}|}$ and let $\Omega = (0,1)^2$, $E = 1$, and $\nu = 0.4$. Hence, the Lamé parameters $\lambda = E\nu/((1+\nu)(1-2\nu))$, $\mu = E/(2(1+\nu))$ satisfy the assumption in Lemma 5.2.4. For a fixed δ, we solve the following peridynamic Navier equation

$$\begin{cases} -\mathcal{L}_\delta^S \boldsymbol{u}(\boldsymbol{x}) = \boldsymbol{f}_\delta(\boldsymbol{x}), & \boldsymbol{x} \in \Omega, \\ \boldsymbol{u}(\boldsymbol{x}) = [x_1^2(1-x_1^2) + x_2^2(1-x_2^2), 0]^T, & \boldsymbol{x} \in \Omega_{\mathcal{I}}. \end{cases} \tag{5.82}$$

When δ gots to zero, we substitute $\boldsymbol{f}_\delta$ with $\boldsymbol{f}_0$ in eq. (5.82), and obtain the following nonlocal problem

$$\begin{cases} -\mathcal{L}_\delta^S \boldsymbol{u}(\boldsymbol{x}) = \boldsymbol{f}_0(\boldsymbol{x}), & \boldsymbol{x} \in \Omega, \\ \boldsymbol{u}(\boldsymbol{x}) = [x_1^2(1-x_1^2) + x_2^2(1-x_2^2), 0]^T, & \boldsymbol{x} \in \Omega_{\mathcal{I}}, \end{cases} \tag{5.83}$$

which converges to the local problem

$$\begin{cases} -\mathcal{L}_0^S \boldsymbol{u}(\boldsymbol{x}) = \boldsymbol{f}_0(\boldsymbol{x}), & \boldsymbol{x} \in \Omega, \\ \boldsymbol{u}(\boldsymbol{x}) = \boldsymbol{0}, & \boldsymbol{x} \in \partial\Omega. \end{cases}$$

We apply the two collocation schemes as eqs. (5.21) and (5.22) and investigate their convergence properties.

5.4.1 RK collocation for the peridynamic Navier equation

We first use the scheme as described in eq. (5.21) to solve eq. (5.82) for a fixed δ and investigate the convergence property to the nonlocal limit. Then we study the convergence of the numerical solution to the local limit by solving eq. (5.83) and letting δ go to zero.

Figure 5.1 shows the convergence profiles. When δ is fixed, the numerical solution converges to the nonlocal solution at a second-order convergence rate. Then we couple δ and $h_{\max}$ by letting both δ and $h_{\max}$ go to zero at different rates, numerical solutions converge to the local limit. Second-order convergence rates are observed when δ goes to zero faster ($\delta = h_{\max}^2$) and at the same rate as $h_{\max}$ ($\delta = h_{\max}$). We only obtain a first-order convergence rate when $\delta = \sqrt{h_{\max}}$. The convergence behaviours agree with Theorem 5.2.8 and 5.2.10 and the numerical examples have verified that the RK collocation method is an AC scheme.

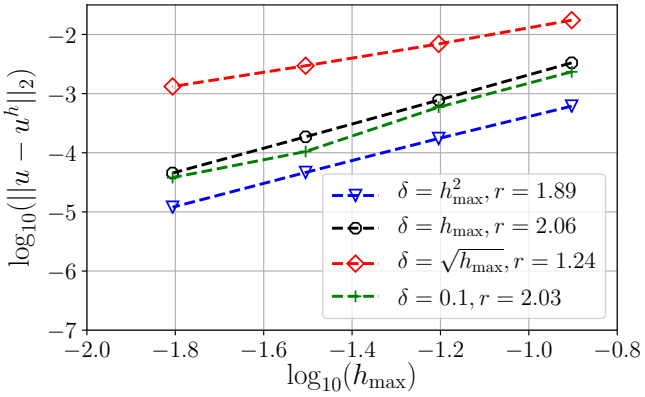

Figure 5.1: Convergence profiles using the RK collocation method.

5.4.2 RK collocation for the quasi-discrete peridynamic Navier equation

To avoid the need of using high-order Gauss quadrature rules, we have reformulated the peridynamic Navier equation in subsection 5.1.2, using quasi-discrete

nonlocal operators. Moreover, it is more practical to couple the grid size with horizon as $\delta = M_0 h_{\max}$ because this leads to banded linear systems amenable to traditional preconditioning techniques. Now, we use the RK collocation method for the quasi-discrete peridynamic Navier equation as discussed in eq. (5.22) to solve eq. (5.83) and study the convergence to the local limit because δ and $h_{\max}$ goes to 0 at the same rate. Figure 5.2 presents the convergence profiles and second-order convergence rates are observed. The numerical findings agree with our analysis in Theorem 5.3.6 and verify that the RK collocation for quasi-discrete peridynamic Navier equation converges to the correct local limit.

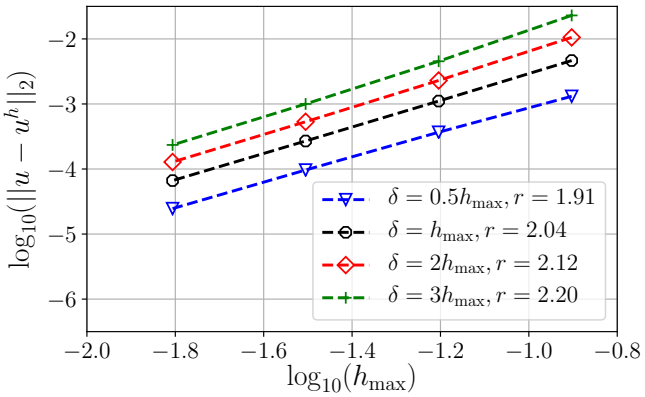

Figure 5.2: Convergence profiles using the RK collocation for quasi-discrete peridynamic Navier equation.

5.5 Near incompressibility

In this section, we study the case when the Poisson ratio ν is close to 0.5 (λ is large but finite), this corresponds to that the material is nearly incompressible. If $\nu = 0.5$ ($\lambda = \infty$), the material is incompressible and the classical (local) linear elasticity model can be cased into a saddle-point problem. The incompressible limit ($\nu \to 0.5$) has been an active research topic in the FEM community because the FEM solution of the pure displacement form deteriorates at this limit as discussed in [56]. A common

remedy is to reformulate and solve the problem in a mixed formulation by introducing an additional variable, pressure. However, for the incompressible case, the FEM functional spaces have to satisfy the famous inf-sup condition (or Ladyzhenskaya-Babuška-Brezzi condition), see [3, 14]. The inf-sup condition is defined as, there exists $C > 0$, such that,

$$\alpha_h = \inf_{q_h \in Q_h} \sup_{u_h \in V_h} \frac{\int_\Omega q_h \operatorname{div} u_h \, \mathrm{d}\Omega}{\|q_h\|_{L^2} \|u_h\|_{V_h}} \geq C, \tag{5.84}$$

where Q_h and V_h are the test spaces for pressure and displacements respectively. For a finite element discretization, there are two phenomena corresponding to eq. (5.84), as discussed in [4, 15]. The *locking phenomenon* means α_h is not bounded away from zero uniformly in h and the *spurious pressure modes phenomenon* corresponds to $\alpha_h = 0$ for such $q_h \in Q_h$ and $u_h \in V_h$.

For the discretization of the local linear elasticity model in mixed form, we end up solving the following system of equations,

$$\begin{bmatrix} \boldsymbol{A} & \boldsymbol{B} \\ \boldsymbol{B}^T & -\frac{1}{\kappa}\boldsymbol{T} \end{bmatrix} \begin{bmatrix} \boldsymbol{U} \\ \boldsymbol{P} \end{bmatrix} = \begin{bmatrix} \boldsymbol{F} \\ \boldsymbol{0} \end{bmatrix}, \tag{5.85}$$

where $\boldsymbol{A}$ is the discrete deviatoric strain, $\boldsymbol{B}$ is the discrete gradient operator, $\boldsymbol{B}^T$ is the discrete divergence operator, $\boldsymbol{T}$ is the mass matrix for pressure, $\kappa = \lambda$, $\boldsymbol{U}$ is displacements unknowns, $\boldsymbol{P}$ is pressure unknown, and $\boldsymbol{F}$ is the forcing term. If $\kappa = \infty$, the coefficient matrix of eq. (5.85) is invertible if only eq. (5.84) is strictly satisfied: no locking or spurious pressure modes are allowed. As long as κ is finite, the system eq. (5.85) is always regular despite the existence of spurious pressure modes. Therefore, when ν is close but not equal to 0.5 (λ is finite), it is sufficient to study if the discretization locks, which is carried out through the inf-sup test proposed in

[4, 15]. The inf-sup test is to calculate the following expression

$$\beta_h = \inf_{v_h \in V_h} \sup_{u_h \in V_h} \frac{\int_\Omega \mathcal{P}_h(\operatorname{div} v_h) \operatorname{div} u_h \, \mathrm{d}\Omega}{\|\mathcal{P}_h(\operatorname{div} v_h)\|_{L^2} \|u_h\|_{V_h}}, \tag{5.86}$$

where $\mathcal{P}_h$ is the L^2 projector onto Q_h. The evaluation of β_h is equivalent to solving the following generalized eigenvalue problem

$$\boldsymbol{G}\boldsymbol{V} = \gamma \boldsymbol{S}\boldsymbol{V}, \tag{5.87}$$

where $\boldsymbol{G} = \boldsymbol{B}^T \boldsymbol{T}^{-1} \boldsymbol{B}$ using matrices from eq. (5.85), $\boldsymbol{V}$ is the eigenvector, γ is the corresponding eigenvalue and $\boldsymbol{S}$ is the matrix corresponding to the V_h norm. We let γ_0 be the first nonzero eigenvalue, then $\beta_h = \sqrt{\gamma_0}$; γ can be zero if spurious pressure modes are present. The discretization passes the inf-sup test if β_h is bounded away from zero uniformly as $h_{\max}$ is refined.

The local poro-elasticity model has an embedded saddle-point problem, see [87, 88], and the functional spaces for displacement and pressure have to be inf-sup stable in order to obtain optimal convergence for both displacement and pressure; nonlocal poro-elasticity has a similar analogy. We are motivated to study the nearly incompressible peridynamic Navier equation because this can be extended to the peridynamics-based hydraulic fracturing model using penalty techniques or artificial compressibility as shown in [42, 57].

Even though there are many open questions for the nonlocal mixed problem, such as, well-posedness, how to impose boundary conditions, etc., we next carry out some preliminary study for the nonlocal mixed problem. We borrow the idea from the local mixed problem and adapt the matrix, which is in the form of eq. (5.85) and is obtained from the mixed form of the quasi-discrete peridynamic Navier equation (eq. (5.18)), to perform the inf-sup test. As discussed in the subsection 5.1.2, we use

equal order (linear RK) approximation for displacements and pressure to solve the peridynamic Navier equation, then in eq. (5.85), $\boldsymbol{A}$ becomes the discrete bond-based peridynamic Navier operator, $\boldsymbol{B}$ is the discrete nonlocal gradient operator, $\boldsymbol{B}^T$ is the discrete nonlocal divergence operator, $\boldsymbol{T}$ is derived from RK interpolation of pressure, and $\kappa = \lambda - \mu$. It is not difficult to see that there are spurious pressure modes, for instance, constant pressures are in the trial space. We first conduct the inf-sup test eq. (5.87) of the RK collocation method. As shown in Figure 5.3, β_h is bounded below as we refine $h_{\max}$, hence the RK collocation method passes the inf-sup test.

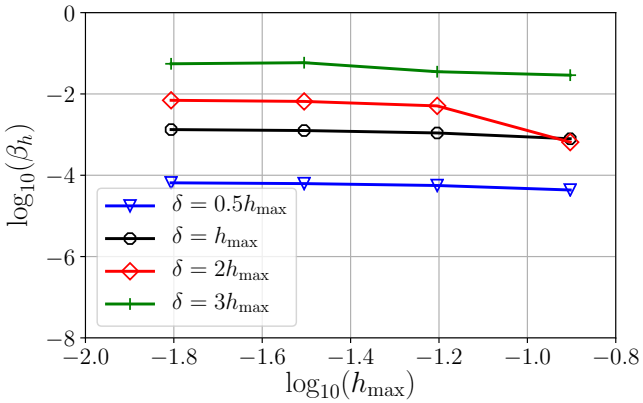

Figure 5.3: Inf-sup test of the RK collocation for quasi-discrete peridynamic Navier equation.

Then, we conduct a two-dimensional numerical example to validate the above analysis. We choose the following manufactured local solution,

$$\begin{cases} u_1^0(\boldsymbol{x}) = \sin(x_1)\sin(x_2), \\ u_2^0(\boldsymbol{x}) = -\cos(x_1)\cos(x_2), \\ p^0 = (\lambda - \mu)\theta^0, \end{cases} \tag{5.88}$$

where $\theta^0(\boldsymbol{x}) = 2\cos(x_1)\sin(x_2)$. The right hand side of eq. (5.9) is obtained,

$$\boldsymbol{f}_0(\boldsymbol{x}) = (2\lambda + 4\mu)[\sin(x_1)\sin(x_2), -\cos(x_1)\cos(x_2)]^T.$$

We can recast the problem as, find $\boldsymbol{u} \in S(\square \cap \Omega; \mathbb{R}^2)$ and $p \in S(\square \cap \Omega; \mathbb{R})$ such that

$$\begin{cases} -16\mu\, \mathcal{L}^B_{\delta,\epsilon}\boldsymbol{u} - 2\mathcal{G}_{\delta,\epsilon}\, p = \boldsymbol{f}_0, \\ (\lambda - \mu)\mathcal{D}_{\delta,\epsilon}\boldsymbol{u} - p = 0, \end{cases} \tag{5.89}$$

and impose the values of eq. (5.88) on $\Omega_{\mathcal{I}}$. The nonlocal kernel is the same as in section 5.4 and let $\Omega = (0,1)^2$, $E = 1$, and $\mu = 0.499$, then the material is slightly compressible. We use uniform discretization (64×64) and choose $\delta = 3h$; the exact and numerical solutions are presented in Figure 5.4. As predicted by the inf-sup test Figure 5.3, the discrete nonlocal solution do not suffer from instabilities near the incompressible limit. This shows that the RK collocation method combined with the quasi-discrete nonlocal operators is promising in solving the peridynamics-based hydraulic fracturing model.

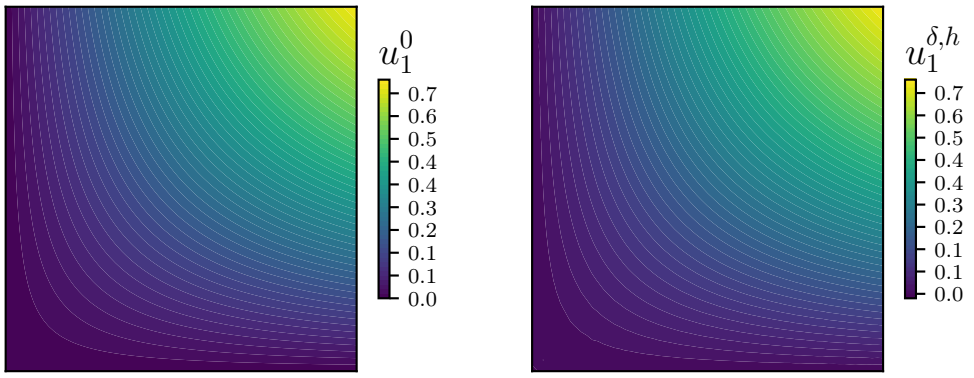

(a) u_1, exact local solution (left) and discrete nonlocal solution (right)

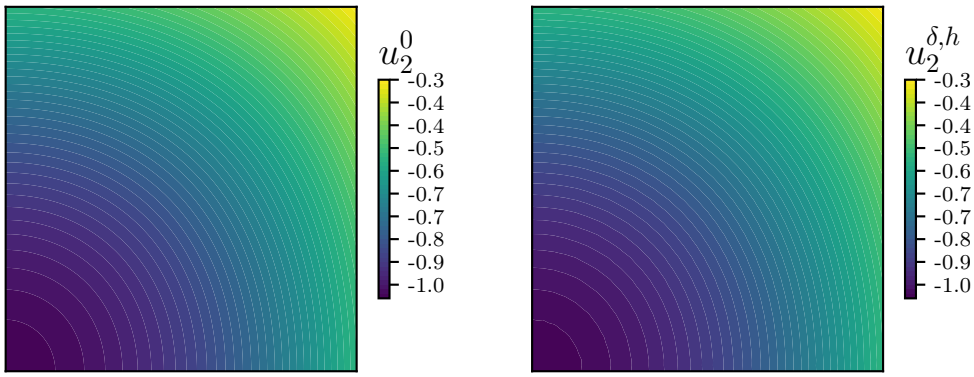

(b) u_2, exact local solution (left) and discrete nonlocal solution (right)

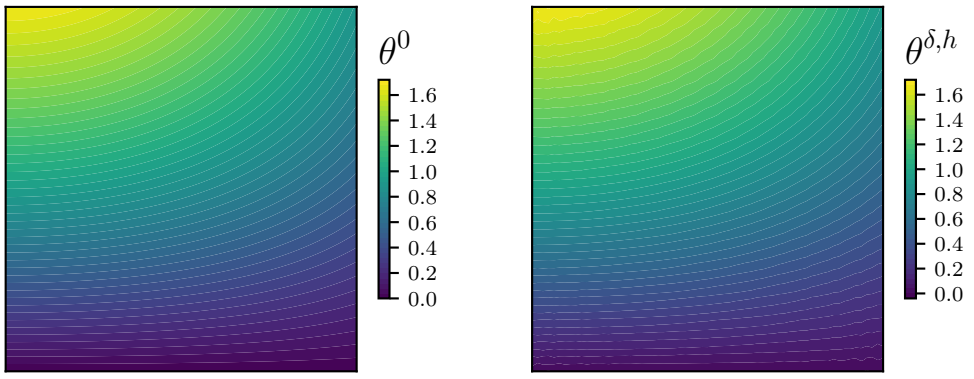

(c) θ, exact local solution (left) and discrete nonlocal solution (right)

Figure 5.4: Exact and numerical solution of eq. (5.89) with uniform grid (64×64) on $\Omega = (0,1)^2$, $h = 0.015625$, $\nu = 0.499$, and $\delta = 3h$.

Chapter 6

Conclusions

This dissertation provided numerical analysis of the linear RK collocation method for linear nonlocal models: nonlocal diffusion and peridynamic Navier equation.

We first addressed the super-convergence behavior of the RK approximation in Chapter 2. We have shown that the error estimates under all Sobolev norms can be improved for all even order RK approximations over the entire domain of interest. The analysis is based on the observation that in the interior of the domain, the RK shape function of even order interpolation is in fact identical to the shape function of one order higher. Error estimates in Sobolev spaces are given for both continuous and discrete RK approximations. Although in practice integrals are always replaced by finite sums, the discussion of continuous RK approximation followed by its discrete counterpart bears the significance of helping us to see in a clear way the origin of the super-convergence phenomenon. It turns out that the discrete RK approximation is super-convergent for even interpolation order p only when the window function satisfies the Strang-Fix condition. This can be achieved, for instance, by choosing B-spline functions as the window function and selecting RK support size wisely. However, when the RK support size is chosen arbitrarily, super-convergence is sometimes observed in numerical experiments within certain range of numerical resolutions. We have proposed a concept of pseudo super convergence to explain that in the case of arbitrary RK support size, the super-convergence is not true for all scales of numerical

resolutions but is a numerical artifact.

Chapter 3 provided a convergence analysis of RK collocation method for linear nonlocal diffusion models and this discretization scheme is AC. Numerical solution of the method converges to both the nonlocal solution (δ fixed) and its local limit ($\delta \to 0$). We have shown stability analysis of this scheme in the case of Cartesian grids with varying resolution in each dimension. Since the standard Galerkin scheme has been proved to be stable, the key idea to show the stability of the collocation scheme is to establish a relationship between the two schemes. Consistency of the collocation scheme is achieved using the synchronized convergence property of the RK approximation. The analysis are verified by numerical examples

In Chapter 4, we have developed a practical numerical scheme for nonlocal models. To this end, we introduce a quasi-discrete nonlocal diffusion operator which replaces the integral with a finite summation of quadrature points inside the horizon. We have generalized the RK technique to calculate the quadrature weights. It is well known that RK and MLS shape functions are equivalent, up to a rescaling of the weighting function and for particular reproducing spaces as in [17]; we have shown that the construction of quadrature weights using the RK technique is similarly equivalent under certain conditions to this generalized MLS approach proposed in [113]. Therefore the stability proof provided here applies equally to this second class of schemes which currently lack a proof of stability. Numerical experiments are conducted to complement the theoretical analysis.

In Chapter 5, we have extended the RK collocation framework developed in Chapters 3 and 4 to the peridynamic Navier equation. We apply linear RK approximation to both displacements and dilatation, then back-substitute dilatation, and solve the equation in a pure displacement form; the collocation scheme is AC. Fol-

lowing similar strategy as proving the stability of the nonlocal diffusion models, we have established a relationship between the standard Galerkin scheme and the RK collocation scheme using Fourier analysis. The Fourier symbol of the peridynamic Navier operator is a matrix and consists of two parts, which adds more complexity to the stability analysis. When showing stability, in order to avoid constraining the nonlocal kernel, we also assume the material parameters satisfy $\lambda \geq \mu$ and our analysis is applicable for materials with Poisson ratio between $[0.25, 0.5)$.

Then, we formulated the quasi-discrete version of the peridynamics Navier equation using the quasi-discrete nonlocal operators proposed in Chapter 4. Under the assumption that the quadrature points are symmetrically distributed and the quadrature weights are positive, we have shown the stability of the RK collocation method for the quasi-discrete peridynamic Navier equation. A reformulation of the bounded second-order moment condition is required to guarantee consistency. The solution of the RK collocation method for the quasi-discrete peridynamic Navier equation converges to the correct local limit.

For classical (local) linear elasticity, FEM solutions obtained from the pure displacement form often suffer from instability near the incompressible limit. For the peridynamic Navier equation, however, numerical results in [112] show that the meshfree discretization converges to the local limit with a second-order convergence rate even for $\nu = 0.495$. We have shown that the matrices obtained from the RK collocation for the mixed form of the quasi-discrete peridynamic Navier equation pass the inf-sup test and the pressure does not oscillate near incompressiblity. Hence, the RK collocation method is promising in solving nonlocal poro-elasticity problem using penalty techniques or artificial compressibility. Showing more rigorous analysis on why the peridynamic Navier equation does not have an instability is a challenging

subject.

Finally, we remark that this is the first step of developing meshfree methods for nonlocal models. Some interesting topics remain to be addressed. Our analysis is restricted on rectilinear Cartesian grids but rigorous analysis on a more general grid, such as quasi-uniform grid, should be studied in the future. The proposed RK collocation method has second order convergence rate. It is challenging to develop higher order methods for the strong form of nonlocal models and the major difficulty is the stability analysis. Moreover, more fundamental works, including well-posedness, how to impose boundary condition, etc., of the nonlocal mixed problems, should be addressed next. Last but not the least, it is interesting to see how the proposed RK collocation method perform in the peridynamics-based hydraulic fracturing model.

Bibliography

[1] D. N. Arnold and J. Saranen, *On the asymptotic convergence of spline collocation methods for partial differential equations*, SIAM Journal on Numerical Analysis, 21 (1984), pp. 459–472.

[2] D. N. Arnold and W. L. Wendland, *On the asymptotic convergence of collocation methods*, Mathematics of Computation, 41 (1983), pp. 349–381.

[3] I. Babuška, *Error-bounds for finite element method*, Numer. Math., 16 (1971), pp. 322–333.

[4] K.-J. Bathe, *Finite element procedures*, Klaus-Jurgen Bathe, 2006.

[5] T. Belytschko, Y. Lu, and L. Gu, *Crack propagation by element-free Galerkin methods*, Engineering Fracture Mechanics, 51 (1995), pp. 295–315.

[6] T. Belytschko and M. Tabbara, *Dynamic fracture using element-free Galerkin methods*, International Journal for Numerical Methods in Engineering, 39 (1996), pp. 923–938.

[7] M. Bessa, J. T. Foster, T. Belytschko, and W. K. Liu, *A meshfree unification: reproducing kernel peridynamics*, Computational Mechanics, 53 (2014), pp. 1251–1264.

[8] F. Bobaru, J. T. Foster, P. H. Geubelle, and S. A. Silling, *Handbook of peridynamic modeling*, CRC press, 2016.

[9] F. Bobaru and Y. D. Ha, *Adaptive refinement and multiscale modeling in 2D peridynamics*, International Journal for Multiscale Computational Engineering, 9 (2011), pp. 635–660.

[10] F. Bobaru, Y. D. Ha, and W. Hu, *Damage progression from impact in layered glass modeled with peridynamics*, Central European Journal of Engineering, 2 (2012), pp. 551–561.

[11] F. Bobaru, M. Yang, L. F. Alves, S. A. Silling, E. Askari, and J. Xu, *Convergence, adaptive refinement, and scaling in 1D peridynamics*, International Journal for Numerical Methods in Engineering, 77 (2009), pp. 852–877.

[12] S. D. Bond, R. B. Lehoucq, and S. T. Rowe, *A Galerkin radial basis function method for nonlocal diffusion*, in Meshfree Methods for Partial Differential Equations VII, Springer, 2015, pp. 1–21.

[13] S. Brenner and R. Scott, *The mathematical theory of finite element methods*, vol. 15, Springer Science & Business Media, 2007.

[14] F. Brezzi, *On the existence, uniqueness and approximation of saddle-point problems arising from Lagrangian multipliers*, ESAIM: Mathematical Modelling and Numerical Analysis - Modélisation Mathématique et Analyse Numérique, 8 (1974), pp. 129–151.

[15] D. Chapelle and K.-J. Bathe, *The inf-sup test*, Computers & Structures, 47 (1993), pp. 537–545.

[16] A. Chen, Q. Du, C. Li, and Z. Zhou, *Asymptotically compatible schemes for space-time nonlocal diffusion equations*, Chaos, Solitons & Fractals, 102 (2017),

pp. 361–371.

[17] J. S. Chen, M. Hillman, and S. W. Chi, *Meshfree methods: progress made after 20 years*, Journal of Engineering Mechanics, 143 (2017), p. 04017001.

[18] J.-S. Chen, C. Pan, C. Roque, and H.-P. Wang, *A Lagrangian reproducing kernel particle method for metal forming analysis*, Computational Mechanics, 22 (1998), pp. 289–307.

[19] J.-S. Chen, C. Pan, and C.-T. Wu, *Large deformation analysis of rubber based on a reproducing kernel particle method*, Computational Mechanics, 19 (1997), pp. 211–227.

[20] J.-S. Chen, C. Pan, C.-T. Wu, and W. K. Liu, *Reproducing kernel particle methods for large deformation analysis of non-linear structures*, Computer Methods in Applied Mechanics and Engineering, 139 (1996), pp. 195–227.

[21] X. Chen and M. Gunzburger, *Continuous and discontinuous finite element methods for a peridynamics model of mechanics*, Computer Methods in Applied Mechanics and Engineering, 200 (2011), pp. 1237–1250.

[22] Z. Chen and F. Bobaru, *Selecting the kernel in a peridynamic formulation: a study for transient heat diffusion*, Computer Physics Communications, 197 (2015), pp. 51–60.

[23] C. Chukwudozie, B. Bourdin, and K. Yoshioka, *A variational approach to the modeling and numerical simulation of hydraulic fracturing under in-situ stresses*, in Proceedings of the 38th Workshop on Geothermal Reservoir Engineering, Stanford Geothermal Program Stanford, Calif, 2013.

[24] M. P. Cleary, M. Kavvadas, K. Y. Lam, et al., *Development of a fully three-dimensional simulator for analysis and design of hydraulic fracturing*, in SPE/DOE Low Permeability Gas Reservoirs Symposium, Society of Petroleum Engineers, 1983.

[25] R. Clifton, A. Abou-Sayed, et al., *On the computation of the three-dimensional geometry of hydraulic fractures*, in Symposium on Low Permeability Gas Reservoirs, Society of Petroleum Engineers, 1979.

[26] R. J. Clifton, A. S. Abou-Sayed, et al., *A variational approach to the prediction of the three-dimensional geometry of hydraulic fractures*, in SPE/DOE Low Permeability Gas Reservoirs Symposium, Society of Petroleum Engineers, 1981.

[27] T. Cook and J. Perrin, *Hydraulic fracturing accounts for about half of current US crude oil production*, Today in Energy, (2016).

[28] M. Costabel, F. Penzel, and R. Schneider, *Error analysis of a boundary element collocation method for a screen problem in* $\mathbb{R}^3$, Mathematics of Computation, 58 (1992), pp. 575–586.

[29] A. Dahi Taleghani, J. E. Olson, et al., *How natural fractures could affect hydraulic-fracture geometry*, SPE Journal, 19 (2013), pp. 161–171.

[30] I. Daubechies, A. Grossmann, and Y. Meyer, *Painless nonorthogonal expansions*, Journal of Mathematical Physics, 27 (1986), pp. 1271–1283.

[31] P. R. Devloo, P. D. Fernandes, S. M. Gomes, C. M. A. A. Bravo, and R. G. Damas, *A finite element model for three dimensional hydraulic fracturing*, Mathematics and Computers in Simulation, 73 (2006), pp. 142–155.

[32] Q. Du, *Nonlocal Modeling, Analysis, and Computation: Nonlocal Modeling, Analysis, and Computation*, SIAM, 2019.

[33] Q. Du, M. Gunzburger, R. B. Lehoucq, and K. Zhou, *Analysis and approximation of nonlocal diffusion problems with volume constraints*, SIAM Review, 54 (2012), pp. 667–696.

[34] Q. Du, M. Gunzburger, R. B. Lehoucq, and K. Zhou, *Analysis of the volume-constrained peridynamic navier equation of linear elasticity*, Journal of Elasticity, 113 (2013), pp. 193–217.

[35] Q. Du, M. Gunzburger, R. B. Lehoucq, and K. Zhou, *A nonlocal vector calculus, nonlocal volume-constrained problems, and nonlocal balance laws*, Mathematical Models and Methods in Applied Sciences, 23 (2013), pp. 493–540.

[36] Q. Du, L. Ju, L. Tian, and K. Zhou, *A posteriori error analysis of finite element method for linear nonlocal diffusion and peridynamic models*, Mathematics of Computation, 82 (2013), pp. 1889–1922.

[37] Q. Du, Y. Tao, X. Tian, and J. Yang, *Asymptotically compatible discretization of multidimensional nonlocal diffusion models and approximation of nonlocal Green's functions*, IMA Journal of Numerical Analysis, 39 (2018), pp. 607–625.

[38] Q. Du and X. Tian, *Stability of nonlocal Dirichlet integrals and implications for peridynamic correspondence material modeling*, SIAM Journal on Applied Mathematics, 78 (2018), pp. 1536–1552.

[39] ——, *Mathematics of smoothed particle hydrodynamics: A study via nonlocal stokes equations*, Foundations of Computational Mathematics, (2019), pp. 1–26.

[40] Q. Du and J. Yang, *Asymptotically compatible fourier spectral approximations of nonlocal Allen–Cahn equations*, SIAM Journal on Numerical Analysis, 54 (2016), pp. 1899–1919.

[41] T. Dupont and R. Scott, *Polynomial approximation of functions in Sobolev spaces*, Mathematics of Computation, 34 (1980), pp. 441–463.

[42] A. Ern and J.-L. Guermond, *Theory and practice of finite elements*, vol. 159, Springer Science & Business Media, 2013.

[43] R. Fung, S. Vilayakumar, D. E. Cormack, et al., *Calculation of vertical fracture containment in layered formations*, SPE Formation Evaluation, 2 (1987), pp. 518–522.

[44] J. Geertsma, F. De Klerk, et al., *A rapid method of predicting width and extent of hydraulically induced fractures*, Journal of Petroleum Technology, 21 (1969), pp. 1–571.

[45] H. Gu, E. Siebrits, A. Sabourov, et al., *Hydraulic fracture modeling with bedding plane interfacial slip*, in SPE Eastern Regional/AAPG Eastern Section Joint Meeting, Society of Petroleum Engineers, 2008.

[46] P. Gupta and C. A. Duarte, *Simulation of non-planar three-dimensional hydraulic fracture propagation*, International Journal for Numerical and Analytical Methods in Geomechanics, 38 (2014), pp. 1397–1430.

[47] ——, *Coupled formulation and algorithms for the simulation of non-planar three-dimensional hydraulic fractures using the generalized finite element method*, International Journal for Numerical and Analytical Methods in Geomechanics, 40 (2016), pp. 1402–1437.

[48] ——, *Coupled hydromechanical-fracture simulations of nonplanar three-dimensional hydraulic fracture propagation*, International Journal for Numerical and Analytical Methods in Geomechanics, 42 (2018), pp. 143–180.

[49] Y. D. Ha and F. Bobaru, *Studies of dynamic crack propagation and crack branching with peridynamics*, International Journal of Fracture, 162 (2010), pp. 229–244.

[50] W. Han and W. K. Liu, *Flexible piecewise approximations based on partition of unity*, Advances in Computational Mathematics, 23 (2005), pp. 191–199.

[51] W. Han and X. Meng, *Error analysis of the reproducing kernel particle method*, Computer Methods in Applied Mechanics and Engineering, 190 (2001), pp. 6157–6181.

[52] Y. Heider and B. Markert, *A phase-field modeling approach of hydraulic fracture in saturated porous media*, Mechanics Research Communications, 80 (2017), pp. 38–46.

[53] S. F. Henke and S. Shanbhag, *Mesh sensitivity in peridynamic simulations*, Computer Physics Communications, 185 (2014), pp. 181–193.

[54] M. Hillman and J. S. Chen, *Nodally integrated implicit gradient reproducing kernel particle method for convection dominated problems*, Computer Methods in Applied Meciics and Engineering, 299 (2016), pp. 381–400.

[55] L. Hua, *Stable element-free Galerkin solution procedures for the coupled soil–pore fluid problem*, International Journal for Numerical Methods in Engineering, 86 (2011), pp. 1000–1026.

[56] T. J. Hughes, *The finite element method: linear static and dynamic finite element analysis*, Courier Corporation, 2012.

[57] T. J. Hughes, W. K. Liu, and A. Brooks, *Finite element analysis of incompressible viscous flows by the penalty function formulation*, Journal of Computational Physics, 30 (1979), pp. 1–60.

[58] P. K. Jha and R. Lipton, *Finite element approximation of nonlinear nonlocal models*, Mathematical Models and Methods in Applied Sciences, (2017).

[59] P. K. Jha and R. Lipton, *Numerical analysis of nonlocal fracture models in Holder space*, SIAM Journal on Numerical Analysis, 56 (2018), pp. 906–941.

[60] P. K. Jha and R. Lipton, *Finite element convergence for state-based peridynamic fracture models*, Communications on Applied Mathematics and Computation, (2019).

[61] P. K. Jha and R. Lipton, *Numerical convergence of finite difference approximations for state based peridynamic fracture models*, Computer Methods in Applied Mechanics and Engineering, 351 (2019), pp. 184–225.

[62] R.-Q. Jia and J. Lei, *A new version of the Strang-Fix conditions*, Journal of Approximation Theory, 74 (1993), pp. 221–225.

[63] S. Jun, W. K. Liu, and T. Belytschko, *Explicit reproducing kernel particle methods for large deformation problems*, International Journal for Numerical Methods in Engineering, 41 (1998), pp. 137–166.

[64] A. Katiyar, J. T. Foster, H. Ouchi, and M. M. Sharma, *A peridynamic formulation of pressure driven convective fluid transport in porous media*, Journal of Computational Physics, 261 (2014), pp. 209–229.

[65] R. Keshavarzi and S. Mohammadi, *A new approach for numerical modeling of hydraulic fracture propagation in naturally fractured reservoirs*, in SPE/EAGE European Unconventional Resources Conference & Exhibition-From Potential to Production, 2012.

[66] H. Lee and Q. Du, *Asymptotically compatible SPH-like particle discretizations of one dimensional linear advection models*, SIAM Journal on Numerical Analysis, 57 (2019), pp. 127–147.

[67] S. Lee, A. Mikelic, M. F. Wheeler, and T. Wick, *Phase-field modeling of two phase fluid filled fractures in a poroelastic medium*, Multiscale Modeling & Simulation, 16 (2018), pp. 1542–1580.

[68] S. Lee, M. F. Wheeler, and T. Wick, *Pressure and fluid-driven fracture propagation in porous media using an adaptive finite element phase field model*, Computer Methods in Applied Mechanics and Engineering, 305 (2016), pp. 111–132.

[69] R. Lehoucq, F. Narcowich, S. Rowe, and J. Ward, *A meshless Galerkin method for non-local diffusion using localized kernel bases*, Mathematics of Computation, 87 (2018), pp. 2233–2258.

[70] Y. Leng, X. Tian, and J. T. Foster, *Super-convergence of reproducing kernel approximation*, Computer Methods in Applied Mechanics and Engineering, 352 (2019), pp. 488–507.

[71] Y. Leng, X. Tian, N. Trask, and J. T. Foster, *Asymptotically compatible reproducing kernel collocation and meshfree integration for nonlocal diffusion*, arXiv preprint arXiv:1907.12031, (2019).

[72] ——, *Asymptotically compatible reproducing kernel collocation and meshfree integration for the peridynamic navier equation*, arXiv preprint arXiv:2001.00649, (2019).

[73] S. Li and W. K. Liu, *Moving least-square reproducing kernel method, part II: Fourier analysis*, Computer Methods in Applied Mechanics and Engineering, 139 (1996), pp. 159–193.

[74] ——, *Synchronized reproducing kernel interpolant via multiple wavelet expansion*, Computational Mechanics, 21 (1998), pp. 28–47.

[75] ——, *Reproducing kernel hierarchical partition of unity, part II—applications*, International Journal for Numerical Methods in Engineering, 45 (1999), pp. 289–317.

[76] ——, *Reproducing kernel hierarchical partition of unity, part I—formulation and theory*, International Journal for Numerical Methods in Engineering, 45 (1999), pp. 251–288.

[77] W. K. Liu, S. Jun, and Y. F. Zhang, *Reproducing kernel particle methods*, International Journal for Numerical Methods in Fluids, 20 (1995), pp. 1081–1106.

[78] W.-K. Liu, S. Li, and T. Belytschko, *Moving least-square reproducing kernel methods (I) methodology and convergence*, Computer Methods in Applied Mechanics and Engineering, 143 (1997), pp. 113–154.

[79] R. W. Macek and S. A. Silling, *Peridynamics via finite element analysis*, Finite Elements in Analysis and Design, 43 (2007), pp. 1169–1178.

[80] T. Mengesha and Q. Du, *The bond-based peridynamic system with Dirichlet-type volume constraint*, Proceedings of the Royal Society of Edinburgh Section A: Mathematics, 144 (2014), pp. 161–186.

[81] ——, *Nonlocal constrained value problems for a linear peridynamic navier equation*, Journal of Elasticity, 116 (2014), pp. 27–51.

[82] C. Miehe and S. Mauthe, *Phase field modeling of fracture in multi-physics problems. Part III. Crack driving forces in hydro-poro-elasticity and hydraulic fracturing of fluid-saturated porous media*, Computer Methods in Applied Mechanics and Engineering, 304 (2016), pp. 619–655.

[83] A. Mikelić, M. Wheeler, and T. Wick, *Phase-field modeling through iterative splitting of hydraulic fractures in a poroelastic medium*, GEM-International Journal on Geomathematics, 10 (2019), p. 2.

[84] A. Mikelic, M. F. Wheeler, and T. Wick, *A phase-field method for propagating fluid-filled fractures coupled to a surrounding porous medium*, Multiscale Modeling & Simulation, 13 (2015), pp. 367–398.

[85] D. Mirzaei, R. Schaback, and M. Dehghan, *On generalized moving least squares and diffuse derivatives*, IMA Journal of Numerical Analysis, 32 (2012), pp. 983–1000.

[86] T. Mohammadnejad and J. Andrade, *Numerical modeling of hydraulic fracture propagation, closure and reopening using XFEM with application to in-situ stress estimation*, International Journal for Numerical and Analytical Methods in Geomechanics, 40 (2016), pp. 2033–2060.

[87] M. A. Murad and A. F. Loula, *Improved accuracy in finite element analysis of Biot's consolidation problem*, Computer Methods in Applied Mechanics and Engineering, 95 (1992), pp. 359–382.

[88] ——, *On stability and convergence of finite element approximations of Biot's consolidation problem*, International Journal for Numerical Methods in Engineering, 37 (1994), pp. 645–667.

[89] R. Nordgren et al., *Propagation of a vertical hydraulic fracture*, Society of Petroleum Engineers Journal, 12 (1972), pp. 306–314.

[90] J. Olson et al., *Multi-fracture propagation modeling: Applications to hydraulic fracturing in shales and tight gas sands*, in The 42nd US Rock Mechanics Symposium (USRMS), American Rock Mechanics Association, 2008.

[91] H. Ouchi, J. T. Foster, and M. M. Sharma, *Effect of reservoir heterogeneity on the vertical migration of hydraulic fractures*, Journal of Petroleum Science and Engineering, 151 (2017), pp. 384–408.

[92] H. Ouchi, A. Katiyar, J. T. Foster, M. M. Sharma, et al., *A peridynamics model for the propagation of hydraulic fractures in naturally fractured reservoirs*, SPE Journal, 22 (2017), pp. 1–082.

[93] H. Ouchi, A. Katiyar, J. York, J. T. Foster, and M. M. Sharma, *A fully coupled porous flow and geomechanics model for fluid driven cracks: a peridynamics approach*, Computational Mechanics, 55 (2015), pp. 561–576.

[94] M. Pasetto, *Enhanced meshfree methods for numerical solution of local and nonlocal theories of solid mechanics*, PhD thesis, University of California at San Diego, 2019.

[95] M. Pasetto, Y. Leng, J.-S. Chen, J. T. Foster, and P. Seleson, *A reproducing kernel enhanced approach for peridynamic solutions*, Computer Methods in Applied Mechanics and Engineering, 340 (2018), pp. 1044–1078.

[96] T. Perkins, L. Kern, et al., *Widths of hydraulic fractures*, Journal of Petroleum Technology, 13 (1961), pp. 937–949.

[97] S. Salimzadeh and N. Khalili, *A three-phase XFEM model for hydraulic fracturing with cohesive crack propagation*, Computers and Geotechnics, 69 (2015), pp. 82–92.

[98] I. J. Schoenberg, *Contributions to the problem of approximation of equidistant data by analytic functions*, in IJ Schoenberg Selected Papers, Springer, 1988, pp. 3–57.

[99] P. Seleson, *Improved one-point quadrature algorithms for two-dimensional peridynamic models based on analytical calculations*, Computer Methods in Applied Mechanics and Engineering, 282 (2014), pp. 184–217.

[100] P. Seleson, Q. Du, and M. L. Parks, *On the consistency between nearest-neighbor peridynamic discretizations and discretized classical elasticity models*, Computer Methods in Applied Mechanics and Engineering, 311 (2016), pp. 698–722.

[101] P. Seleson and D. J. Littlewood, *Convergence studies in meshfree peridynamic simulations*, Computers & Mathematics with Applications, 71 (2016), pp. 2432–2448.

[102] E. Siebrits and A. P. Peirce, *An efficient multi-layer planar 3D fracture*

growth algorithm using a fixed mesh approach, International Journal for Numerical Methods in Engineering, 53 (2002), pp. 691–717.

[103] S. A. Silling, *Reformulation of elasticity theory for discontinuities and long-range forces*, Journal of the Mechanics and Physics of Solids, 48 (2000), pp. 175–209.

[104] S. A. Silling and E. Askari, *A meshfree method based on the peridynamic model of solid mechanics*, Computers & Structures, 83 (2005), pp. 1526–1535.

[105] S. A. Silling, M. Epton, O. Weckner, J. Xu, and E. Askari, *Peridynamic states and constitutive modeling*, Journal of Elasticity, 88 (2007), pp. 151–184.

[106] S. A. Silling and R. B. Lehoucq, *Convergence of peridynamics to classical elasticity theory*, Journal of Elasticity, 93 (2008), p. 13.

[107] ——, *Peridynamic theory of solid mechanics*, in Advances in Applied Mechanics, vol. 44, Elsevier, 2010, pp. 73–168.

[108] E. Simonson, A. Abou-Sayed, R. Clifton, et al., *Containment of massive hydraulic fractures*, Society of Petroleum Engineers Journal, 18 (1978), pp. 27–32.

[109] H. Tian, L. Ju, and Q. Du, *A conservative nonlocal convection–diffusion model and asymptotically compatible finite difference discretization*, Computer Methods in Applied Mechanics and Engineering, 320 (2017), pp. 46–67.

[110] X. Tian and Q. Du, *Analysis and comparison of different approximations to nonlocal diffusion and linear peridynamic equations*, SIAM Journal on Numerical Analysis, 51 (2013), pp. 3458–3482.

[111] X. Tian and Q. Du, *Asymptotically compatible schemes and applications to robust discretization of nonlocal models*, SIAM Journal on Numerical Analysis, 52 (2014), pp. 1641–1665.

[112] N. Trask, B. Huntington, and D. Littlewood, *Asymptotically compatible meshfree discretization of state-based peridynamics for linearly elastic composite materials*, arXiv preprint arXiv:1903.00383, (2019).

[113] N. Trask, H. You, Y. Yu, and M. L. Parks, *An asymptotically compatible meshfree quadrature rule for nonlocal problems with applications to peridynamics*, Computer Methods in Applied Mechanics and Engineering, 343 (2019), pp. 151–165.

[114] D. Z. Turner, *A non-local model for fluid-structure interaction with applications in hydraulic fracturing*, International Journal for Computational Methods in Engineering Science and Mechanics, 14 (2013), pp. 391–400.

[115] United States Energy Information Administration, *Hydraulically fractured wells provide two-thirds of US natural gas production*, 2016.

[116] ——, *Annual energy outlook 2015: with projections to 2040*, (2017).

[117] H. Wei, J.-S. Chen, and M. Hillman, *A stabilized nodally integrated meshfree formulation for fully coupled hydro-mechanical analysis of fluid-saturated porous media*, Computers & Fluids, 141 (2016), pp. 105–115.

[118] M. F. Wheeler, T. Wick, and W. Wollner, *An augmented-Lagrangian method for the phase-field approach for pressurized fractures*, Computer Methods in Applied Mechanics and Engineering, 271 (2014), pp. 69–85.

[119] Z. A. Wilson and C. M. Landis, *Phase-field modeling of hydraulic fracture*, Journal of the Mechanics and Physics of Solids, 96 (2016), pp. 264–290.

[120] K. Wu, *Numerical modeling of complex hydraulic fracture development in unconventional reservoirs*, PhD thesis, University of Texas at Austin, 2014.

[121] Y. Xie and G. Wang, *A stabilized iterative scheme for coupled hydro-mechanical systems using reproducing kernel particle method*, International Journal for Numerical Methods in Engineering, 99 (2014), pp. 819–843.

[122] F. Xu, M. Gunzburger, and J. Burkardt, *A multiscale method for nonlocal mechanics and diffusion and for the approximation of discontinuous functions*, Computer Methods in Applied Mechanics and Engineering, 307 (2016), pp. 117–143.

[123] K. Yu, X. Xin, and K. Lease, *A new adaptive integration method for the peridynamic theory*, Modelling and Simulation in Materials Science and Engineering, 19 (2011), p. 045003.

[124] X. Zhang, J. Wu, and L. Ju, *An accurate and asymptotically compatible collocation scheme for nonlocal diffusion problems*, Applied Numerical Mathematics, 133 (2018), pp. 52–68.

[125] A. K. Zheltov et al., *3. Formation of vertical fractures by means of highly viscous liquid*, in 4th World Petroleum Congress, World Petroleum Congress, 1955.